P-///

Composite Trans Wing Technology Deve ent

Design Development T nd Advanced Structural C ts

Charles F. Griffin and Willia ll

Composite Transport Wing Technology Development

Design Development Tests and Advanced Structural Concepts

Charles F. Griffin and William E. Harvill
Lockheed Aeronautical Systems Company
Burbank, California

NASA

National Aeronautics
and Space Administration

Scientific and Technical
Information Division

1988

FOREWORD

This report was prepared by the Lockheed-Aeronautical Systems Company under Contract NAS1-17699. The program was sponsored by the National Aeronautics and Space Administration (NASA), Langley Research Center. The Program Manager for Lockheed is Mr. A. M. James and the Project Manager for NASA is Mr. M. Dow. Lockheed's Georgia activity is managed by Mr. W.E. Harvill.

The following personnel were principal contributors to the program:

	California	Georgia
Engineering Managers	C. Griffin	L. Reynolds
Structural Design	M. Niu	R. Barrie
	R. Bernard	A. Larman
Structural Analysis & Test/Evaluation	D. Kramer	
	M. Bidinger	V. Pigott
	G. Carayanis	G. Gilbert
	D. Petit	D. Bierce
	T. Gillete	
Manufacturing & Tooling	P. Flowers	G. Reynolds
	R. Hooper	F. Snipes
Materials/Processing/ Value Analysis	G. Hull	L. Ott
	R. Turpin	G. Walters
	B. Towery	
Quality Assurance	D. Russel	F. Malik
	S. Kracher	

CONTENTS

PRECEDING PAGE BLANK NOT FILMED

PAGE __LV__ INTENTIONALLY BLANK

CONTENTS

P-111

Composite Transport Wing Technology Development

Design Development Tests and
Advanced Structural Concepts

Charles F. Griffin and William Sorvill

NASA Contractor Report 4177

Composite Transport Wing Technology Development

Design Development Tests and Advanced Structural Concepts

Charles F. Griffin and William E. Harvill
Lockheed Aeronautical Systems Company
Burbank, California

NASA

National Aeronautics
and Space Administration

Scientific and Technical
Information Division

1988

FOREWORD

This report was prepared by the Lockheed-Aeronautical Systems Company under Contract NAS1-17699. The program was sponsored by the National Aeronautics and Space Administration (NASA), Langley Research Center. The Program Manager for Lockheed is Mr. A. M. James and the Project Manager for NASA is Mr. M. Dow. Lockheed's Georgia activity is managed by Mr. W.E. Harvill.

The following personnel were principal contributors to the program:

	California	Georgia
Engineering Managers	C. Griffin	L. Reynolds
Structural Design	M. Niu	R. Barrie
	R. Bernard	A. Larman
Structural Analysis	D. Kramer	
& Test/Evaluation	M. Bidinger	V. Pigott
	G. Carayanis	G. Gilbert
	D. Petit	D. Bierce
	T. Gillete	
Manufacturing &	P. Flowers	G. Reynolds
Tooling	R. Hooper	F. Snipes
Materials/Processing/	G. Hull	L. Ott
Value Analysis	R. Turpin	G. Walters
	B. Towery	
Quality Assurance	D. Russel	F. Malik
	S. Kracher	

CONTENTS

PRECEDING PAGE BLANK NOT FILMED

PAGE __IV__ INTENTIONALLY BLANK

CONTENTS

LIST OF FIGURES

LIST OF FIGURES (Continued)

LIST OF FIGURES (Continued)

LIST OF FIGURES (Continued)

LIST OF TABLES

SUMMARY

Numerous design concepts, materials and manufacturing methods were investigated for the covers and spars of a transport wing box. Cover panels and spar segments were fabricated and tested to verify the structural integrity of design concepts and fabrication techniques.

Compression tests on stiffened panels demonstrated the ability for graphite/epoxy wing upper cover designs to achieve a 35 percent weight savings compared to the aluminum baseline. The impact damage tolerance of the designs and materials used for these panels limits the allowable compression strain and therefore the maximum achievable weight savings.

Bending and shear tests on various spar designs verified an average weight savings of 37 percent compared to the aluminum baseline. Impact damage to spar webs did not significantly degrade structural performance. Predictions of spar web shear instability correlated very well with measured performance. The structural integrity of spars manufactured by filament winding equaled or exceeded those fabricated by hand lay-up.

The information obtained will be applied to the design, fabrication, and test of a full scale section of a wing box. When completed, the tests on the technology integration box beam will demonstrate the structural integrity of an advanced composite wing design which is 25 percent lighter than the metal baseline.

INTRODUCTION

Current applications of composite materials to transport aircraft structure, most of which are stiffness critical secondary structural components and medium size primary structural components, have demonstrated weight savings from 20 to 30 percent. The greatest impact on aircraft performance and cost will be made when these materials are used for fabrication of primary wing and fuselage structures that are 30-to-40 percent lighter than their metal counterparts and which have a reduced acquisition cost. Achievement of this goal requires the integration of innovative design concepts, improved composite materials and low cost manufacturing methods.

In 1984, the Lockheed Aeronautical Systems Company began a program to develop engineering and manufacturing technology for advanced composite wing structures on large transport aircraft. The program was sponsored by the National Aeronautics and Space Administration (NASA).

The selected baseline component is the center wing structural box of an advanced version of the C-130 aircraft. The existing structural box, shown in figure 1, is a two-spar multirib design, 440 inches long, 80 inches wide, and 35 inches deep at the crown. A preliminary design of a composite box was completed. Within the last three years several design concepts for the wing covers and spars were evaluated by fabricating and testing components. Integration of the design concepts into a box beam will follow. This box beam will be of sufficient size and complexity to interrogate the many engineering and manufacturing technology issues which must be resolved before composite wing structures can be confidently applied to large transport aircraft.

1

This report summarizes major technical achievements from the program. Cover and spar components were fabricated and tested to evaluate various design concepts, composite materials and low cost manufacturing processes.

Use of commercial products or names of manufacturers in this report does not constitute official endorsement of such products or manufacturers, either expressed or implied, by either the National Aeronautics and Space Administration or the Lockheed Aeronautical Systems Company.
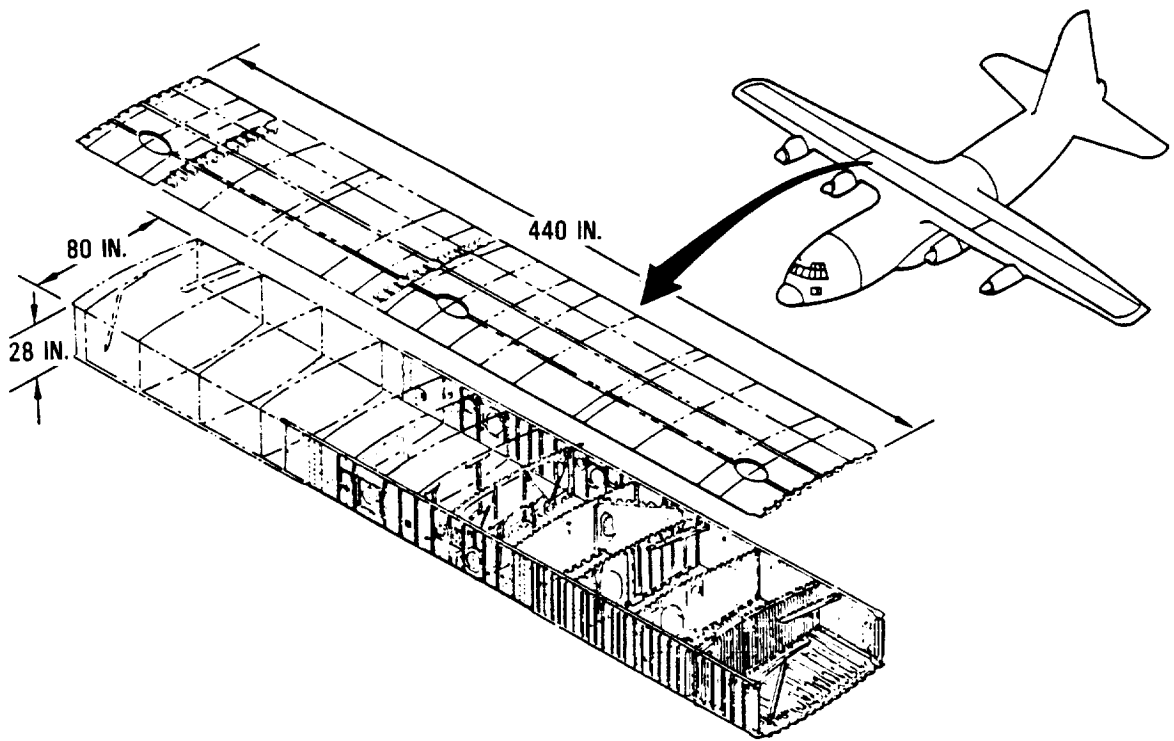
Figure 1. - Existing Lockheed C-130 center wing - metallic design.

WING DEVELOPMENT

Cover Design Criteria

Geometry

Upper and lower covers of the wing box are 80 inches wide by 440 inches long as shown in figure 2. The covers are supported by the forward and aft spars and by ribs which are typically spaced at 30 inch centers. Three large cut-outs are placed in the upper cover to provide access to the integral fuel tanks which span from Wing Station 61 to Wing Station 178. An inner wing to outer wing joint is located at Wing Station 220.

Design Loads and Stiffness Requirements

The design loads for the composite wing box are based on the baseline aircraft requirements. Figure 3 presents the maximum spanwise cover end loads as a function of wing station. The maximum level of 22,000 lb/in. is a relatively high value which is representative of design load levels for current and future transport aircraft. The maximum surface loads are developed for an up bending condition which puts the upper cover in compression and the lower cover in tension. Combined with the spanwise loads are inplane shear loads, which have a magnitude less than 20 percent of the axial load and pressure loads due to beam bending curvature and fuel pressures.

Stiffness requirements for the composite wing have been established which will meet the commercial flutter requirements as specified in Federal Aviation Regulation (FAR) Part 25. The requirements for the composite wing box are presented as an envelope (figure 4) of stiffness ratios for the composite wing box to those of the baseline aircraft. Points that fall within the envelope indicate the wing box is acceptable from a flutter standpoint. The torsional stiffness requirements for the inner wing box translate to an average inplane shear stiffness (GT) value for the covers of 0.73×10^6 lb/in. As shown in figure 4, variations from this value are acceptable as limited by the axial stiffness of the cover.

Damage Tolerance

Damage tolerance requirements are flight safety considerations intended to provide the required level of residual strength for specified periods of unrepaired service usage resulting from designated threats. Damage could possibly occur and remain undetected for some period of usage. The required safe operational interval is either the interval until the damage is detected or, if not detected, the entire service life. Throughout this operational interval, the residual strength of the structure must be capable of sustaining a load level that is very unlikely to be exceeded.

FWD
UP

WS 20.50 TRUSS FUSELAGE
ATTACH RIB

WS 61.62 FUEL
CONTAINMENT RIB

WS 150.00, 120.0 AND 90.0
TRUSS SUPPORT RIB

WS 178.78 FUEL CONTAINMENT RIB

WS 220.0
WS 192.12
WS 178.782
WS 120.0
WS 108.12
WS 90.0
WS 61.625
WS 20.5
WS 0.0
WS 20.50
WS 61.5
WS 90.0
WS 108.12
WS 120.0
WS 150.00
WS 178.78
WS 220.0
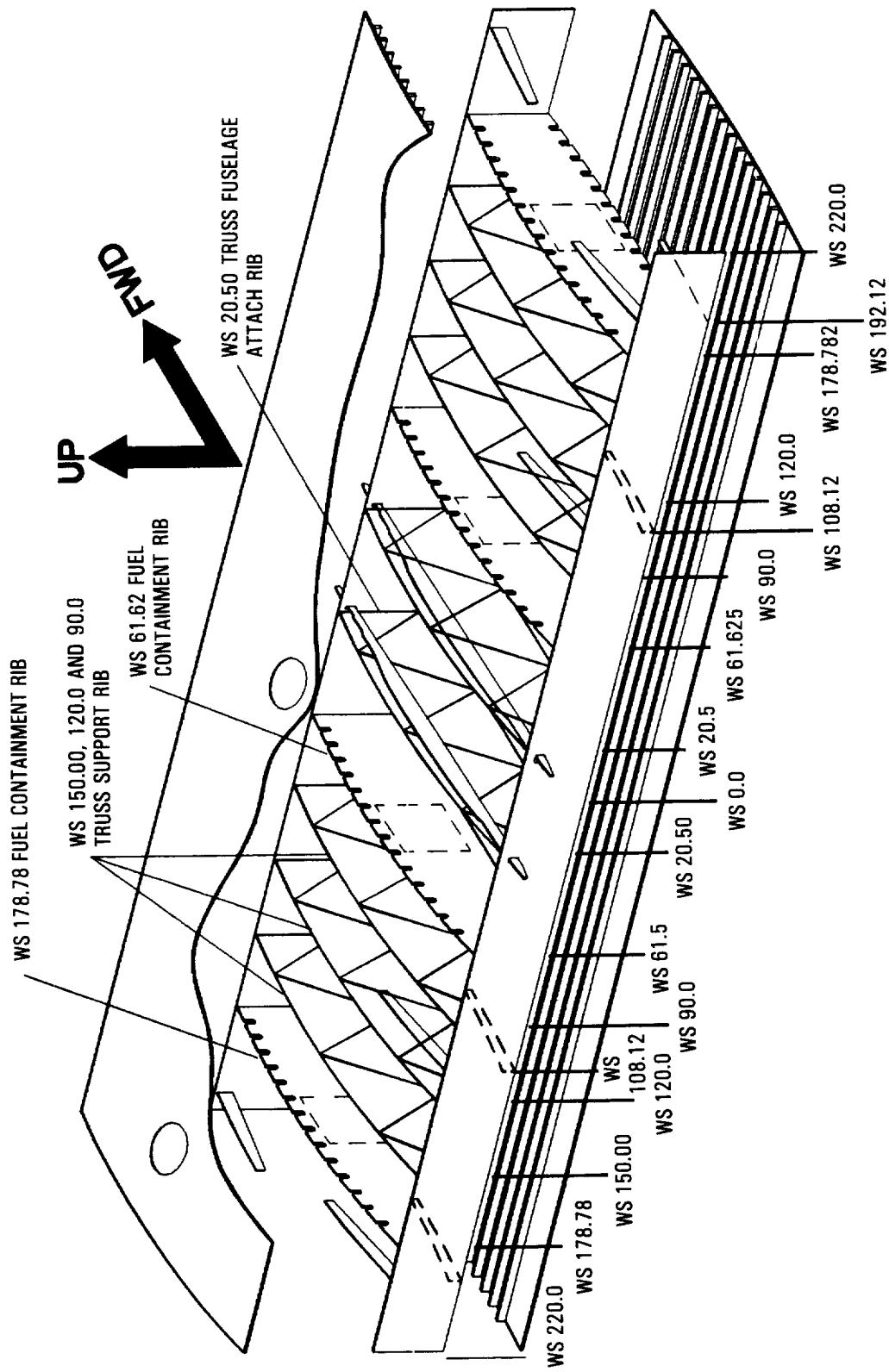
Figure 2. – Wing box assembly.

4
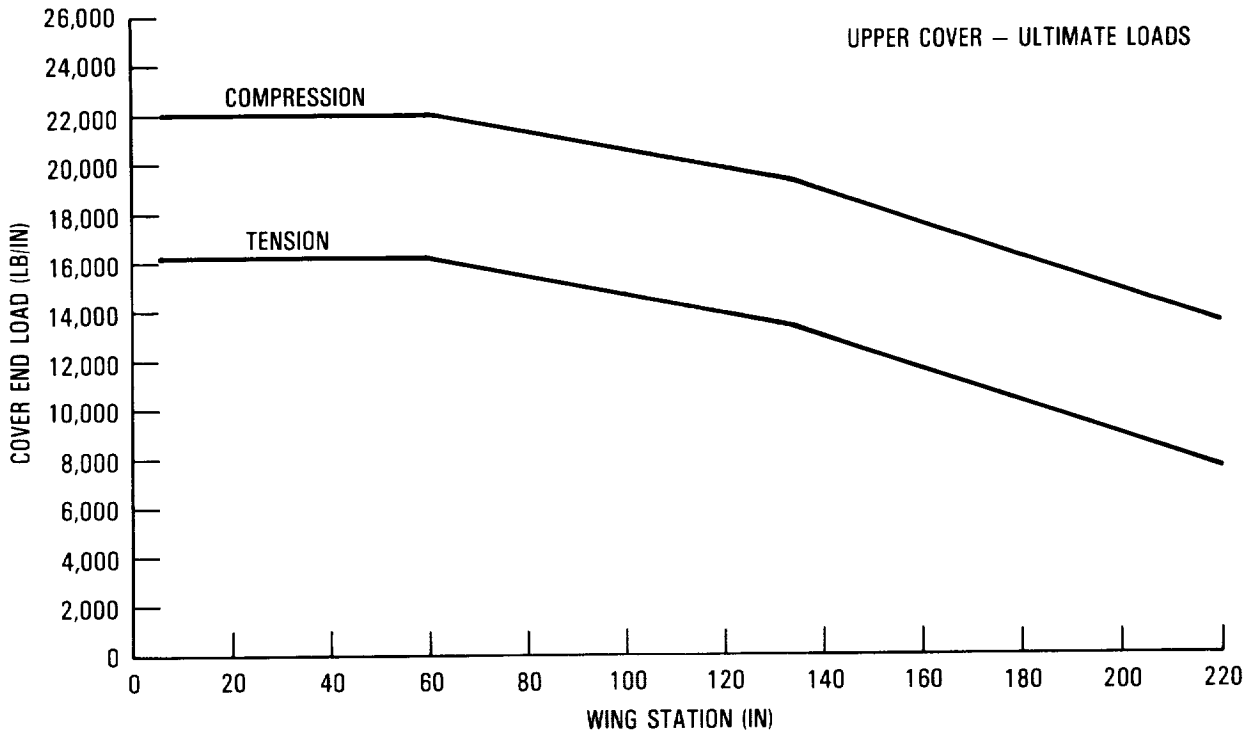
Figure 3. - Cover end loads.
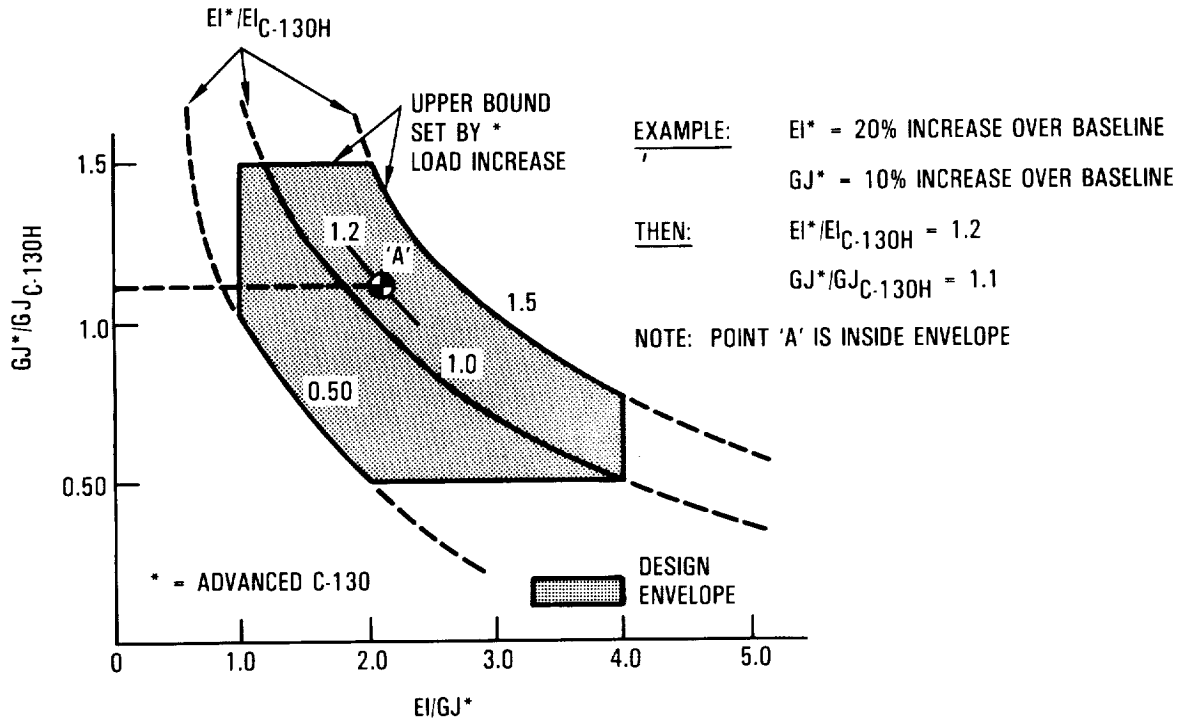
Figure 4. - Flutter envelope.

Structural requirements for damage tolerance consider civil as well as military criteria. The damage tolerance requirements for commercial aircraft, as specified in (FAR) 25.571, were used where applicable. Advisory Circular 25-571 provides guidance for interpreting the intent of the regulation and the means of showing compliance with the requirements. More specific guidance for the particular application of the criteria to damage tolerance design of composite aircraft structure is contained in Advisory Circular 20-107A. This document states "that impact damage that can be realistically expected from manufacturing and service, but not more than the established threshold of detectability for the selected inspection procedure, will not reduce the structural strength below ultimate load capability."

The military requirements for damage tolerance of composite structures are being developed under Air Force Contract F33615-82-C-3213, "Damage Tolerance of Composites." This program has defined the principal impact damage as a 1.0 inch diameter hemispherical impactor with 100 ft-lb of kinetic energy or with the kinetic energy required to cause a 0.10 inch deep dent, whichever is least. The residual strength requirement for non-inspectable damage is limit load.

For the wing, the damage tolerance criteria used for this program requires the structure to have ultimate strength capability with the presence of barely visible impact damage anywhere within the structure. Barely visible impact damage is either the kinetic energy required to cause a 0.1 inch deep dent or a kinetic energy of 100 ft-lb with a 1.0 inch diameter hemispherical impactor, whichever is least.

BASELINE J-STIFFENED COVER DESIGN

Design

Early in this program, design trade studies were conducted on various configurations for the wing covers. These evaluations included quantitative weight and cost analysis and a qualitative assessment of the merits of each design.

After evaluating numerous concepts for the wing covers, three concepts were selected for a more in-depth investigation. The three concepts, shown in figure 5, were a blade stiffened design, a corrugated design, and a J-stiffened design.

The blade stiffened skin represents one of the simplest designs from the manufacturing standpoint. The design consists of a pultruded stiffener cocured to a uniform thickness skin. The shape of the stiffener simplifies fuel sealing where the stiffener penetrates the fuel bulkhead. With this design, the stiffener carries most of the axial load since the skin has been configured with a high percentage of ± 45 degree material to enhance damage tolerance.

CORRUGATED COVER DESIGN

PRECURED HIGH % 0° LAMINATES
INTERLEAVED INTO CROWN

FOAM

SOFT SKIN

0° INSERTS INTERLEAVED INTO SKIN

BLADE STIFFENED COVER DESIGN

FIBERGLASS
OVERWRAP

PULTRUDED 'T'

PAN

FASTENERS AT
RIB LOCATIONS

SOFT SKIN

J-STIFFENED COVER DESIGN

PULTRUDED J-STIFFENER

FIBERGLASS WRAP

PAN

FASTENERS AT
RIB LOCATIONS

0° PAD-UP IN SKIN

SOFT SKIN
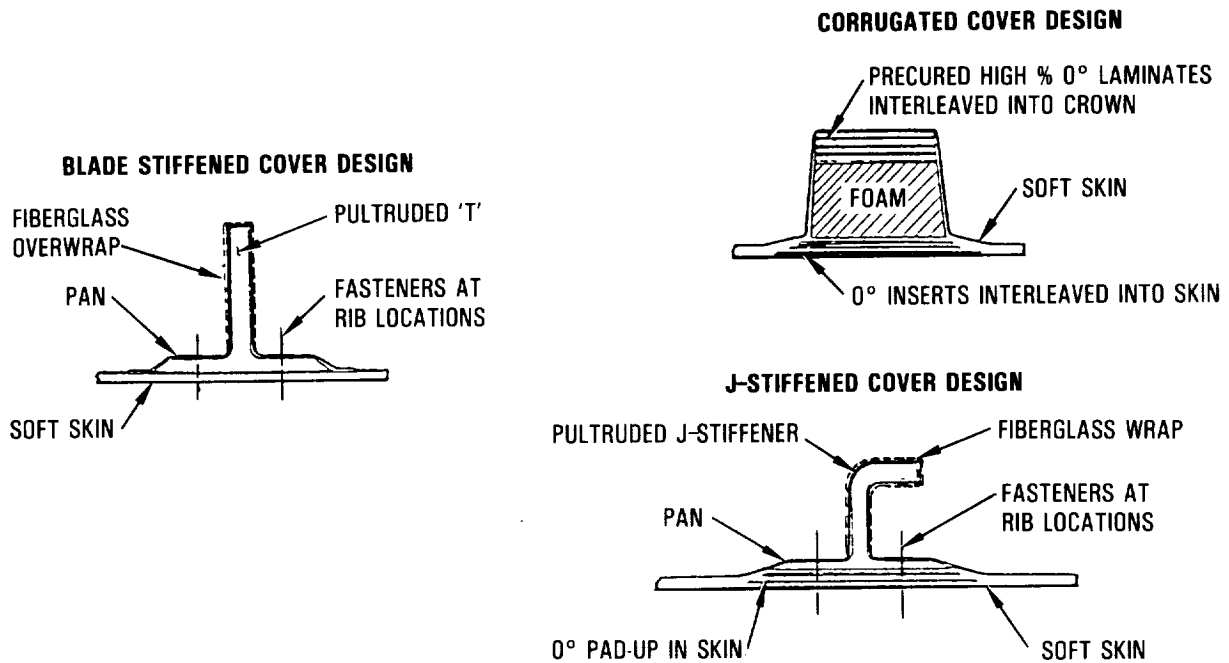
Figure 5. - Cover designs.

The second design is a corrugated skin. This design offers good structural efficiency because the high modulus material can be optimally placed to achieve the required panel bending stiffness for stability. However, the structural efficiency of the design is severely reduced by manufacturing considerations which include a discontinuous inner skin which is lapped at the crown of the stiffener. The discontinuous inner skin is required to simplify layup and eliminate the possibility of bridging in the radii of the stiffener. Furthermore, the stiffener must be filled with foam to eliminate the need for mandrels during fabrication and to prevent fuel transfer from the wet bay to dry bay areas of the wing.

The third design is a J-stiffened skin. The significant features of this design are a skin with a high modulus pad-up under the stiffener and a stiffener shape which has improved bending stiffness compared to a blade.

A weight comparison of the three cover designs is presented in Table 1. These designs are for the upper cover of the wing at the most highly loaded location. All of the designs meet the load and stiffness structural requirements. The J-stiffened skin concept has the best weight savings potential of the three designs.

Analysis of the upper and lower covers indicated that the minimum margin of safety was obtained for compression loading to the upper cover. This result is due to the compression design allowable being less than the tension design allowable in graphite/epoxy composites. Thus, it was decided to

7

TABLE 1. - WEIGHT FACTORS FOR COVER DESIGNS

DESIGN	WEIGHT FACTOR
J-STIFFENED	100%
BLADE STIFFENED	108%
CORRUGATED	137%

fabricate a test panel typical of a highly loaded region in the upper wing cover. The loads used to design the panels were an axial compression loading of 22,000 lb/in., combined with an inplane shear load of 1,900 lb/in., and a normal pressure of 6.82 psi.

The material selected for fabrication of the test panels was AS4/1806 graphite fabric/epoxy. Three types of fabric were designed; each having a cured ply thickness of 0.012 inches at 32 percent resin content by weight.

Unidirectional - 9 end/in. AS4, 12K warp
                - 10 end/in. S2 150 1/0 fill
                - plain weave, 325 g/m^2

Bidirectional   - 9 end/in. AS4, 6K warp
                - 9 end/in. AS4, 6K fill
                - 5 harness satin weave, 310 g/m^2

$\pm 45°$ and $\pm 45°$ bias - 18 end/in., AS4, 3K at $45°$
                              - 18 end/in., AS4, 3K at $-45°$
                              - 2 ply knit with Dacron thread, 333 g/m^2

The reason for selecting woven and knit fabrics for the test panels, rather than unidirectional tape, was reduction of manufacturing cost. Cost studies predict that fabrics, which are generally much thicker than tape, would be less expensive to lay down by hand than tape laid down with an automated machine. Note that use of these three fabrics eliminates the need for crossplying and permits all plies to be laid down at zero degrees, which is a major simplification in the manufacturing process.

As part of a Lockheed funded research program, the physical and mechanical properties of these fabric composites were obtained by an extensive test program. Table 2 summarizes the properties used for designing the J-stiffened panels described below and the spars discussed later.

The test panel design, shown in figure 6, has several unique design features. The principal load carrying element within the panel is the J-stiffener which contains 75 percent $0°$ plies and 25 percent $\pm 45°$ plies. The stiffener was designed to be pultruded or contact molded and machined prior to being cobonded to the skin laminate. The skin laminate is a "soft" configuration consisting of 16.7 percent $0°$ plies. Panel optimization studies indicated that the soft skin was most efficient for compression stability and is inherently resistant to delamination due to impact damage. Six $0°$ plies are interleaved into the skin at the base of the stiffener as a pad-up.

8

TABLE 2. - AS4/1806 DESIGN PROPERTIES

Property	Unidirectional Fabric	Bidirectional Fabric	$\pm45^{\circ}$ Bias Knit Fabric
Resin Content By Weight (%)	33 ± 3	33 ± 3	33 ± 3
Density (lb/in.^{3})	0.057	0.057	0.057
Nominal Thickness (in.)	0.012	0.012	0.012
0° Tensile Modulus (msi)	19.7	9.7	8.5 ①
0° Compression Modulus (msi)	17.0	9.7	8.5 ①
90° Modulus (msi)	1.47	8.8	8.7 ②
Poissons Ratio	0.30	0.05	0.05 ①
0° Inplane Shear Modulus (msi)	0.62	0.62	0.62 ①
Tension Design Strain (10^{-6} in./in.) -65°F, Dry	5000	5000	5000 ①
Compression Design Strain (10^{-6} in./in.) 180°F, Wet	4500	4500	4500 ①

① At 45° to Warp   ② At 135° to Warp

A double lap shear joint of the stiffener to the skin is created via 16.7% 0°/66.7% $\pm45^{\circ}$/16.7% 90° pans which are placed between the stiffeners. FM 300 adhesive is used at the interfaces of the stiffeners to the pans and skin.

Fabrication

A sequential manufacturing process was selected for the J-stiffened panels. First the J-stiffeners were laid up and cured. Then the cured stiffeners were combined with an uncured skin and pans and this assembly cocured. This technique was selected to enable the stiffeners to be pultruded in a production application.

FIBERGLASS 2 PLIES (100/0/0)

J CAP 24 PLIES (75/25/0)

PAN 3 PLIES (17/66/17)

J BASE 14 PLIES (79/21/0)

BASIC SKIN 15 PLIES (17/66/17)

MATERIAL AS4/1806 FABRIC .012 CURED THICKNESS

1.73 REF

.328 REF

.410 REF

.466 REF

2.88 REF

PAD-UP SKIN 21 PLIES (40/48/12)

.216 REF

6.60
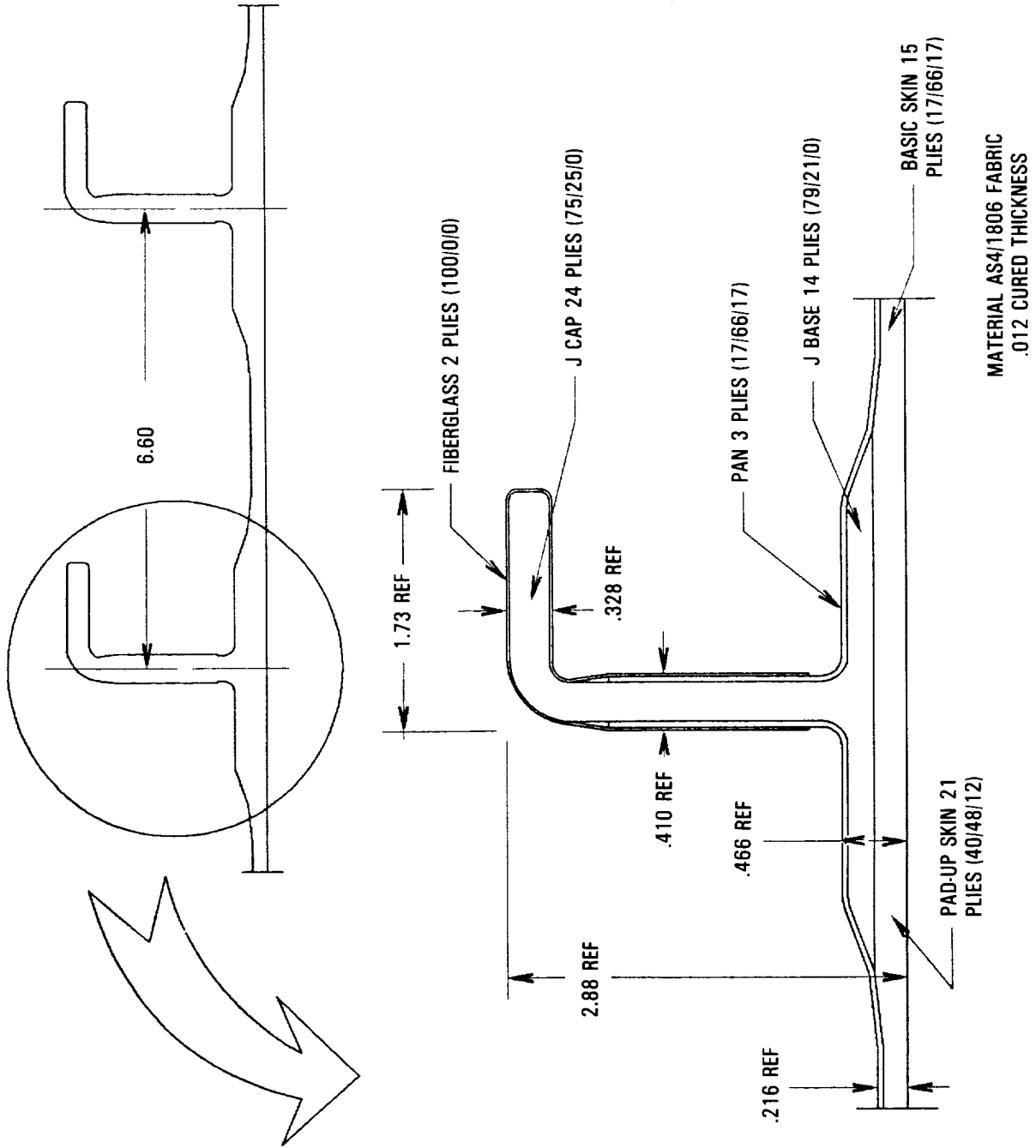
Figure 6. – J-Stiffened panel design.

For the test panels, the J-stiffeners were formed by combining three pieces; a 'Z' section, a 'C' section and a flat base. Separate lay-up blocks were employed for each detail. Each piece was vacuum debulked at room temperature for 20 minutes. The details were then assembled in a curing tool, shown in figure 7, and cured in an autoclave. After being cured, the J-stiffeners were ultrasonically inspected and machined to the proper dimensions for the next step in the panel assembly.

Stiffened panel assembly was accomplished by wrapping the J-stiffeners with FM-300 film adhesive and placing them on the uncured skin laminate. A graphite/epoxy tooling aid was used to locate the J's on the skin. Preformed pans were then added between the stiffeners and the assembly was bagged. Formed silicon rubber inserts were used to fill the cavity between the upper flange of the J-stiffener and the base to simplify the bagging procedure. The panel was then cured in an autoclave. As with the J-stiffeners, a straight-up cure cycle was used for the panel with 100 psi pressure applied during the heat-up period and 350°F temperature held for two hours.

After being cured, the J-stiffened panels were ultrasonically inspected, trimmed, and the fiberglass stiffener wraps cocured in place. Figure 8 shows a panel after it has been machined in preparation for application of the fiberglass overwraps.

Test

As previously noted, analysis of the wing cover design indicated that the minimum margin of safety was for compression loading on the upper cover. Therefore, static compression tests were conducted on J-stiffened panels to evaluate their strength for both the unimpacted and impacted test conditions.

A J-stiffened panel was impacted at numerous locations to determine the relationship between impact energy and the amount of damage. From previous tests, it had been determined that impact damage to the stiffener flange or to the skin/stiffener interface caused the largest reduction in compression strength. The panel was impacted at these locations, see figure 9, using a 12 pound drop weight having a 1.0-inch-diameter-hemispherical tup. For all impacts, the panel was clamped between wooden blocks as shown in figure 10. The spacing between the interior pair of blocks was 8.0 inches.

After the panel was impacted, it was visually and ultrasonically inspected. A summary of the data from these inspections is shown in Table 3. The impacts to the outside surface of the panel at the skin/stiffener interface caused very little visual damage, even at the higher impact energies. It is interesting to note that, based on the ultrasonic inspections, the 100 ft-lb impact caused less damage than did the 80 ft-lb impact. This behavior has been seen on other stiffened panels. At 100 ft-lb, the impactor partially punctures the surface, as evidenced by the broken fibers on the outside surface. It is theorized that partial puncture reduces the laminate deformation and, thus, the extent of the interlaminar and translaminar damage is decreased. However, the local damage to the laminate, under the head of the impactor, is greater. A micrographic inspection made of a section of the laminate cut through the 100 ft-lb impact damage area is shown in figure 11.

11
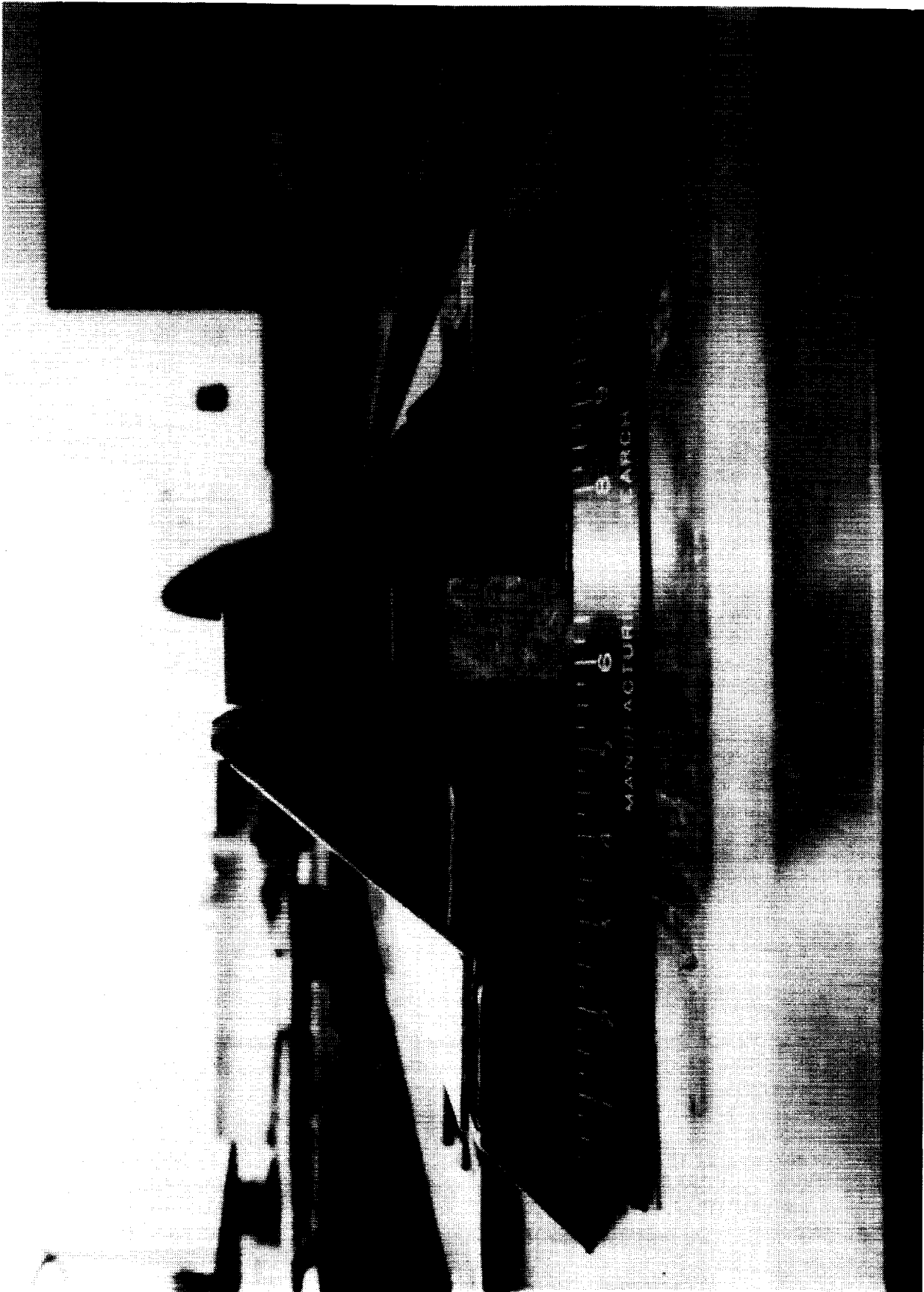
Front View

Figure 7. – Stiffener tool (Sheet 1 of 2).

Top View

Figure 7. – Stiffener tool (Sheet 2 of 2).
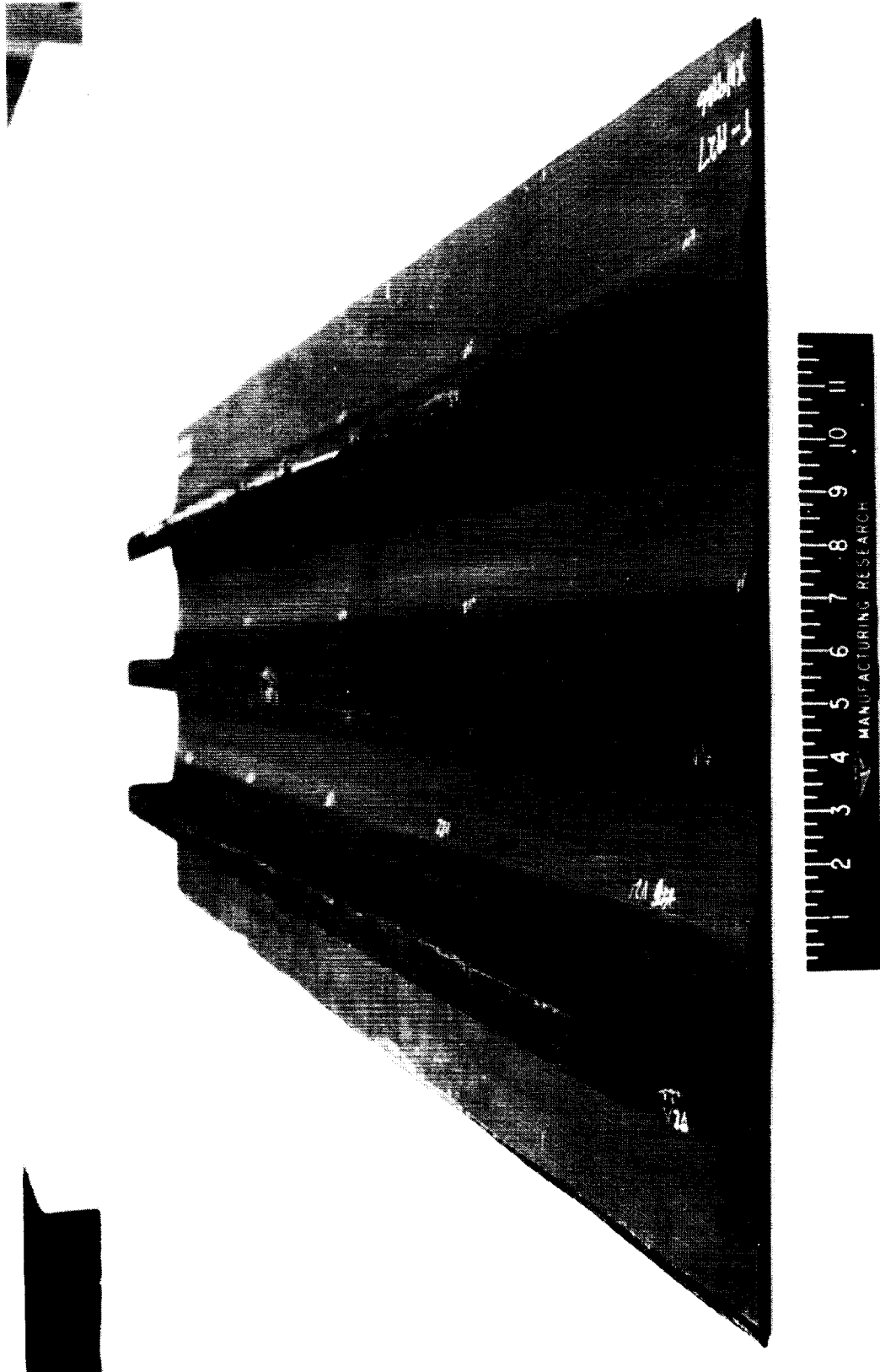
Figure 8. – J-stiffened panel.
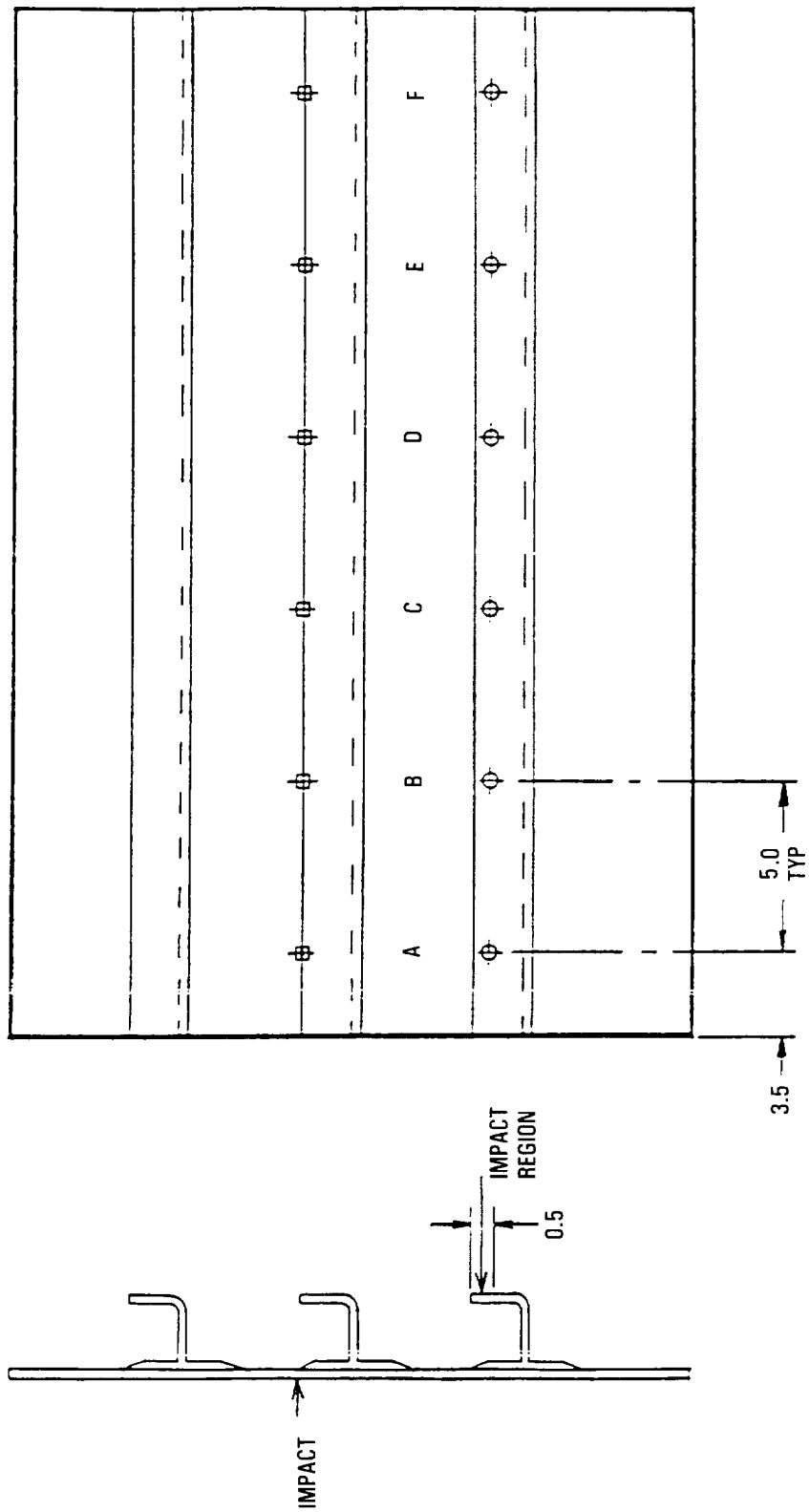
Figure 9. – Impact locations on test panel.

15
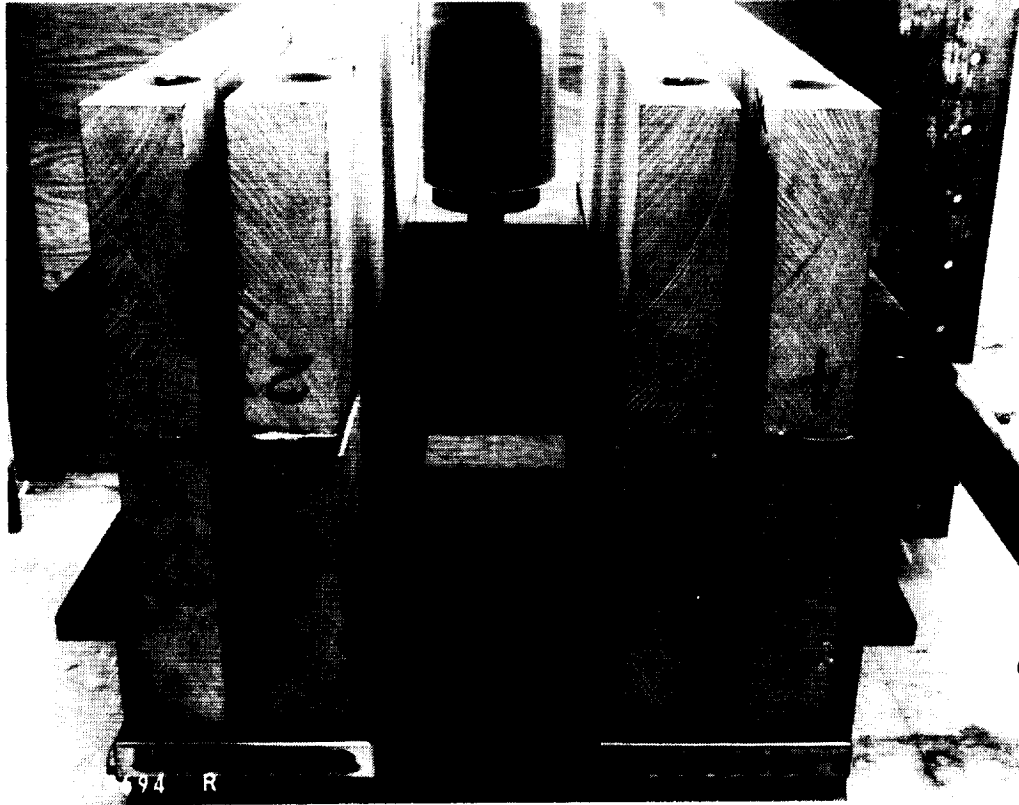
Figure 10. – Impact test fixture.

The stiffeners were covered by two plies of fiberglass fabric/epoxy. Thus, impacts to the stiffeners were quite visible because the fiberglass/epoxy crazed at the location of the impact. The typical damage to the stiffener flange was semi-circular delaminations radiating away from the point of impact.

The impact energies selected for the post-impact compression tests on J-stiffened panels were 100 ft-lb for the skin/stiffener location and 60 ft-lb for the flange location. The 100 ft-lb surface impact is consistent with the Air Force requirements for damage tolerance. Lockheed's policy for interior damage requires that the damage be easily detected by visual inspection. Therefore, 60 ft-lb was selected for the flange impact energy.

The unimpacted compression strength of the cover design was determined by testing a 14.2-inch-wide by 24.0-inch-long panel with two J-stiffeners. Prior to testing 0.25 inch fasteners were installed in the skin and stiffeners to duplicate the effect of panel-to-rib cap attachments. The loaded ends of the panel were potted, the side support rails installed and the panel was mounted in the test machine as shown in figure 12. The applied load at failure was 484,200 pounds and the strains ranged from 5771 μin./in. to 6804 μin./in. with an average panel strain of 6431 μin./in. The load-strain plots were linear to failure. Failure occurred through the simulated rib cap attachments at the middle of the panel.

16

TABLE 3. - RESULTS OF TRIAL IMPACTS

Impact Location	Impact Energy (ft-lb)	Impacted Surface Damage	Dent Depth (in.)	Damage① Area (in.²)	Damage Width (in.)
Skin/ Stiffener	20	Not visible	0.005	0.70	0.70
	30	Barely visible	0.004	1.20	1.05
	40	Barely visible	0.002	0	0
	60	Visible	0.005	2.75	1.50
	80	Visible	0.007	5.05	2.20
	100	Visible	0.017	3.65	1.60
Stiffener Flange	20	Barely Visible	0.005	0	0
	30	Barely Visible	0.004	0	0
	40	Visible	0.007	1.10	0.70
	50	Visible	0.007	1.70	1.10
	60	Visible	0.012	2.80	1.06
	80	Visible	0.012	4.55	1.30

①Computed from ultrasonic inspection records.

Column stability was determined by testing a 69-inch-long, two J-stiffener panel. The ends of the panel were potted but no side supports were installed on the panel. The panel failed in end bearing in the potting box at an applied load of 329,700 pounds, with an average panel strain of 4505 μin./in. The measured strains in the middle of the panel ranged from 2830 μin./in. in the stiffener flanges to 5519 μin./in. in the skin. The column buckling load was 290,000 pounds based on an intersecting slope analysis of the plot of the lateral deflection versus load. This is
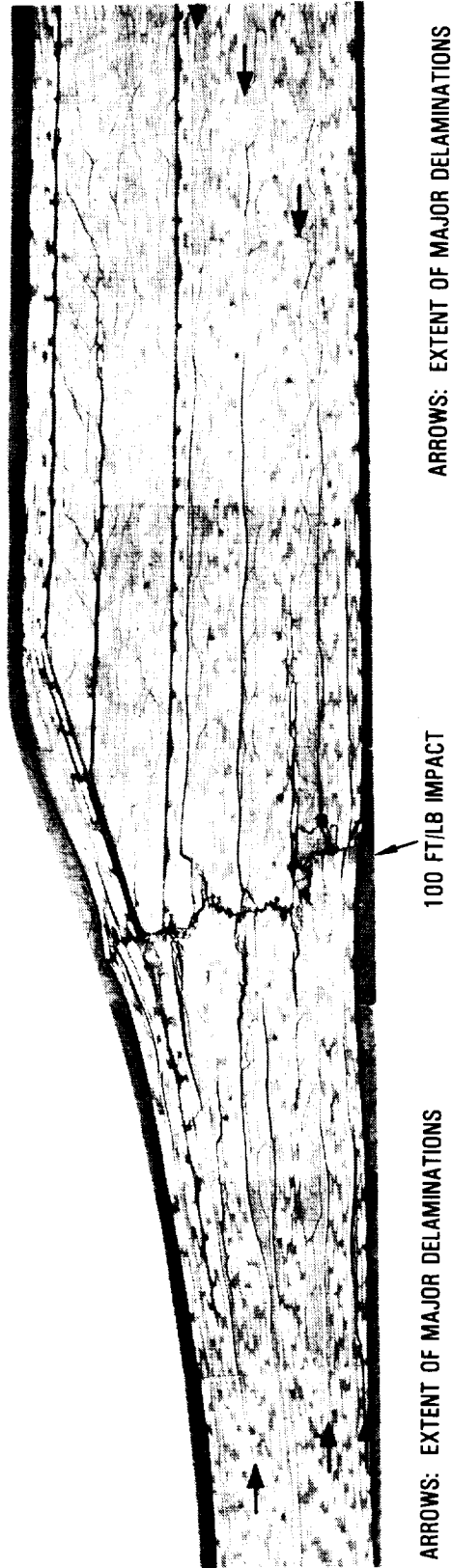
Figure 11. – Photomicrograph of skin impact damage to J-stiffened panel.
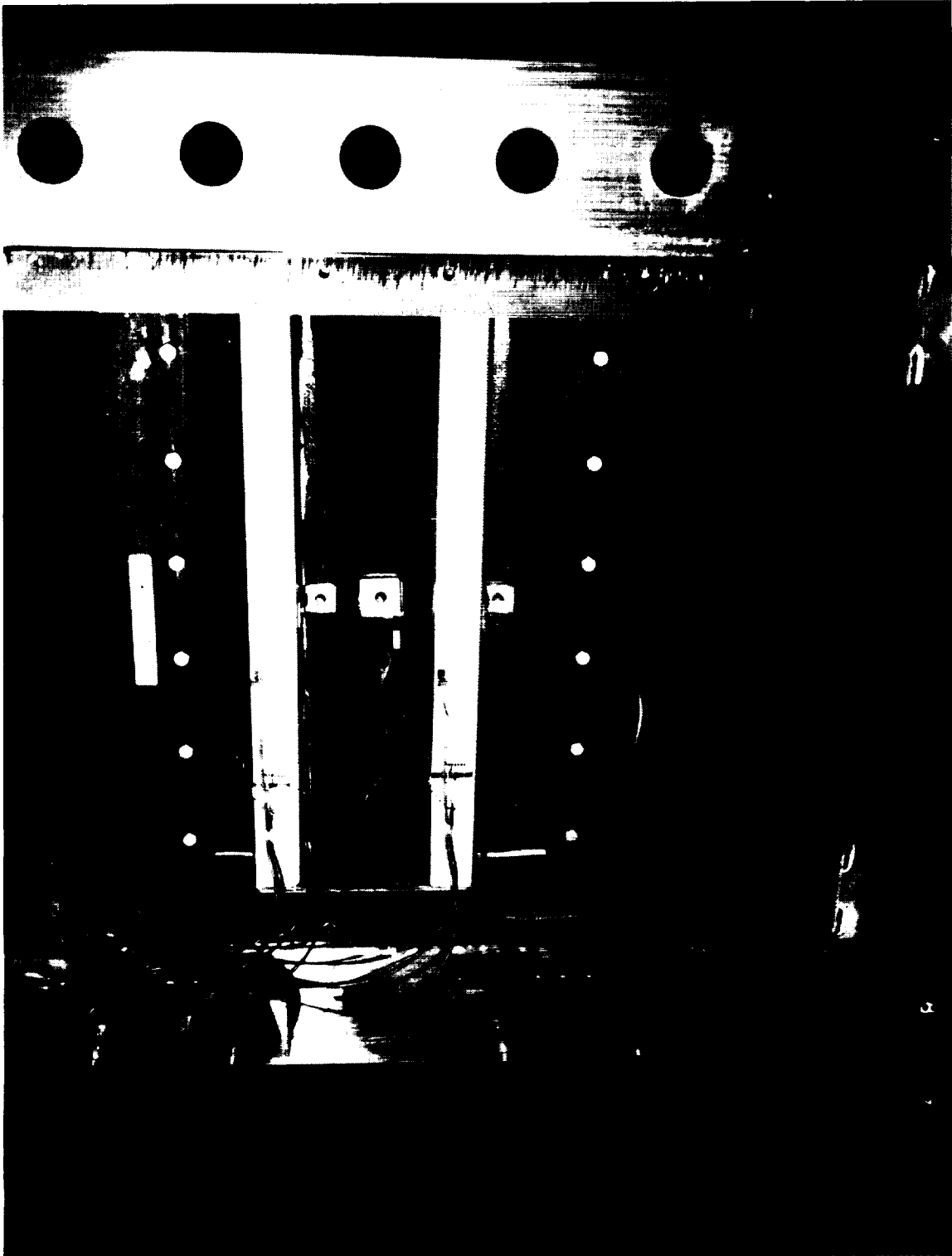
Figure 12. – J-stiffened panel installed in compression test machine.

19

equivalent to a fixity coefficient of 3.2. The predicted column failure load of 340,200 pounds was based upon a PASCO analysis using a simply-supported panel with an effective length of 35.4 inches (simulating a 69-inch panel with an end fixity C = 3.8) and including an inward initial longitudinal bow of .53 inches.

A 20.8-inch-wide, three stiffener panel was impacted on the upper flange of the center stiffener at 60 ft-lb. The impact damage was visible and ultrasonic inspection indicated a damage area of 3.71 in.^{2} The ends of the 24-inch-long panel were potted and side supports were installed.

The panel failed in compression through the damaged area with no evidence of bending. The damaged flange began to fail at a load of 300,000 pounds, which corresponds to an average panel strain of 2,500 μin./in. At an applied load of 400,000 pounds (3,340 μin./in.), both audible and visible indications of failure became apparent. The final panel failure occurred at a load of 541,300 pounds. At this load, the average panel strain was 4,523 μin./in. The measured strains at failure averaged 2,900 μin./in. in the impacted flange, 5,600 μin./in. in the skin, and 6,200 μin./in. in the undamaged flanges. Based upon a design ultimate failure strain of 4,500 μin./in., the predicted panel compression failure load was 538,500 pounds. Figure 13 shows both sides of the panel after failure.

A second 20.8-inch-wide, three stiffener panel was impacted on the skin as shown in figure 14. The 100 ft-lb impact resulted in a 0.017 inch deep dent which was clearly visible on the unpainted surface. A slight crack was observed on the other side of the panel. Ultrasonic inspections indicated a delamination area of 7.24 in.^{2}.

This panel was tested in static compression and failed through the impact damaged area. There was no evidence of panel bending. The failure occurred at a load of 524,900 pounds, which corresponds to an average panel strain of 4836 μin./in. The measured strains at failure ranged from 4836 μin./in. in the flange to 4886 μin./in. in the skin. Based upon a design ultimate failure strain of 4500 μin./in. for post-impact compression and a panel AE of 119,667,950 pounds, the predicted panel compression failure load was 538,500 pounds.

A summary of the J-stiffened panel tests is presented in Table 4. All panels demonstrated failure loads greater than the design ultimate load of 22,000 lb/in.

As a part of a Lockheed funded program, tests were conducted on coupons and J-stiffeners constructed with AS4/1806. Figure 15 compares these data with the results obtained on the J-stiffened panels. Compression failure strains are plotted as a function of the impact damage areas which were obtained from ultrasonic inspections. Note that the data plotted on the ordinate is from test specimens which contain 0.25 inch diameter holes to represent the effects of fasteners. A curve was faired through the coupon data and extrapolated to very large damage sizes. Two observations are made. First, both the notched J-stiffeners and the J-stiffened panel containing fastener holes failed at lower strains than would have been predicted from the

152096 R
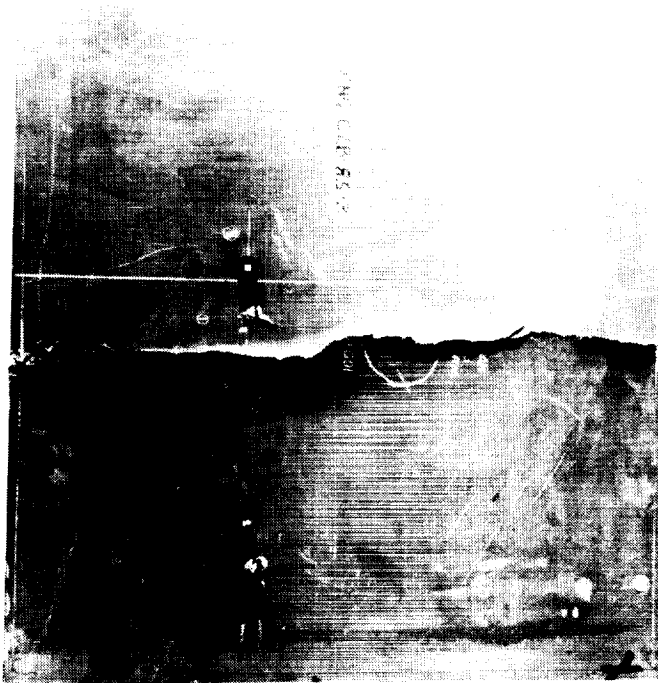
152097R

Figure 13. - Failed J-stiffened panel.

21

100 FT-LBS

1.67 ± .25
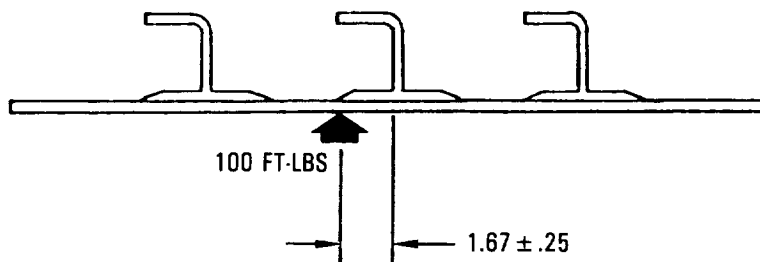
Figure 14. - Impact locations on skin of three stiffener panel.

notched coupon data. Secondly, the impacted J-stiffeners and stiffened panels failed at higher strains than the curve would predict. Accurate methods for predicting the strength of impacted panels need to be developed.

THERMOPLASTIC J-STIFFENER

Design

Thermoplastic resin composites such as polyphenylene sulfide (PPS) and polyetheretherketone (PEEK) are being developed as alternatives to thermosetting resins such as epoxy or bismaleimide. Preliminary tests indicate that thermoplastic matrix composites are tougher than epoxy composites, which will permit designing to greater strain allowables. Furthermore, since thermoplastics are melt fusible, out-of-autoclave consolidation and forming methods and fusion joining techniques may result in lower part fabrication costs than for epoxies.

Several forms of graphite/thermoplastic composites are available in addition to preimpregnated unidirectional tape and fabrics. Co-woven fabrics, which are a hybrid fabric composed of alternating thermoplastic yarns and graphite yarns, and fabrics woven with co-mingled yarns containing graphite and thermoplastic fibers are also available. These latter forms offer a drapable product which can be laid-up over complex shapes and then consolidated by the application of heat and pressure.

A J-stiffener, shown in figure 16, was designed using Celion/PPS co-mingled woven fabric. Configuration details were selected so that stiffeners could be fusion welded to a thermoplastic skin laminate to obtain a stiffened panel. The dimensions and ply layup selected for the stiffener were similar to those described for the graphite/epoxy J-stiffener to permit a direct comparison.

Fabrication

Xerkon was selected as a subcontractor to weave the co-mingled yarn into a fabric and to fabricate the J-stiffeners using their "Autocomp" process. The co-mingled yarn consisted of 34 percent PPS and 66 percent Celion fibers by weight. This yarn was woven into a fabric and then plied and stitched into "C" shaped, "Z" shaped and flat preforms.

22

TABLE 4. – J-STIFFENED PANEL COMPRESSION TESTS

MATL: AS4/1806 FABRIC PANEL WEIGHT: 0.032 LB/IN2
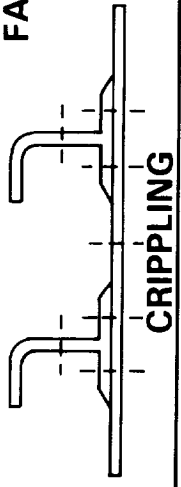
TEST CONFIGURATION	FAILURE LOAD (KIPS)	Nx (LB/IN) Nx$_{ULT}$ = 22000 LB/IN	FAILURE STRAIN (IN/IN)
0.25 DIA FASTENERS CRIPPLING	484.2	34100	0.0064
COLUMN	329.7	27570	0.0045
100 FT–LB POST-IMPACT	524.9	25240	0.0048
60 FT-LB POST-IMPACT	541.3	26020	0.0046
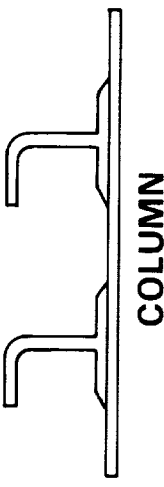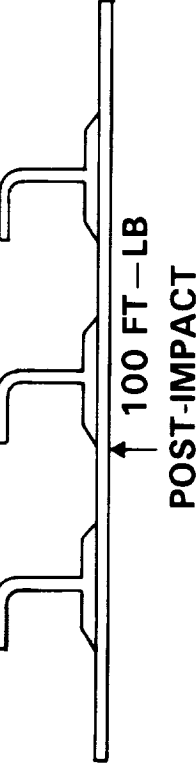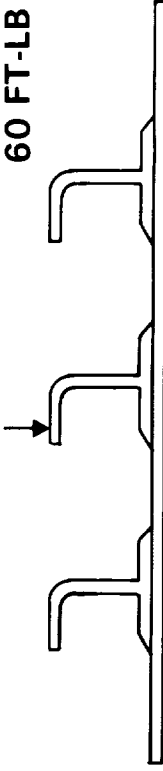
Lockheed

NASA
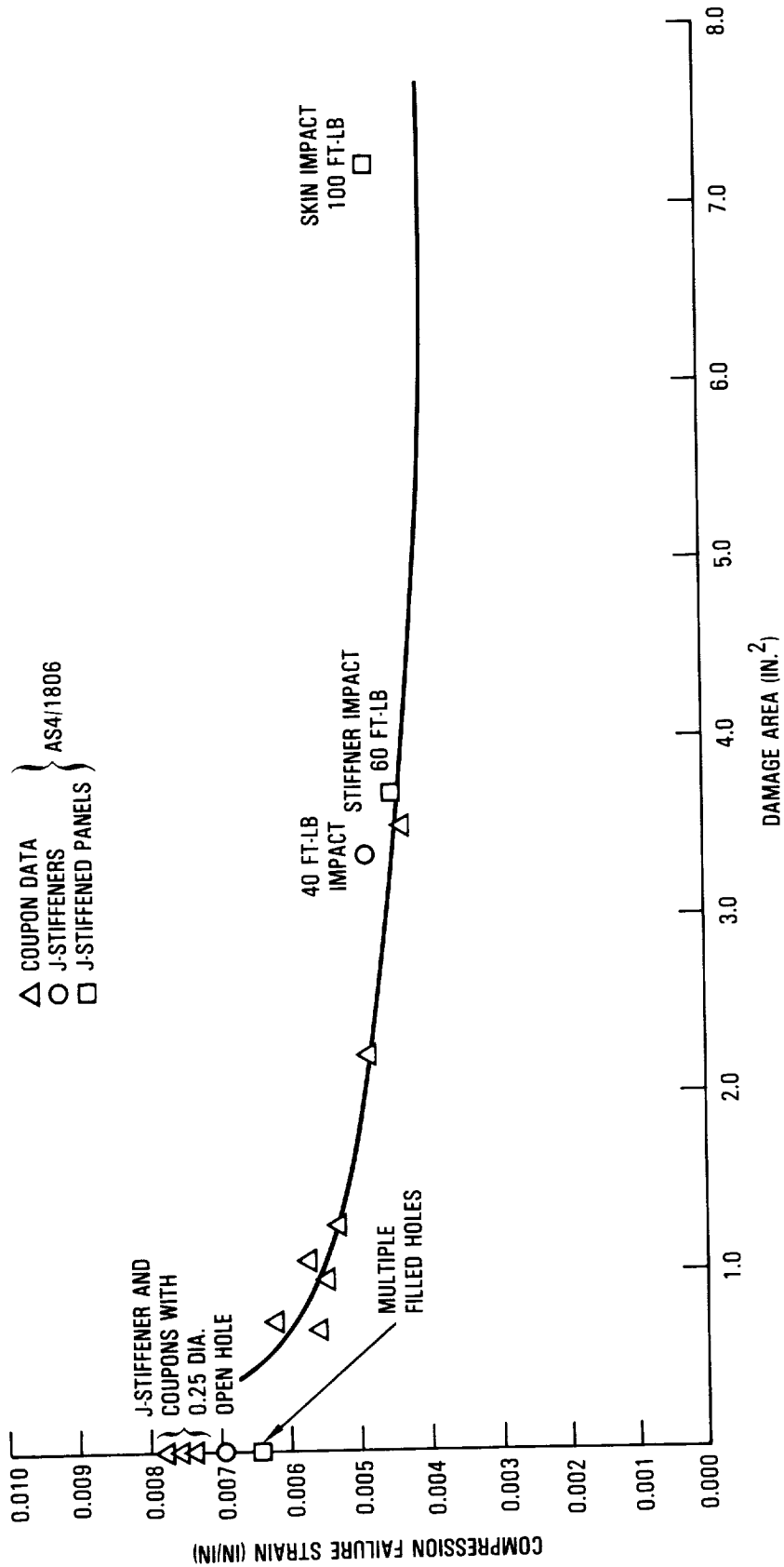
Figure 15. – Comparison of coupon data to J-stiffened panel data.

24

The thickness of the preforms results in a large accumulative compressibility factor. Therefore the "C" and "Z" preforms were preconsolidated in integrally matched steel dies at 630°F and 80 psi. These pieces were then assembled in an integrally heated steel tool and co-consolidated to form the final part. The consolidation cycle was accomplished at a temperature of 630°F at a pressure of 300 psi for one hour. A completed stiffener is shown in Figure 17.

Quality assurance tests conducted on the stiffeners indicated a resin content of 32 percent by weight. Ultrasonic inspections detected a low level of porosity in the parts which was confirmed by photomicrographs. It is hypothesized that the porosity results from the decomposition of the polyester threads used to knit the fabric and preforms. This problem could be eliminated by using a PPS knit thread.

Test

Sections of the J-stiffeners and coupons machined from the web of the stiffeners were tested in compression. Prior to testing a 0.25 inch diameter hole was drilled in the web of the stiffener or in the center of the coupon. Static test results, shown in Table 5, indicated that the predicted stiffness of the laminate was obtained. Failure strains were much lower than anticipated, but are consistent with results obtained by tests on laminates fabricated using preimpregnated unidirectional tape as part of Lockheed funded research program. Scanning electron micrographs of failed laminates indicated poor fiber to matrix adhesion.

BLADE STIFFENED COVER

Design

Upon completion of tests on the AS4/1806 J-stiffened panels and thermoplastic J-stiffeners, a design trade study was conducted to evaluate alternate concepts for the wing box. Two wing box designs were selected for investigation; a two spar configuration with stiffened covers and a multi-spar design with sandwich covers. For these designs a recently developed toughened epoxy, 8551-7, composite containing a high modulus fiber, IM7, was the selected material. Mechanical and physical properties for this material are presented in Table 6.

For the two-spar wing concept a blade-stiffened cover design was selected. Although previous trade studies had indicated that the structural efficiency of a J-stiffened panel was 8 percent greater than a blade-stiffened panel, when the weight of rib to cover clips and fuel sealing clips are included the difference in weight is only 2 percent. Furthermore, producibility analysis indicated that the blade-stiffened panel would be less costly to produce and assemble to the ribs. The covers were sized using a NASA computer code, PASCO, and the cover loads previously reported. Since, tests indicated that the post-impact compression strength of IM7/8551-7 was greater than its 0.25-inch diameter open-hole compression strength, the panel design did not constrain the skin to be a soft laminate with a high percentage
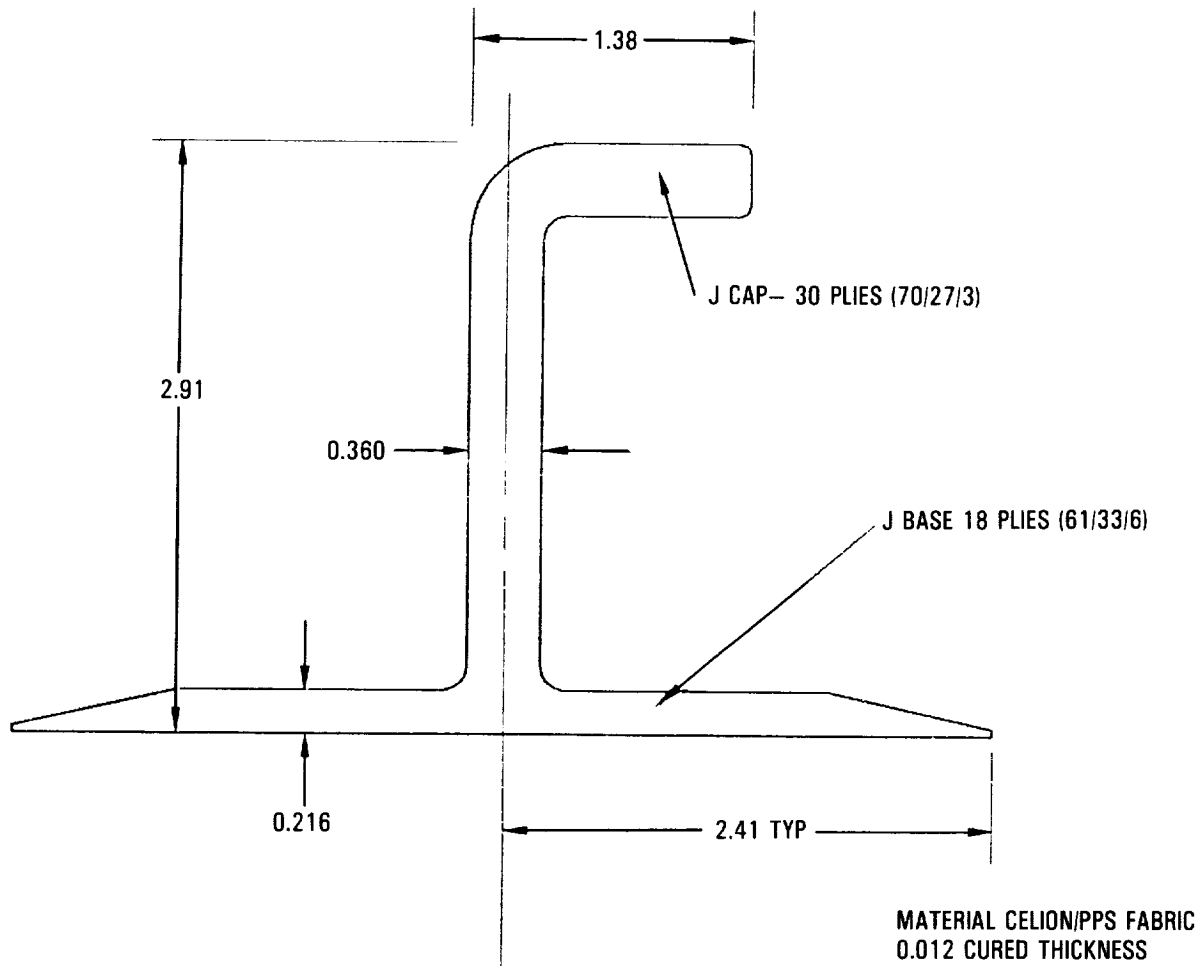
Figure 16. - Thermoplastic J-stiffener designs.

of ±45° plies. The resultant blade-stiffened panel design for the upper cover is shown in figure 18. Note that the panel has been designed as a series of back-to-back channels laid onto a skin laminate. Additional 0°plies are designed into the upstanding legs of the channels to obtain the desired panel bending and inplane stiffness.

For the multi-spar wing box design a unique sandwich construction was selected for the covers. The majority of the material required to obtain the wing box bending strength and stiffness was located integrally in the sandwich directly over the four spars as shown in figure 19. Sandwich cores between the skins were designed for shear stiffness and strength requirements and to react fuel and box crushing pressures. As designed, the cover would be a single piece with the precured spar cap inserts being co-cured to the skins and skin doublers. The smooth inner surfaces would make cover-to-spar and cover-to-rib joints much easier to assemble for fuel sealing and would offer a large cost saving in final assembly.
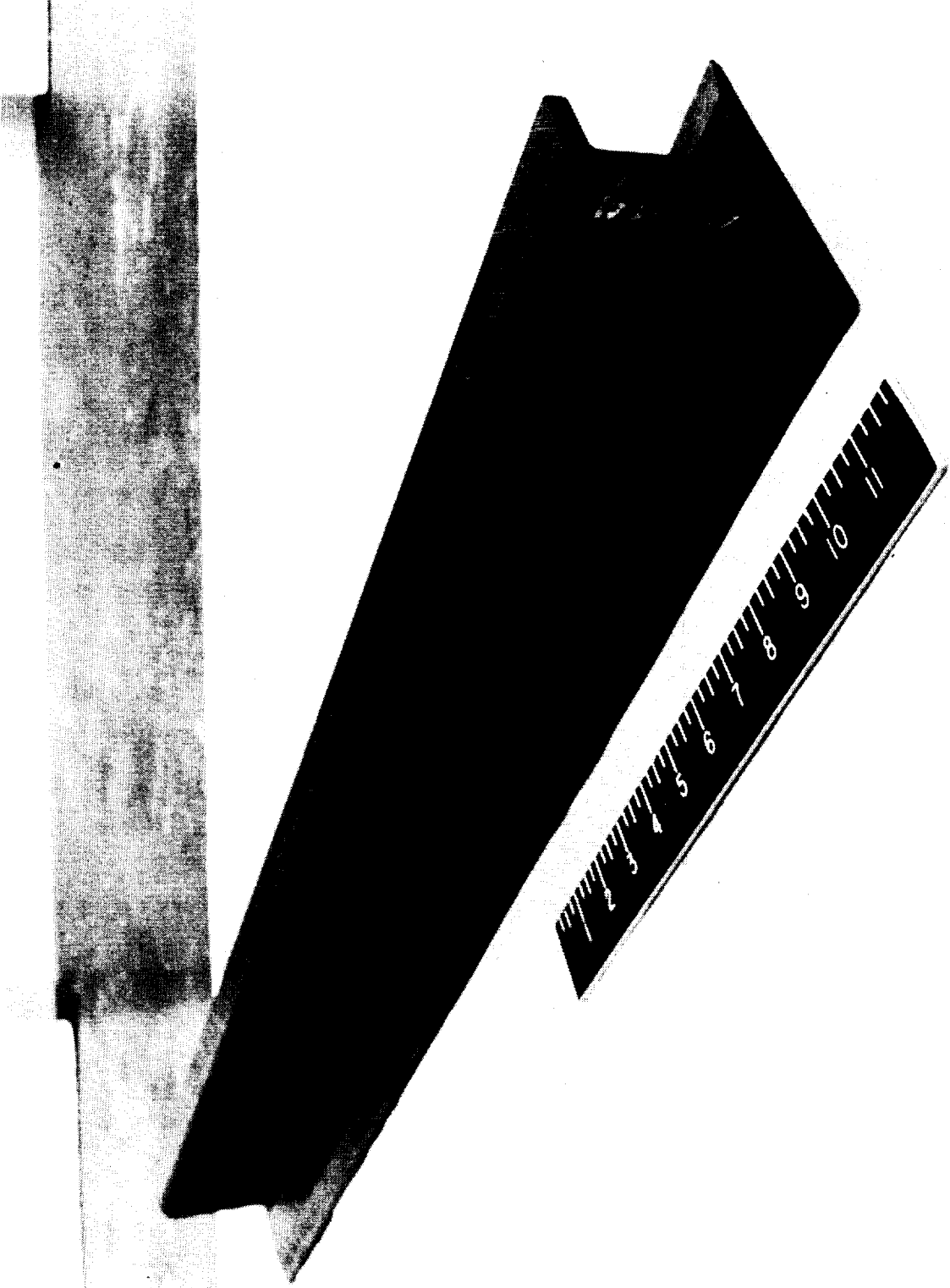
Figure 17. – Thermoplastic J-stiffeners.

TABLE 5.   CO-MINGLED CELION/PPS COMPRESSION DATA

Material Orientation:	
70.0%	0°
26.7%	$\pm45^{\circ}$
3.3%	90°

J-Stiffener Compression (0.25 inch diameter hole in webs)

Coupon ID	Failure Load (kips)	Failure Stress (ksi)	Failure Strain (μin./in.)
C-NJ-1	81.35	45.27	4397
C-NJ-2	87.33	47.05	4265
C-NJ-3	93.81	51.77	5228
AVG		48.03	4630

Notched (0.25 inch diameter hole) Compression on Coupons From Stiffener Webs

Coupon ID	Failure Load (kips)	Failure Stress (ksi)	Failure Strain (μin./in.)	Initial Modulus (msi)
C-5N-1	27.69	50.92	4377	11.68
C-5N-2	28.35	52.85	4488	11.84
C-5N-3	27.50	49.99	4193	11.67
C-5N-4	26.54	48.58	4088	11.75
C-5N-5	26.92	49.28	4271	11.82
AVG		50.32	4283	11.75

Preliminary design and analysis was completed for each wing box concept. This included the covers, ribs, spars, large acess hole reinforcements as well as the wing joints. Weight and production cost estimates were then made for each configuration. The cost figures reflect the use of IM7/8551-7 material and automated manufacturing techniques. Table 7 summarizes the results of these analyses and compares them to the baseline advanced aluminum wing box. Detailed weight comparisons are presented in Table 8. As a result of these investigations, it was decided to fabricate and test blade-stiffened panels constructed with IM7/8551-7 unidirectional tape. Evaluations of the sandwich design were made as part of a Lockheed funded research program.

TABLE 6. - IM7/8551-7 DESIGN PROPERTIES

Property	Unidirectional Tape
Resin Content by Weight (%)	32 + 3
Density (lb/in.^{3})	0.057
Nominal Thickness (in.)	0.0054
0°Tensile Modulus (msi)	21.9
0°Compression Modulus (msi)	20.9
90°Modulus (msi)	1.5
Poisson's Ratio	0.30
0°Inplane Shear Modulus (msi)	0.80
Tension Design Strain (10^{-6} in./in.) -65°F, Dry	5500
Compression Design Strain (10^{-6} in./in.) 180°F, Wet	5000

A detailed design and analysis was completed for a blade stiffened panel located at the most highly loaded station on the wing upper surface. Loads used for this analysis were the same as those used to design the J-stiffened test panel. The resultant design is shown in figure 20.

Fabrication

The blade-stiffened panel was composed of three elements: skin, C-channel and fillet. All of these elements were hand laid up of IM7/8551-7 unidirectional tape on aluminum templates. Skins were laid up, vacuum debulked, and freezer stored pending assembly. C-channels are laid up flat, four to six plies at a time. This ply stack was transferred to a male form block and pin-aligned, maintaining 0° fiber orientation relative to the long axis of the block. The form block and ply stack was bagged and partial vacuum was applied, forcing the ply stack to slowly deform into a C-channel shape. Full vacuum was applied and the formed ply stack was vacuum consolidated at room temperature. This process was repeated until the C-channel preform was completed. The debulked C-channel laminate was removed and placed in freezer storage.
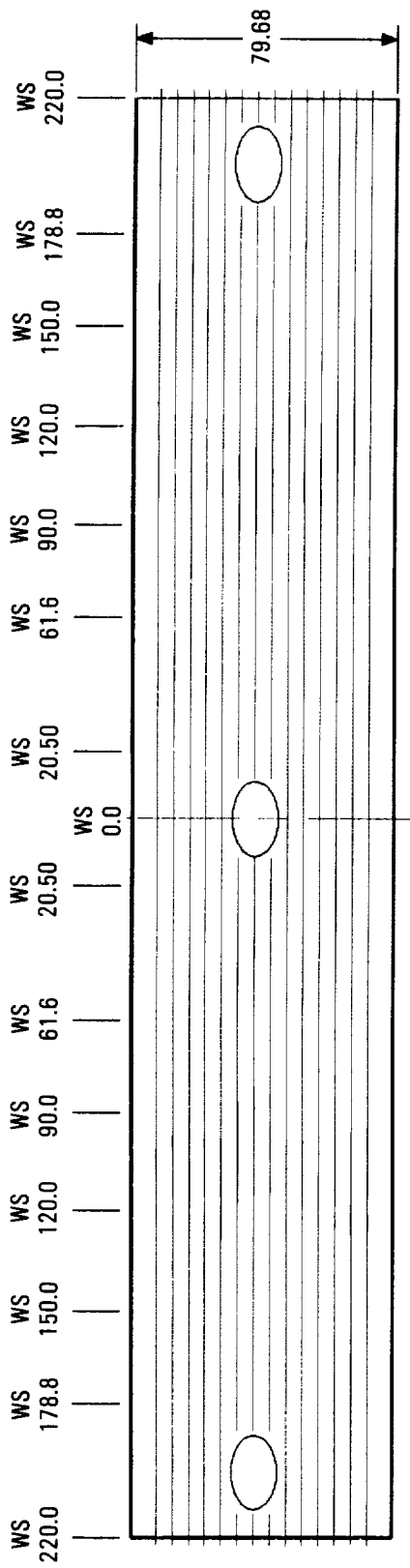
PLANFORM OF UPPER COVER

LAYER OF ADHESIVE
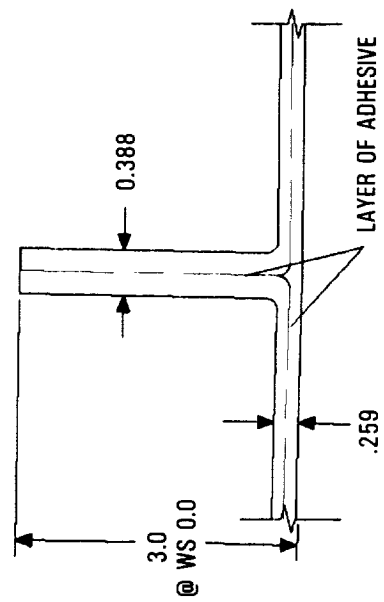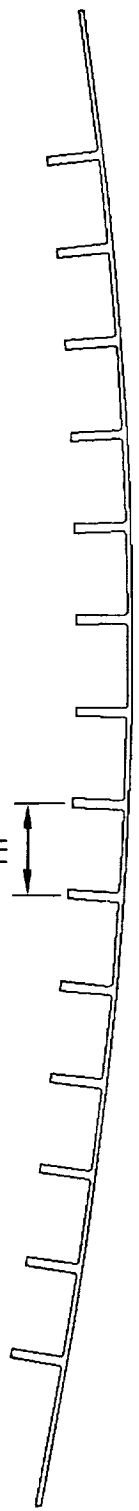
CROSS SECTION

Figure 18. – Blade-stiffened upper cover design.

30
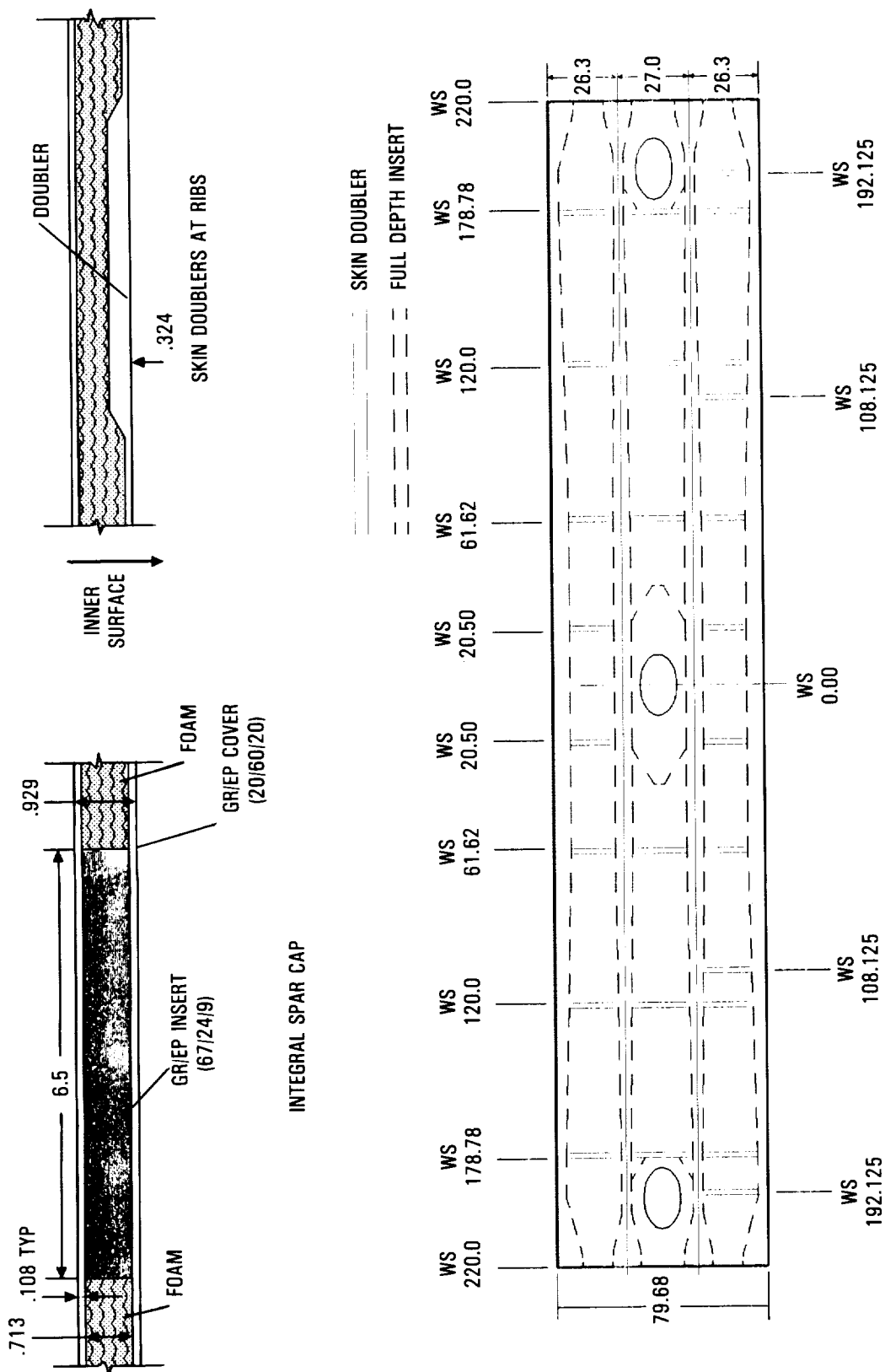
Figure 19. - Sandwich upper cover design.

31

TABLE 7. – SUMMARY OF WING BOX DESIGN TRADES
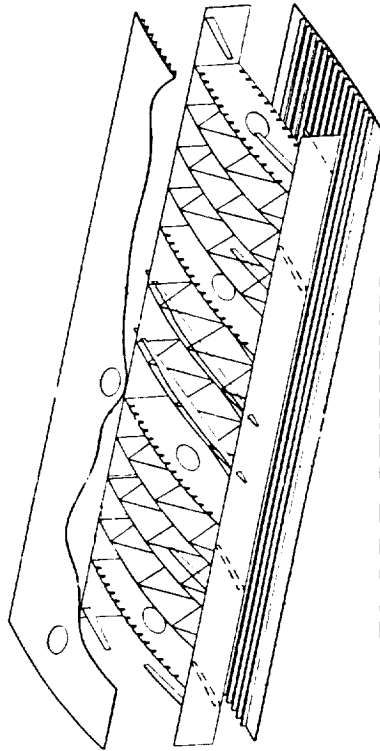
SANDWICH

BLADE STIFFENED
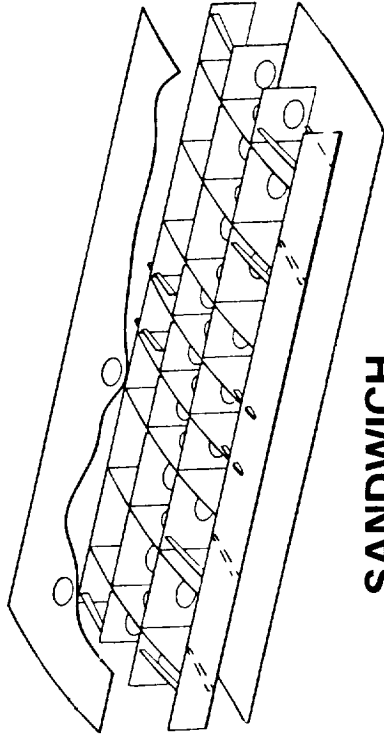
	BASELINE	SANDWICH	BLADE
WEIGHT	100%	76%	71%
COST	100%	114%	94%
MATERIALS	12.7%	35%	55%
LABOR	87.3%	65%	45%

TABLE 8. WING BOX WEIGHT COMPARISON

ITEM	AL BASELINE	TARGET	COMPOSITE	
			MULTI-SPAR (SANDWICH)	MULTI-RIB (BLADE STIF)
COVERS	3872	2672	2458	2434
SPARS	942	683	951	551
RIBS	608	464	307	533
FASTENERS/ETC.	235	203	273	206
WS 220.0 JOINT (1)	183	143	191	176
LIGHTNING PROTECTION	0	38	38	38
GROWTH	0	223	223	223
TOTAL	5845	4388	4441	4161
PERCENTAGE SAVINGS		25%	24%	29%

(1) PRODUCTION JOINT OR MAJOR WING JOINT

BLADE 72 PLIES (61/33/6)

FIBERGLASS 2 PLIES 100/0/0

SKIN 24 PLIES (42/50/8)

MATERIAL IM7/8551-7 TAPE
0.0054 CURED THICKNESS

4.95

0.428

2.82

0.259
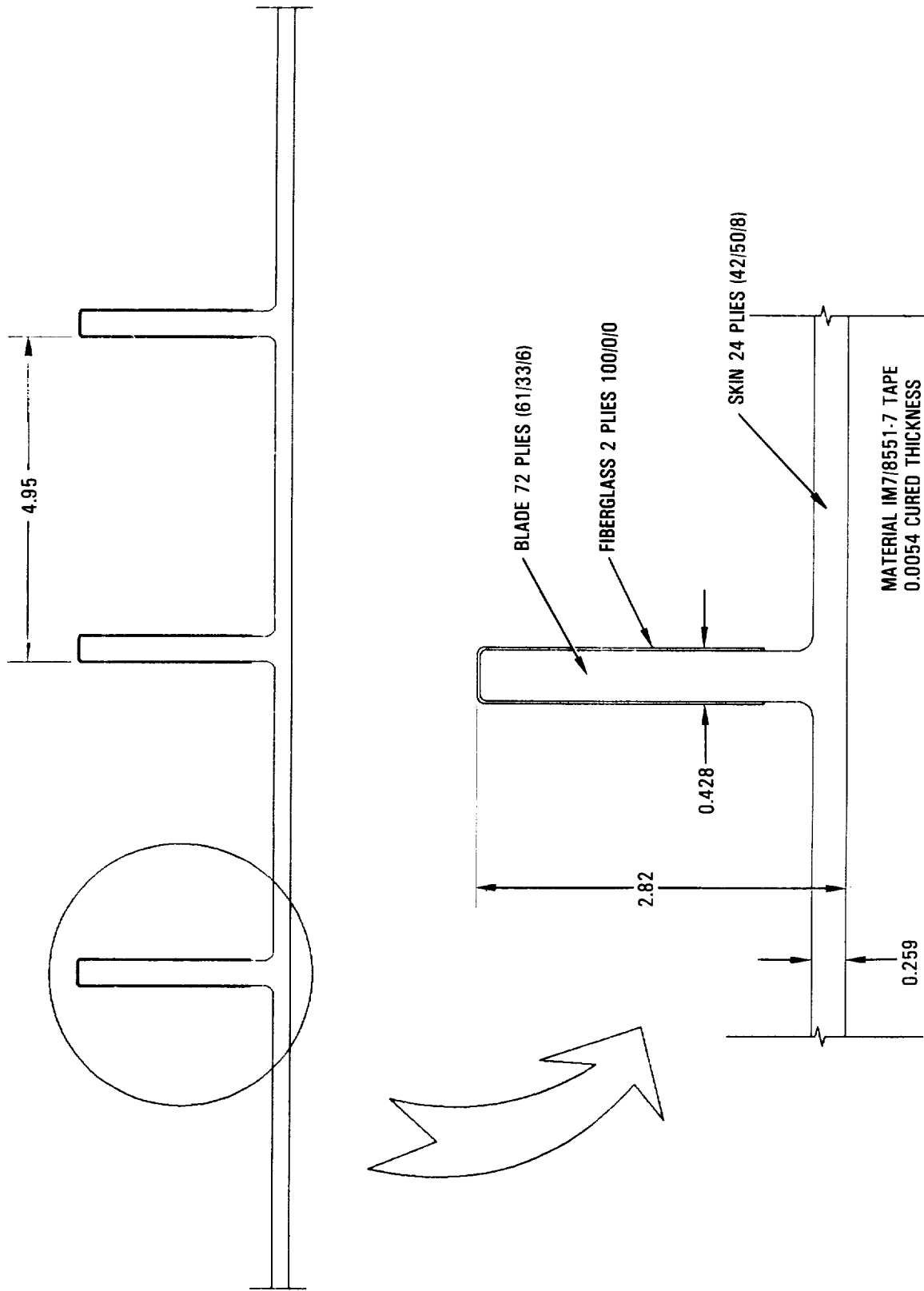
Figure 20. – Blade-stiffened panel design.

Fillets were fabricated by cutting a specific width of prepreg tape the length of the panel. This width was established by empirical tests to determine the amount of material required to fill the C-channel/skin intersection. The tape was hand rolled as tightly as possible to form a cylinder of $0°$ fibers. This preform was then packed into a closed mold, envelope bagged and vacuum consolidated in a $150°F$ oven. The preconsolidated fillet was removed from the mold and placed in freezer storage.

The blade-stiffened panel was tooled on the inner or blade side. Silicone rubber covered, hollow aluminum blocks were arranged on an aluminum plate to provide the required blade height and spacing. One block was fixed to the plate; the other blocks were designed to slide toward the fixed block under autoclave pressure. Mechanical stops were located between blocks to ensure that blades were straight and of a uniform cross-section. Autoclave pressure was augmented by silicone rubber expansion during blade consolidation.

The assembly began by placing uncured graphite/epoxy C-channel preforms over each block segment, shown in figure 21, three to four inches apart on the tool plate. Sliding blocks, with preforms in place, were moved into contact with the fixed block, sequentially. Toe-clamps located along the two long sides of the assembly maintained position and alignment. Shown in figure 22, preformed fillets were placed at each channel intersection and the assembly was covered with a precompacted skin and caul plate, see figure 23. Silicone rubber bag ramps covered the toe-clamps and transmitted autoclave pressure to consolidate the blades, while the skin and channel webs were consolidated by autoclave pressure alone. The entire assembly was covered with a nylon vacuum bag and cured in an autoclave.

Figure 24 shows a panel after removal from the tool. Ater removal the panels were ultrasonically inspected and the blades were machined to the proper height. Fiberglass overwraps were then applied to the blades and cured to complete the panel fabrication.

Test

Tests conducted on the blade-stiffened panels were identical to those done on the J-stiffened panels discussed previously, namely trial impacts and compression tests on notched or impacted panels. This methodology was selected to permit a direct comparison of the test results.

A two bladed panel was impacted at various locations and impact energies with a 12-pound-steel impactor having a 1.0-inch-diameter-hemispherical tup. Prior to being impacted, the panel was clamped to a rigid foundation to represent an area near a rib. After being impacted, the panel was visually and ultrasonically inspected and the dent depths at point of impact were measured. All of the impact locations displayed visual damage. A summary of the inspection results is presented in Table 9. Based on the results of these tests, a 100 ft-lb impact energy was selected for the skin impacts and a 40 ft-lb impact energy was selected for the blade impacts on the compression test panels.
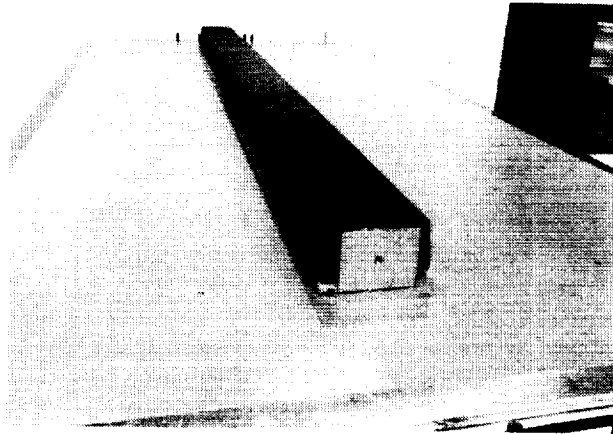
Figure 21.   Layup of channel section.
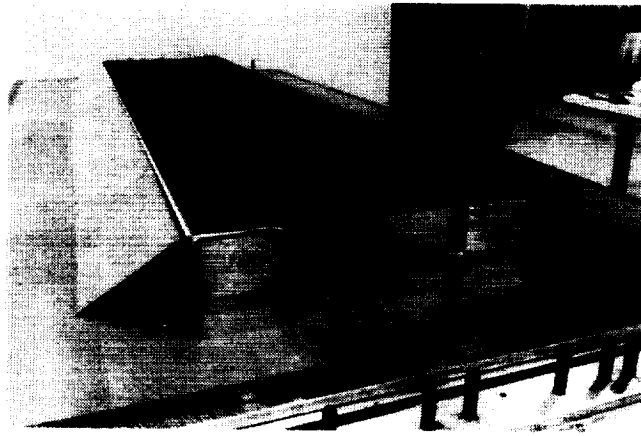
Figure 22.   Channel sections assembled in tool.
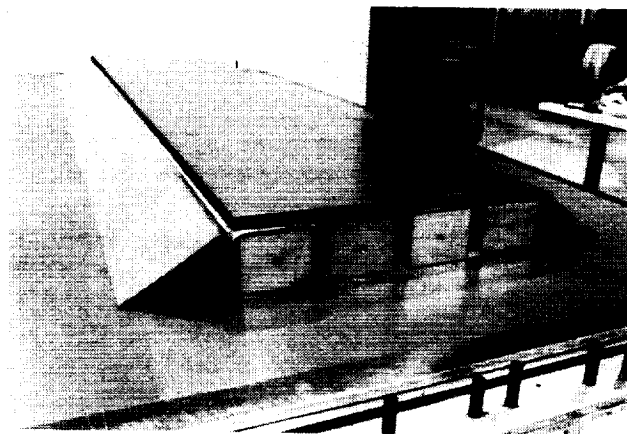
Figure 23.   Tool with GR/EP parts just prior to bagging.

Figure 24. - Blade-stiffened panel.

37

TABLE 9. - TRIAL IMPACT DATA
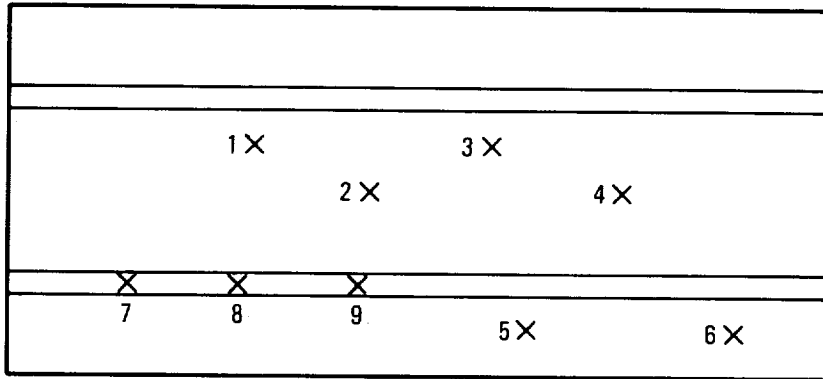
IMPACT LOCATIONS

Location	Energy	Damage Area	Dent Depth
1	80 ft-lb	5.4 in^2	.025 in.
2	80 ft-lb	3.1 in^2	.018 in.
3	100 ft-lb	5.75 in^2	.022 in.
4	100 ft-lb	3.6 in^2	.014 in.
5	80 ft-lb	3.1 in^2	.012 in.
6	100 ft-lb	5.75 in^2	.064 in.
7	20 ft-lb	N/A [1]	N/A [1]
8	40 ft-lb	N/A [1]	N/A [1]
9	60 ft-lb	N/A [1]	N/A [1]

[1] The fiberglass wrap around blade made accurate measurements difficult.

Several areas on the trial impact panel were selected for micrographic examinations. Specimens were cut, polished and photomicrographed for detailed inspections. Figure 25 shows the internal damage to the panel caused by a 100 ft-lb impact to the skin within 0.50 inch of the blade. Note that the delaminations within the skin laminate are arrested at the base of the blade as was indicated by ultrasonic inspections. In addition to the numerous delaminations and translaminar cracks caused by the impact, the micrograph reveals extensive ply fractures near the base of the blade. The unimpacted compression strength of the cover design was determined by testing a 24.0 inch long panel with two stiffeners. Prior to testing, 0.25 inch fasteners were installed in the skin and stiffeners to duplicate the effect of panel-to-rib cap attachments. The loaded ends of the panel were potted, the side support rails were installed and the panel was mounted in the test machine. The applied compression load at failure was 282,100 pounds with an average strain of 5200 μ in./in. The load-strain plots were linear to failure indicating no buckling. Failure occurred through the simulated rib attachment holes in the middle of the panel.

A second two-bladed panel was tested after being impacted on the skin midway between the blades at 100 ft-lb. The damage is shown in Figure 26. Ultrasonic inspections of the panel indicated that the delaminations arrested at the blades with a total damage area of 5.25 in^2. Upon compression loading, this panel failed catastrophically at a load of 211,800 pounds and an average strain of 3600 in./in. The two bladed panel configuration used for this test is probably not representative because the impact caused damage to greater than 50 percent of the panel width. A four-blade panel would probably have resulted in a greater failure strain and more representative results.

Two panels, 15.85 inches wide, containing three blades, were tested to determine the effect of impacts to the skin at the base of the blade and to the top of the blade. The first panel was impacted at 100 ft-lb on the skin at the base of the blade. This panel failed at a load of 373,000 pounds and an average strain of 4600 μin./in. Figure 27 shows this panel after failure. The second panel, which had a 40 ft-lb impact to the top of the central blade, failed at a load of 361,200 pounds and an average strain of 4400 μin./in. Both panels failed catastrophically through the impact damaged areas. All load-strain curves were linear to failure. The panel axial stiffness, 83.3 x 10^6 lb verified predicted results.

For comparison purposes, an identical three-bladed panel was manufactured using AS4/2220 material. This panel was impacted at 100 ft-lb on the skin near the base of the blade. Ultrasonic inspections indicated a damage area of 8.0 in^2, much greater than obtained for similar impacts on the IM7/8551-7 panels. This panel was compression tested and failed at a load of 256,000 pounds and an average strain of 3500 μin./in. This is 1000 μin./in. less than the same test on the IM7/8551-7 blade-stiffened panel.

A summary of the results obtained from the blade-stiffened panel tests is presented in Table 10. All of the impacted panels failed at a strain much lower than the anticipated value of 5000 μin./in. As a part of a Lockheed funded research program, extensive tests were conducted on IM7/8551-7 laminates having a variety of orientations. Results of these tests indicated

Figure 25. - Photomicrograph of impact to skin near blade.
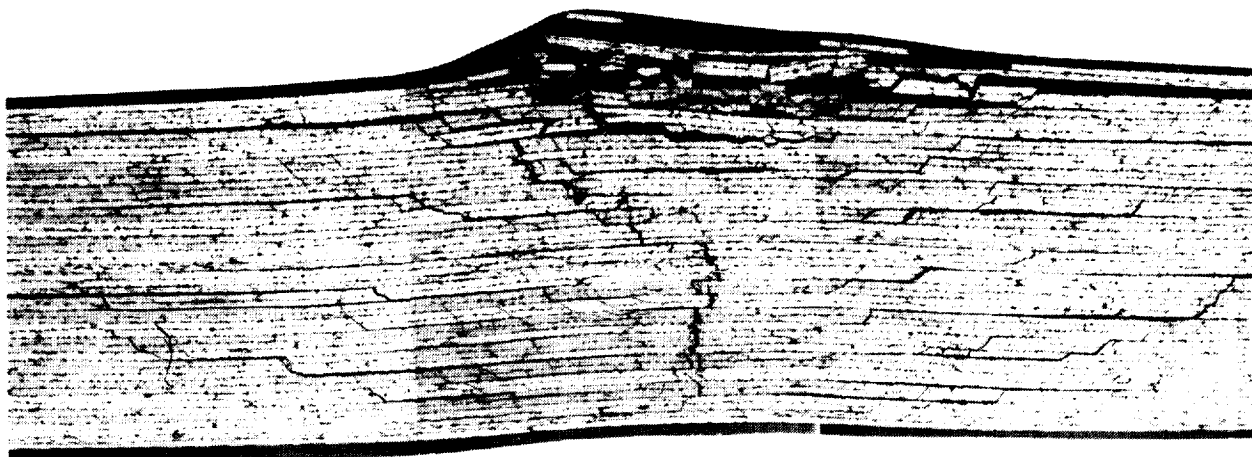
Figure 26. - Photomicrograph of impact to skin between blades.

Figure 27. - Failed blade-stiffened panel.

41

that the failure strain of either impacted laminates or coupons containing an open hole decreased with increasing percentages of 0 degree material within the laminate. Panel test results are compared to coupon data in figure 28. Based on these data, it is concluded that the compression design strain value of 5000 μin./in., which was selected for the blade stiffened panels, was too high. A more appropriate value would have been 4000 μin./in.

Even though coupon test data comparisons indicate that IM7/8551-7 laminates have superior post-impact compression strength to AS4/1806 laminate, the IM7/8551-7 blade stiffened panels failed at slightly lower strains than did the AS4/1806 J-stiffened panels. The principal reason for the difference in performance is attributed to the fact that the blade stiffened panel had a skin which contained a high percentage of 0° material. The J-stiffened panel was a "soft skin" design having a low percentage of 0° plies in the skin. As these test indicate, impact damage tolerance is improved by employing a "soft skin" design concept for stiffened panels even though this may not be the optimum design for compression stability considerations.

TABLE 10. BLADE-STIFFENED PANEL COMPRESSION TESTS MATL:IM7/8551-7
PANEL WEIGHT: 0.027 lb/in^2
FPH
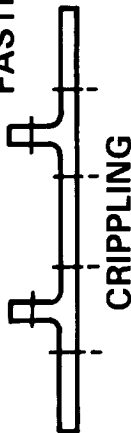
TEST CONFIGURATION	FAILURE LOAD (KIPS)	Nx (LB/IN) NxULT = 22,000 LB/IN	FAILURE STRAIN (IN/IN)
0.25 DIA FASTENERS CRIPPLING	282.1	25,880	0.0052
POST-IMPACT ↑ 100 FT-LB	211.8	19,430	0.0036
POST-IMPACT ↑ 100 FT-LB	373.2	23,550	0.0046
40 FT-LB POST-IMPACT	361.2	22,790	0.0044
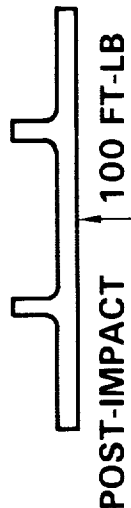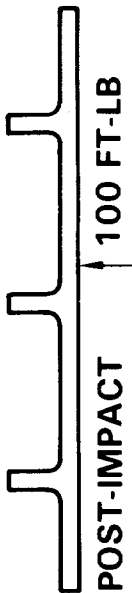
43
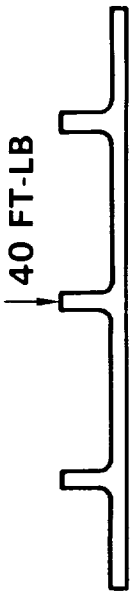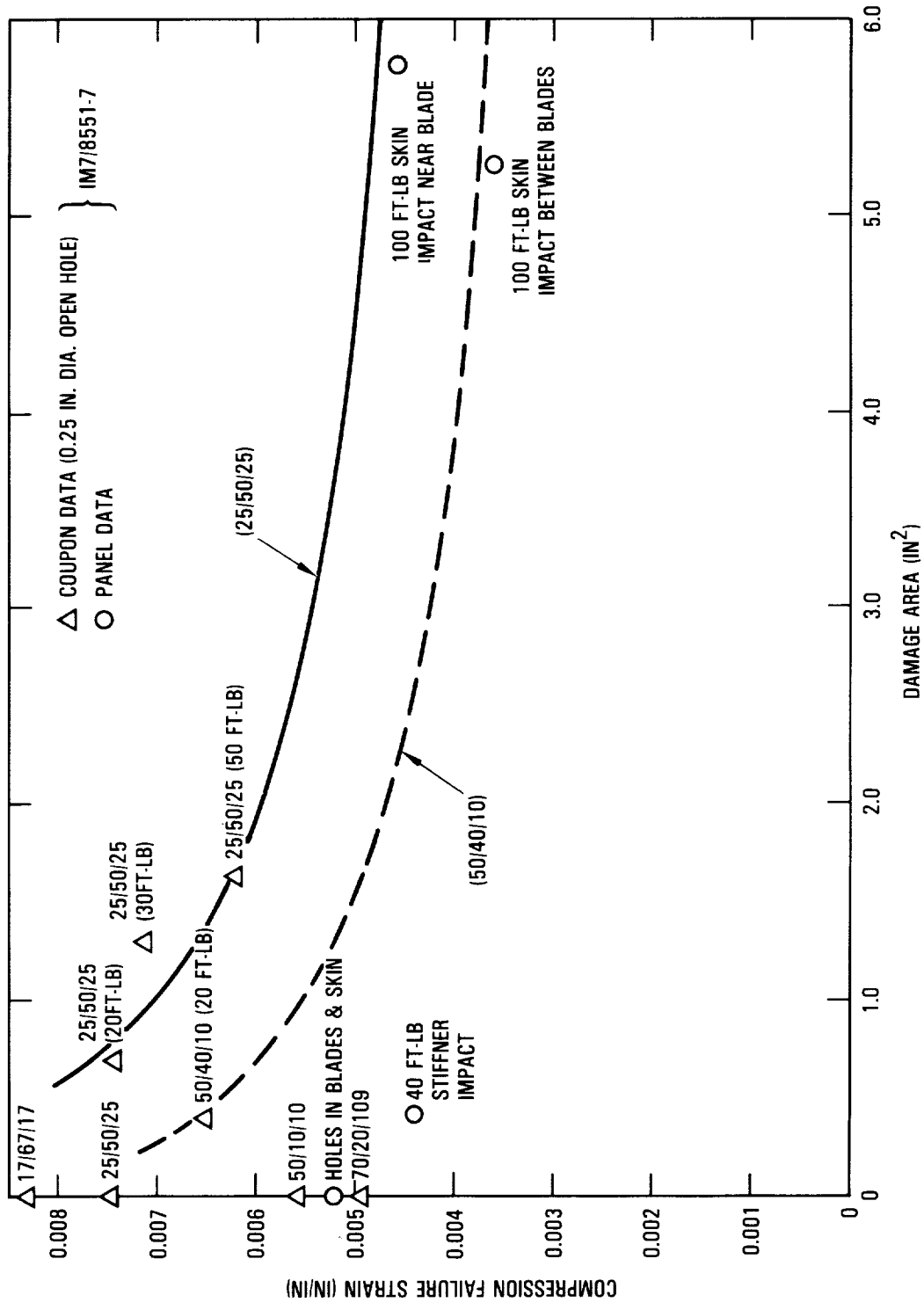
Figure 28. — Comparison of coupon data to blade-stiffened panel data.

SPAR DEVELOPMENT

Spar Design Criteria

Geometry

In early studies on composite transport wing spars a stiffened-web, solid-laminate, C-channel spar configuration was identified as the most appropriate choice for meeting program cost, weight, structural integrity, durability, and damage tolerance goals. The configuration is amenable to filament winding or standard hand layup techniques. Stiffeners can be co-cured, co-bonded, or separately attached as dictated by manufacturing efficiencies and costs. Accurate analysis procedures have been developed to predict structural performance. The selected structural configuration is illustrated in figure 29.

With minor variations the C-configuration is adaptable to a wide spectrum of·materials and manufacturing processes. In this program, four separate spars were designed, fabricated, and tested to allow direct structural performance comparisons. The four spar concepts evaluated were:
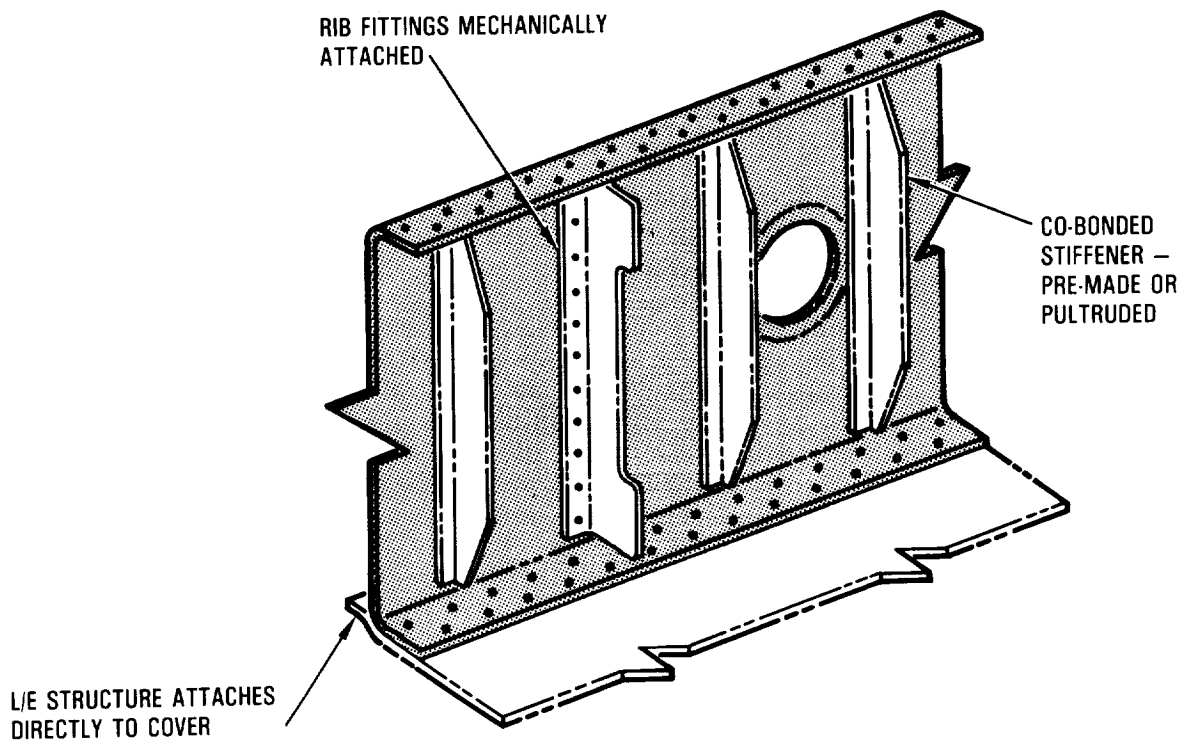
Figure 29. - Stiffened channel spar concept.

45

(1) A "baseline" spar -- hand laid up of AS4/1806 knit and woven fabric prepregs.

(2) A "thermoplastic" spar -- incorporating combinations of roll-forming and hand layup with AS4/PEEK.

(3) A "filament-wound" spar -- of baseline material in towpreg form.

(4) A "postbuckled" spar -- of baseline material and layup but designed to allow the spar web to buckle below ultimate load.

One spar bending test specimen and two shear panel test specimens were produced for each of the designs and statically tested to failure. Details of these test specimens are shown in figure 30, and a discussion of individual specimen design, fabrication, and testing is included in subsequent sections of this report.

Spar Design Loads

As a basis for structural design, Lockheed used wing loads and criteria developed for an advanced military transport aircraft to meet requirements anticipated for the early 1990s. External design loads, compatible with the advanced transport's planned usage were generated for an array of flight and landing conditions. These external loads were then applied to a NASTRAN model representative of this aircraft's complete wing to generate applicable element internal loads. Figure 31 is an envelope plot of the internal shear flows common to the front and rear spars, which were generated from this analysis. In this figure, the maximum shear flow occurs near Wing Station 61, which is the spar-to-fuselage attachment location. The maximum shear flow at this location is above 4600 lb/in. This shear flow was established and used as the design load level for the comparative spar components. These spars were sized to provide minimum margins compatible with static and damage tolerance criteria established for the complete wing. All of the spar test components were dimensionally the same height (14 inches) and same length (63 inches). Because the component height was half that of the full wing component; the shear flow was achieved by using an appropriate applied shear load. The strain levels in the spar caps were controlled to the desired strain level by using simulated wing covers mechanically attached. The attachment was representative of a typical full-scale spar cap-to-wing cover joint.

Baseline Spar

Design

The design concept for the baseline spar is the stiffened channel configuration. The spar web, which has stiffeners located on 10 inch centers, is designed to be buckling resistant, while spar caps are configured to

SPAR
BENDING
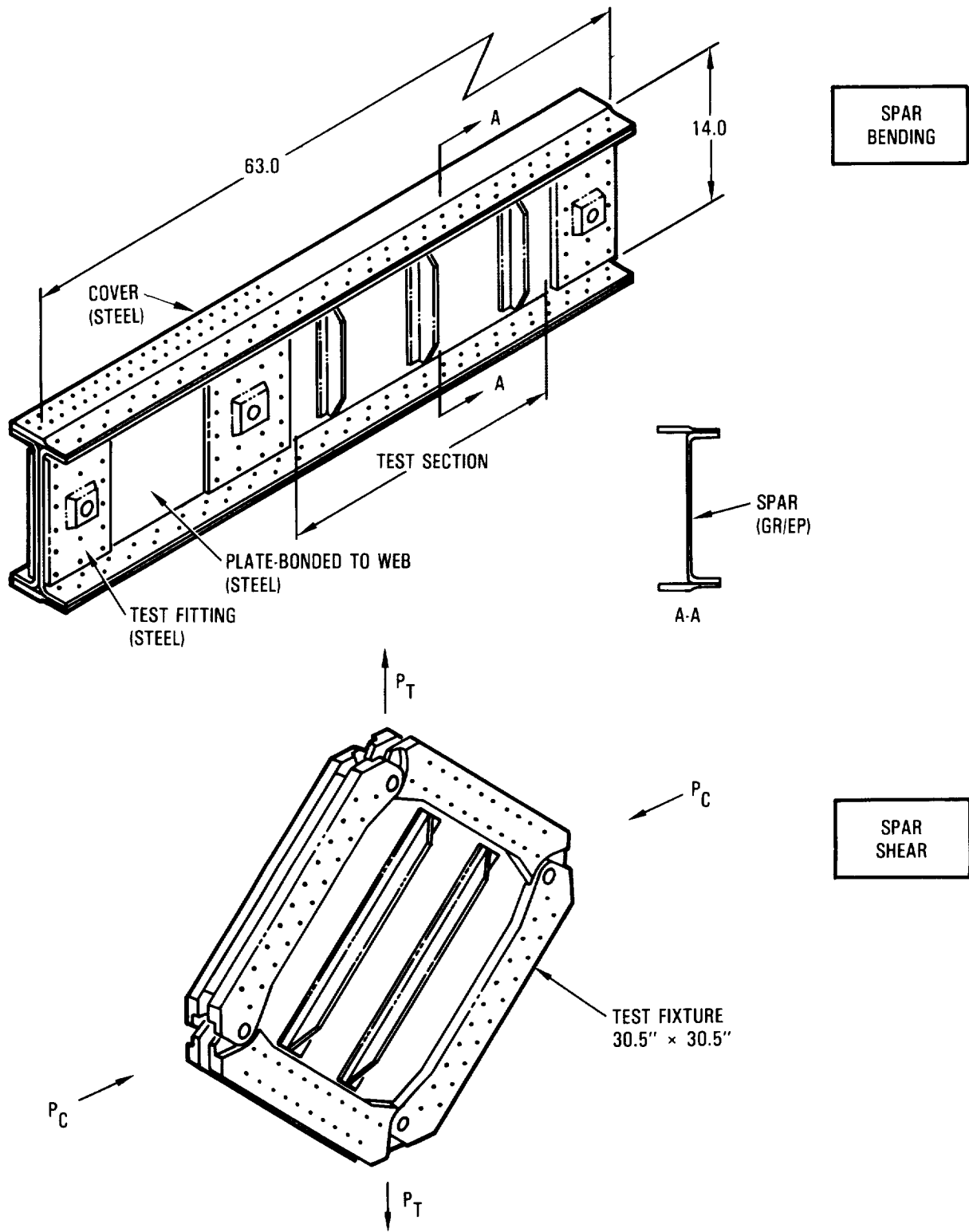
SPAR
SHEAR

Figure 30. – Spar test specimens.
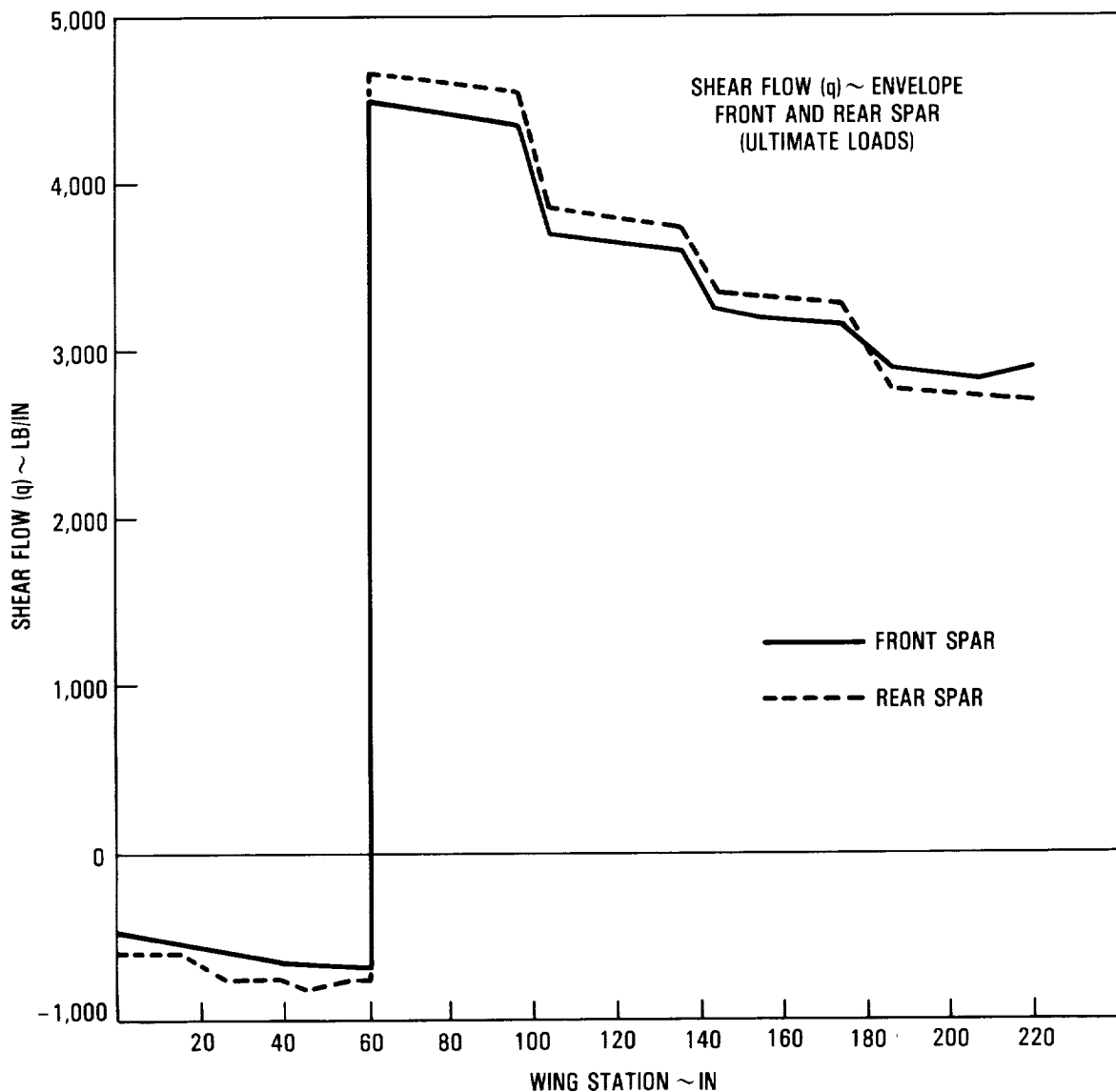
Figure 31. - Shear flow envelope - NASTRAN internal loads.

operate at strain levels equal to those in the covers. Typical ply layups in the spar cap, web, and stiffeners are illustrated in figure 32. Spar bending and shear panel test specimens of this concept were designed utilizing woven and knitted forms of AS4/1806 material.

To guarantee failure of the spar bending test specimen in the test area, all non-test areas were substantially reinforced. Steel doublers, approximately 0.15 inch thick, were bonded to the spar web in these areas, and reusable steel fittings were mechanically attached at the three load introduction points. Steel straps, simulating upper and lower covers, were attached to the spar caps to provide representative loading conditions.

48

UNIDIRECTIONAL
TAPE

0.312 (26 PLIES)
(38%0°/46%±45°/16%90°)

0.12 R

0.216 (18 PLIES)
(17%0°/66%±45%°/17%90°)

MATERIAL: AS4/1806
PREPREG FABRIC (0.012/PLY)

CAP AND WEB

0.216 (18 PLIES)
(44%0°/44%±45°/12%90°)

UNIDIRECTIONAL
TAPE

0.12R

STIFFENER
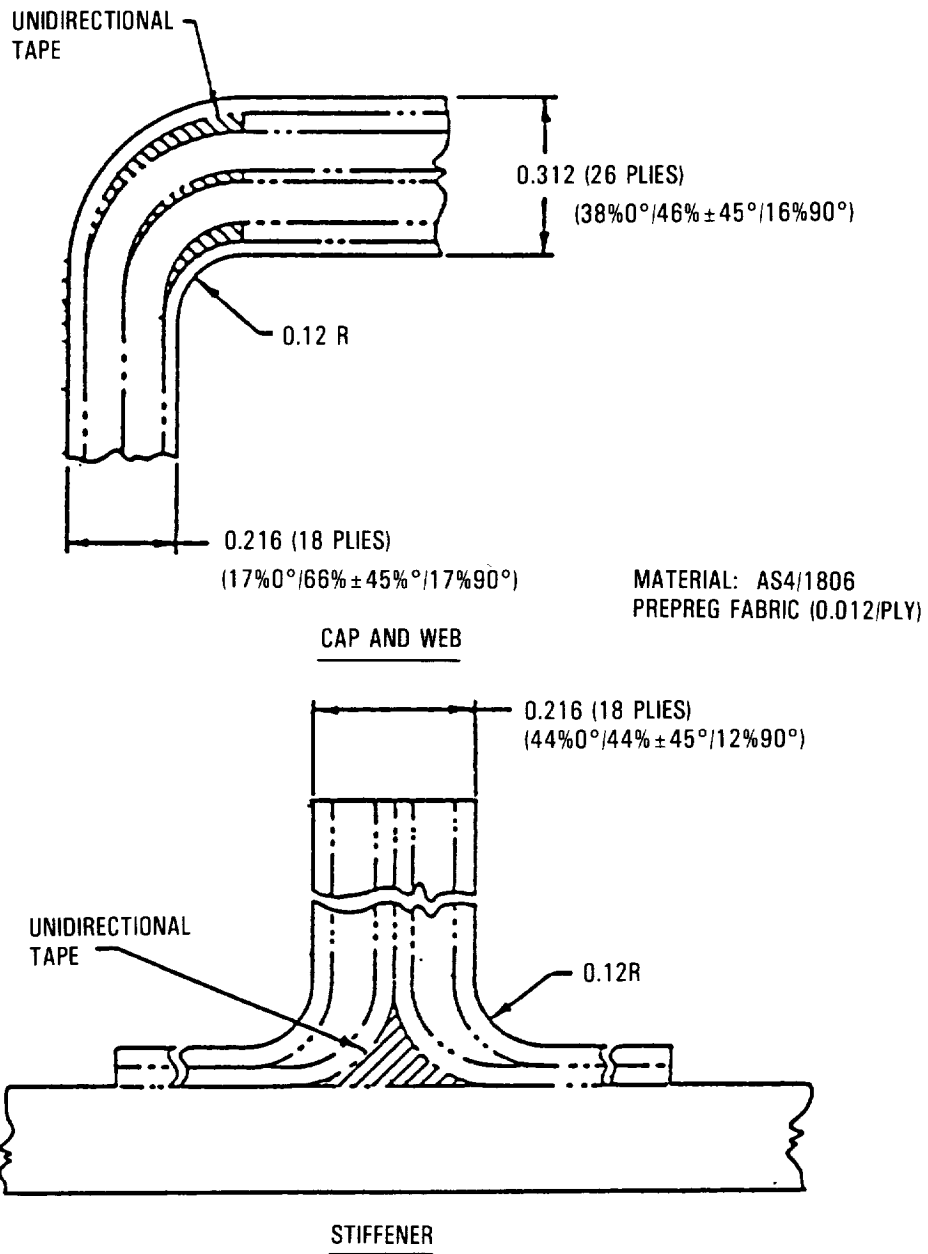
Figure 32. – Baseline design ply layup.

Local reinforcing steel doublers were also utilized on the shear panel test specimens, to improve the test specimen's bearing capability when bolted to the picture frame test fixture.

Fabrication

A development spar tool built with independent funds was modified and used to fabricate the baseline spar test specimen. The basic tool is a female tool, with graphite/epoxy slip sheets adjacent to the composite spar. Side rails, pinned to the graphite base, support the caps and minimize thermal incompatibility. Standard bagging and autoclave preparation were employed before applying heat and pressure to cure the spar.

The modified tool concept is illustrated in figure 33. Modifications included a change in web height from 28 inches to 14 inches, an airpad caul sheet, and side rail pins. The change in web height provided a realistic height-to-width ratio for the test section. The airpad caul sheet was to provide better compaction in the cap-to-web radius during the autoclave cure. The aluminum side rails were undercut and pinned to the graphite slip sheet to minimize the effect of thermal expansion against the spar cap flanges. The graphite/aluminum base of the spar tool was also used to fabricate the baseline spar shear panels. The blade stiffeners for both the baseline specimens were fabricated on a shop-aid tool, illustrated in figure 34.

All baseline specimens were laid up by hand using AS4/1806 fabric and knit prepreg. On these, and all other test components, in-process quality approvals were documented at specified points in the manufacturing paperwork. After autoclave cure and subsequent bonding cycles, 100 percent ultrasonic inspections were conducted before proceeding to the next manufacturing step.

The graphite/epoxy stiffeners and the steel load introduction plates were bonded simultaneously to the composite spar with a $350^{\circ}F$ epoxy adhesive. Ultrasonic inspection revealed some disbonds at stiffener ends and along the longitudinal edges of the load introduction plates. Fasteners were installed along the edges of the plates and at the ends of each stiffener. Inspection also revealed some warpage in the spar web due to the mismatch in the thermal expansion between the graphite/epoxy spar and the steel backup channel. A drawing change was initiated to allow using a room temperature curing adhesive to bond the metal details on subsequent test articles.

Stiffeners were bonded to the baseline spar shear panels with a $350^{\circ}F$ curing adhesive. After ultrasonic inspection acceptance, steel load introduction plates were room-temperature bonded along the periphery of the shear panels to complete the assemblies.

The spar test specimens are shown in figures 35 and 36 just before the final step in assembling test hardware.

50

AIR PAD
CAUL SHEET

PART   SLIP SHEET

ALUM SIDE RAIL

GRAPHITE
SLIP SHEET

ALUM BASE

MOLDED RUBBER   SIDE RAIL
RADIUS FILLET   LOCATING PIN
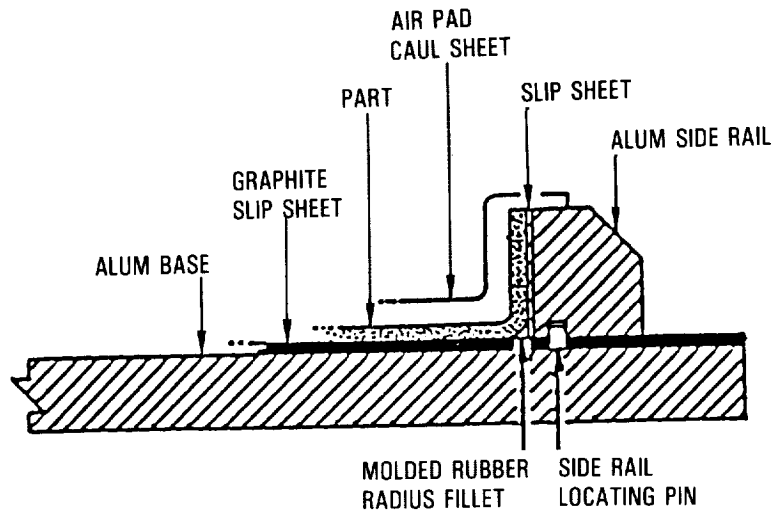
Figure 33. - Baseline spar tool concept.

ALUM CAUL SHEET

ALUM FORM BLOCK

EDGE DAM

TOOL PLATE

PART
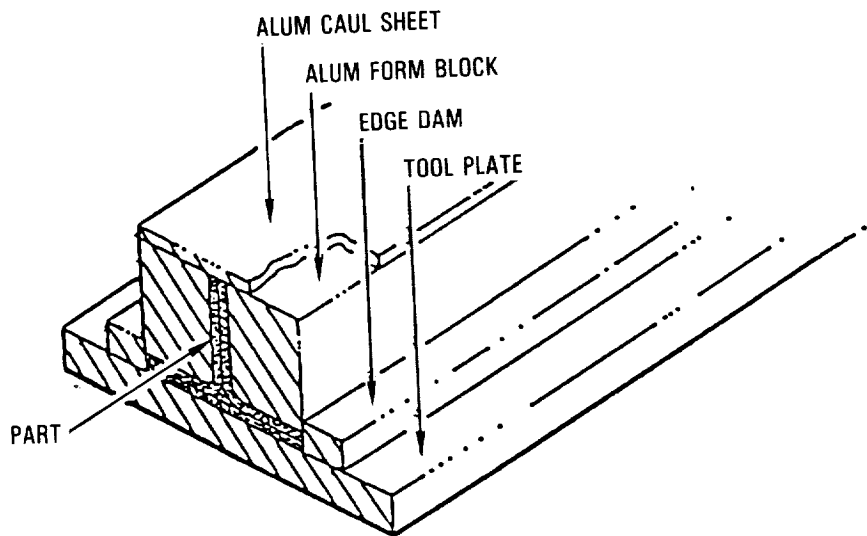
Figure 34. - Shop-aid stiffener tool.
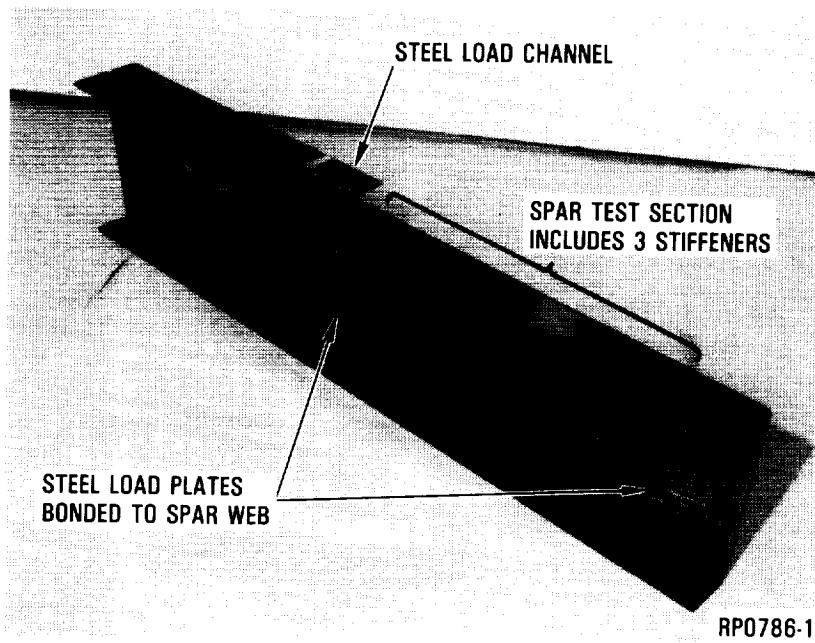
Figure 35. - Baseline spar with metal load plates bonded to spar.
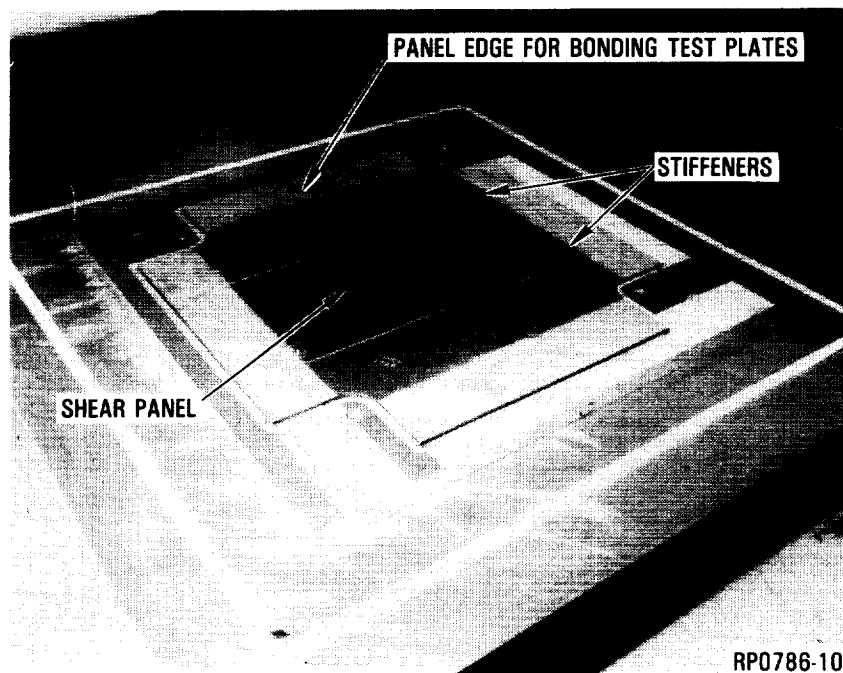
Figure 36. - Baseline shear panel before bonding test fixture to panel.

52

The assembly of the upper and lower steel cover-simulation parts to the spar bending article presented some difficulty in drilling close tolerance holes in the combination of 0.300-inch thick steel and 0.300-inch thick graphite/epoxy. A two-step drilling procedure was used, followed by a final reaming. The first step utilized a 5/16-inch-diameter cobalt drill bit to penetrate the steel cap component only. The graphite cap was then drilled with a 19/64-inch-diameter carbide drill bit, inserted through the larger 5/16 inch diameter hole in the steel component so that only the graphite/epoxy was being drilled. A final reaming was used to open both holes up to the required 0.324 - 0.327 inch diameter. This process produced very good quality holes without excessive drill wear and breakage, and was used on all subsequent spar bending assemblies. Figure 37 shows the fasteners being installed in the baseline spar assembly.

Test

Spar Bending Specimen - The predicted mode of initial failure was the onset of buckling in the spar web. Complete failure, although not predicted during initial design, was expected to occur as a result of stiffener separation after spar web buckling had occurred. During the spar baseline test, severe yielding of the steel plate which simulated the lower cover was indicated by strain data. This yielding resulted in earlier than expected failure through the composite lower cap in the maximum bending
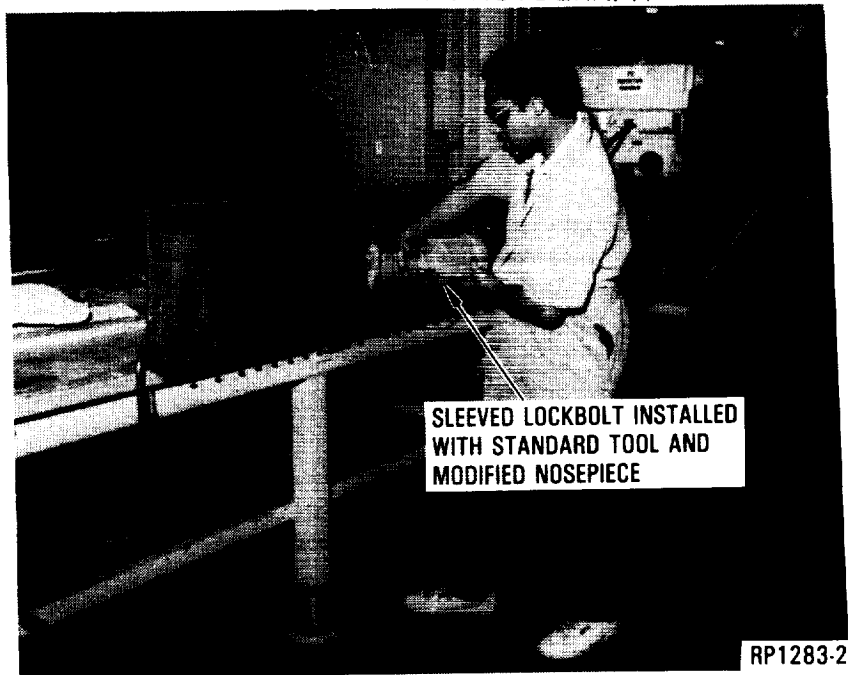
Figure 37. - Installing fasteners in baseline spar test specimen.

section at an indicated strain of 4839 μin./in. The failure, illustrated in figure 38, went through the spar cap attachment holes, then proceeded up the spar web. The yielding of the spar cap was caused by lack of heat treatment on the steel cover. Comparison of predicted and measured strain data showed good correlation. The critical web in the test section buckled at an average shear flow of 4710 lb/in., as compared to an ultimate design shear flow of 4643 lb/in. The applied test load level (at "V" in figure 38) was 63,000 pounds at buckling onset. Figure 39 shows the good correlation between the finite element model analysis and the strain measurements and indicates the onset of buckling.

Gages 65 and 66 were on the lower cap closest to the point of complete failure. Gage 66, which was on the steel portion, shows (figure 40) excessive yielding above the 50 kip load level. The model shows yielding above the 50 kip load level, but not the extreme indicated by the actual gage. Gage 65 on the graphite cap also showed considerably higher strain than that predicted. These readings may have been affected by the close proximity of the gages to a fastener hole. The strain indicated by gage 65 was in excess of 5000 in./in., at final failure and was significantly higher than was intended because of the load transfer from the yielding steel cap. Two changes were required for the remaining specimens to ensure a good test, representative of the initial design analysis; namely, the steel caps were heat treated to 180 ksi strength, and the test fixture was modified to allow extensional movement of the specimen during the bending process.

Spar Shear Specimen - Two baseline shear panel specimens were tested in an existing picture frame fixture. Mounted in a testing machine this test apparatus applies a vertical tensile load to opposite corners of the picture frame fixture while a horizontal compressive load is applied to the opposite corners by an auxiliary hydraulic jack.

The first article was instrumented and tested in the "as manufactured" condition. Strain versus load plots from back-to-back diagonal gages in the web area are shown in figure 41, and clearly indicate the onset of buckling at approximately 75,000 pounds diagonal loading. This load level yields a calculated shear flow loading of 4714 lb/in. The predicted onset of buckling was calculated to be 4235 lb/in. The difference between the measured and predicted values was attributed to the fixture fixity, which approaches a clamped condition at the steel reinforcing member. Subsequent finite element analysis of the specimen indicated buckling at 4608 lb/in. (within 3 percent of the indicated test value).

The specimen was continuously loaded in the postbuckled range until one of the stiffeners completely separated from the panel, and the second stiffener disbonded at an applied load of 90,000 pounds tension and 86,617 pounds compression. The specimen continued to hold load at this level. Thereafter, the specimen was removed from the test machine, and used for trial impact tests to define the impact magnitude to be used on the second baseline spar shear specimen.

HORIZONTAL SUPPORT

V LB

TEST SECTION

WEB BUCKLED @ q = 4710 LB/IN

REACTION R1

SPAR FAILURE LOCATION

REACTION R2

COMPOSITE CAP AND WEB FAILED

$\epsilon_{C/E\ CAP}$ = 4,839 μ IN./IN.

STEEL CAP FAILED 76, 395 LB

VIEW B-B

STEEL

COMPOSITE

SECTION A-A
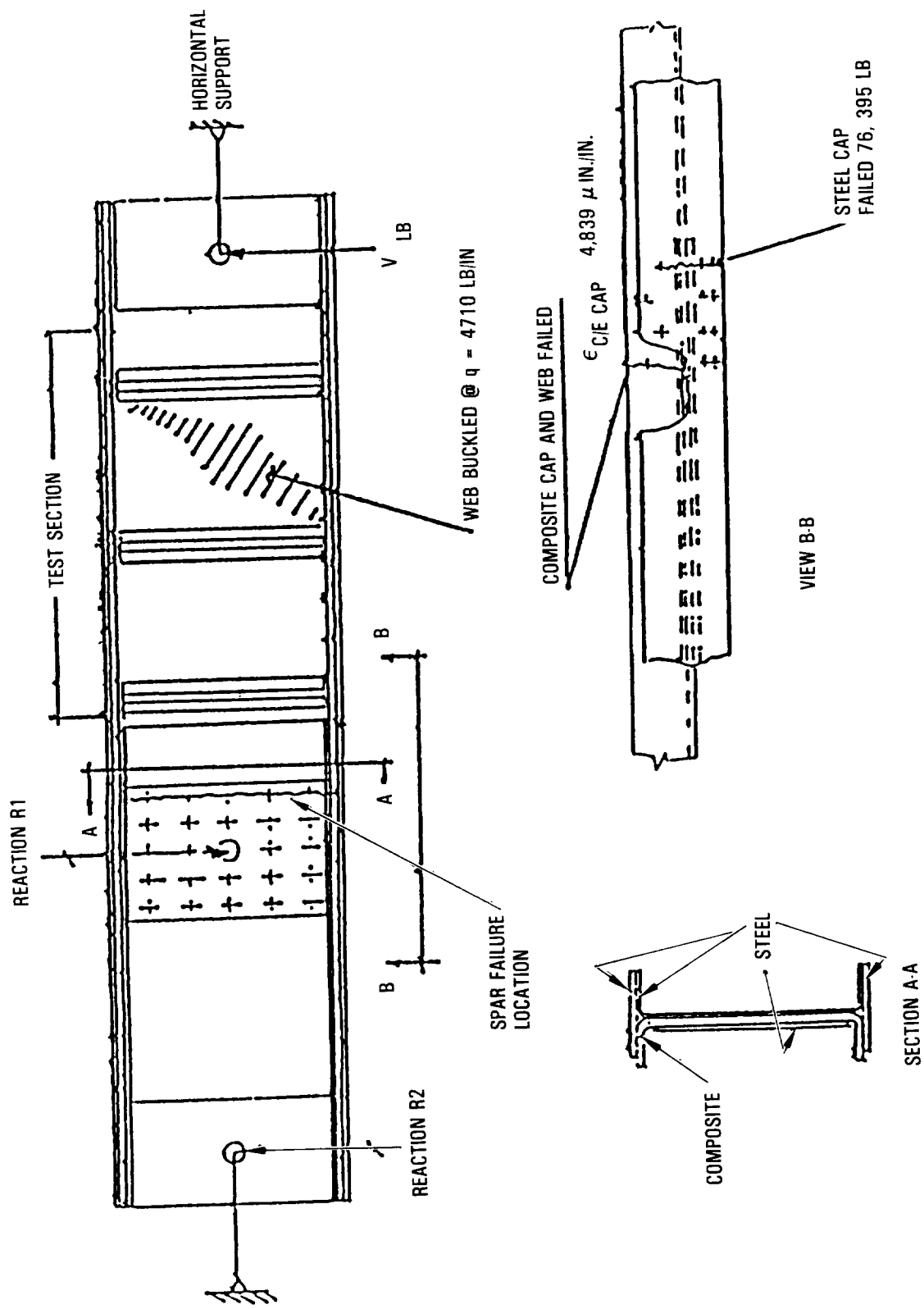
Figure 38. - Baseline spar test results.
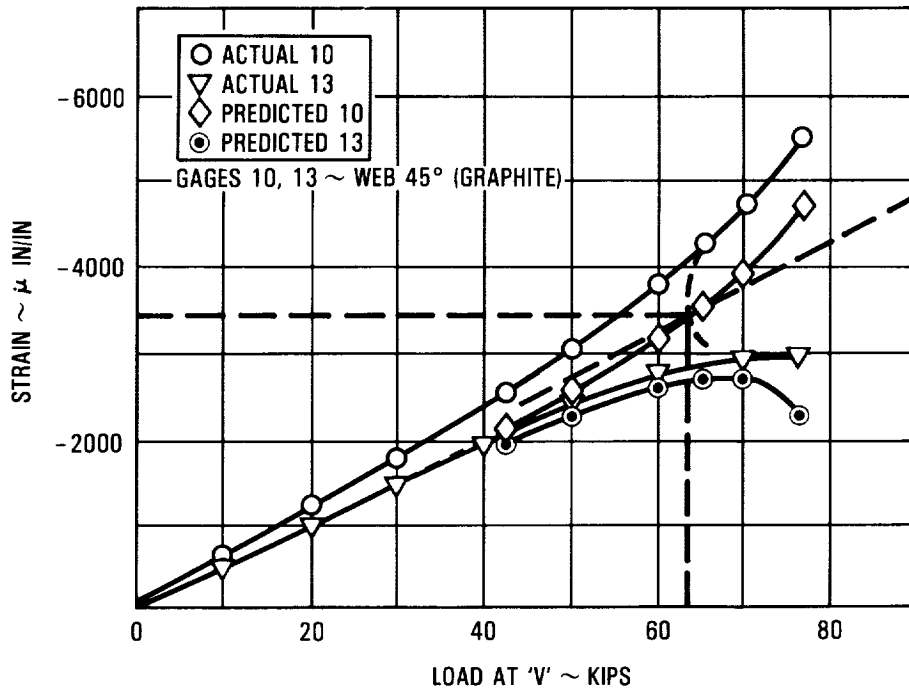
Figure 39. - Baseline spar web strain gage correlation.

The as-manufactured test specimen used for trial impacting had sustained separation of both stiffeners. One stiffener was rebonded before impacting. Figure 42 indicates the locations of trial impacts and resulting damage depth and radiographic damage area. The stiffener on the trial impact specimen remained attached to the web, even after four impacts. Since none of the trial impacts caused a 0.100-inch dent, the 100 ft-lb energy level was used on the post-impact test specimen. All but the 40 ft-lb trial impact produced clearly visible damage.

Two locations along the stiffener were selected as the most critical locations for the predicted mode shape. Both impact sites are illustrated in figure 43, along with measured impact depth and radiographic damage area. The panel was supported on nine-inch centers during impact, consistent with a location close to a cap/rib interface.

Strain gages for the "damaged" specimen were placed at the same location as those for the "as-manufactured" specimen. Strain versus load level plots (fig. 44) indicated that the onset of buckling occurred at a diagonal load level of 64,000 pounds, as compared to the 75,000 pound level for the "as-manufactured" specimen. This actual buckling load occurred sooner than the predicted value of 73,310 pounds, but the analysis did not account for the impact damage. Eccentricities from the impact damage appear to be the cause
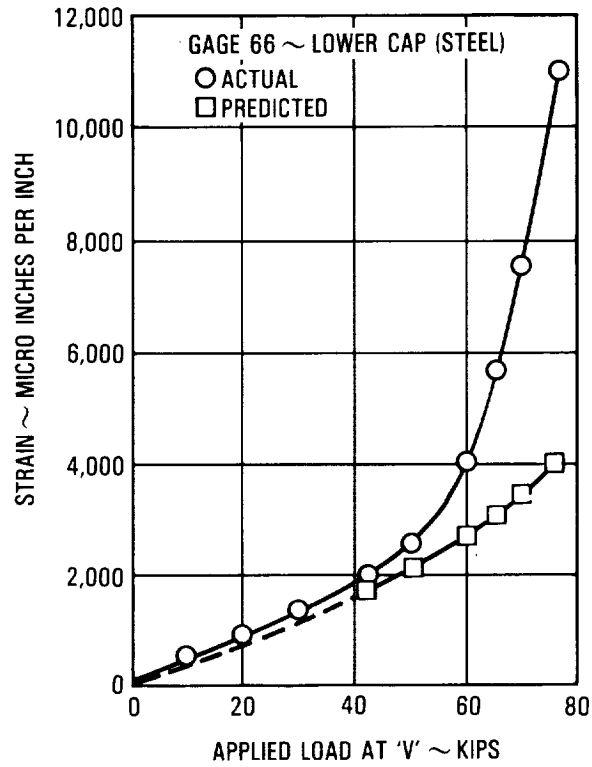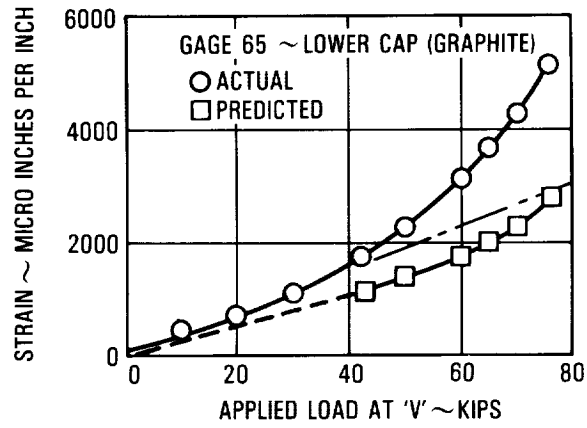
Figure 40. - Baseline spar cap strain gage correlation.
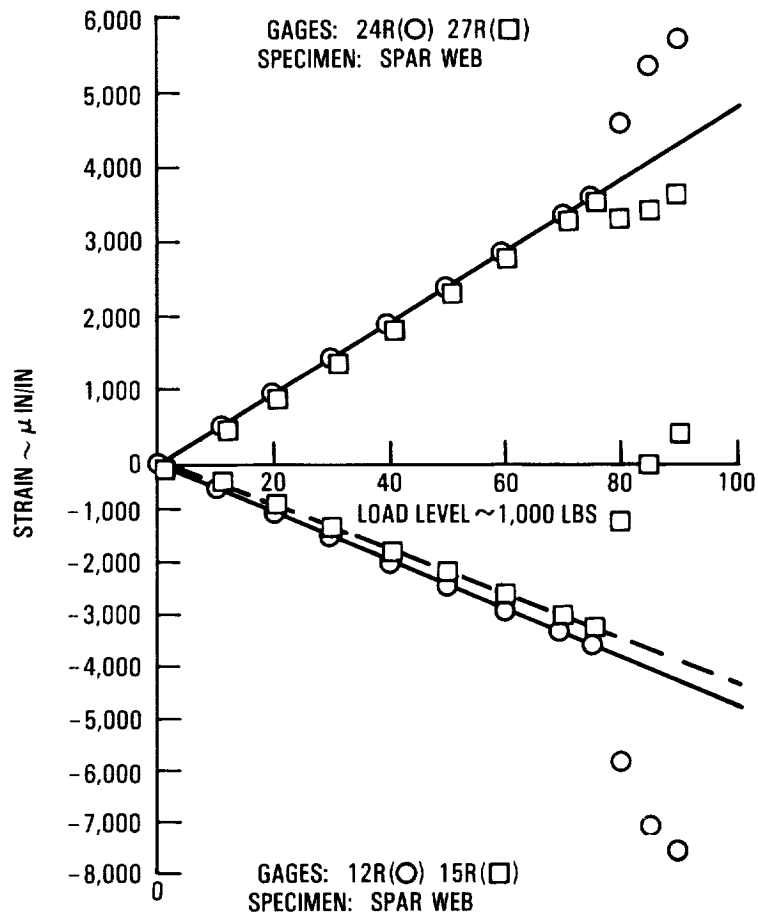
Figure 41. - Baseline shear panel: Strain vs. load level - "as manufactured."
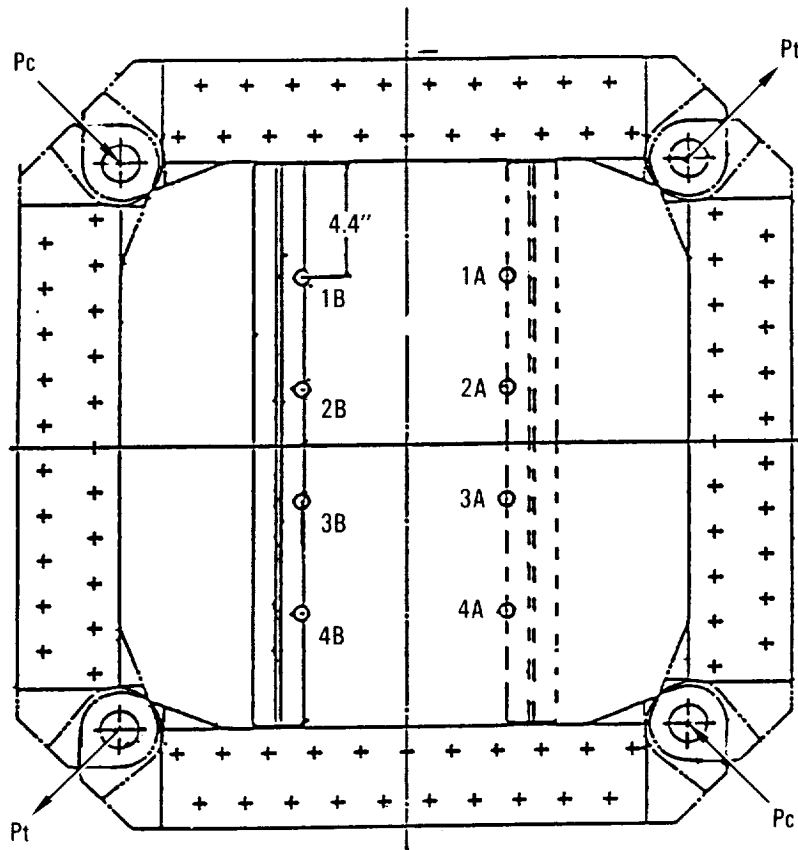
IMPACT SITE	IMPACT ENERGY (FT-LBS)	IMPACTED SIDE DAMAGE DEPTH (IN)	RADIOGRAPHIC DAMAGE AREA (IN^2)
1A	40	.008	0.57
2A	60	.031	1.65
3A	80	.050	2.01
4A	70	.057	1.77
1B	100	.053	1.54
2B	65	.021	1.54
3B	90	.072	1.33
4B	80	.025	0.95

Figure 42. - Trial impact results - baseline spar shear panel.
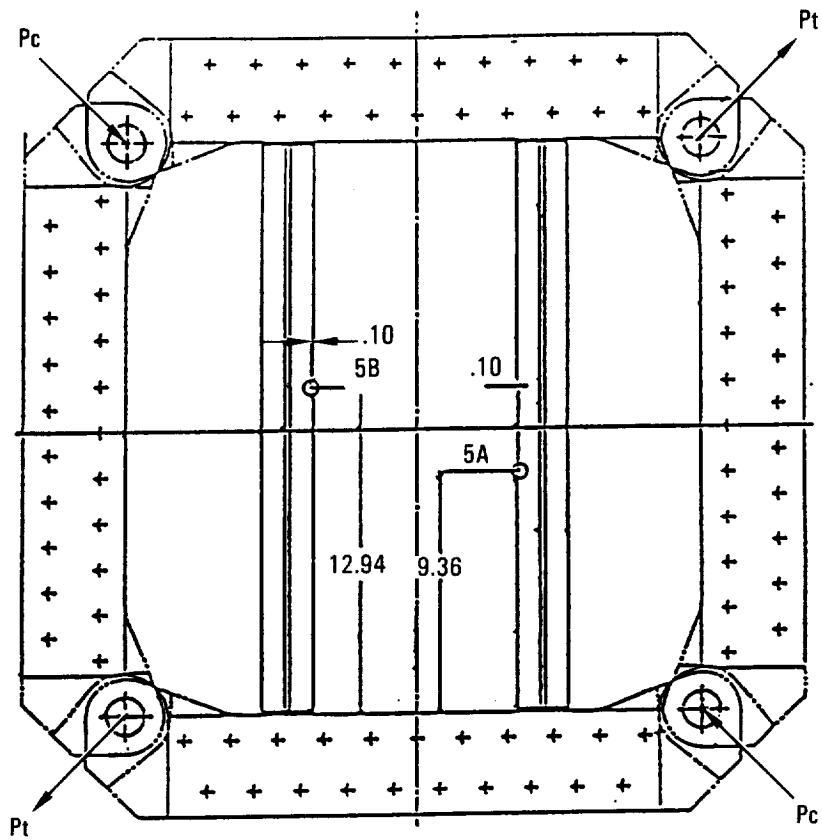
IMPACT SITE	IMPACT ENERGY (FT-LBS)	IMPACTED SIDE DAMAGE DEPTH (IN)	RADIOGRAPHIC DAMAGE AREA (IN^2)
5A	100	.088	3.30
5B	100	.053	2.01

Figure 43. - Impact damage location and extent - baseline spar shear specimen.
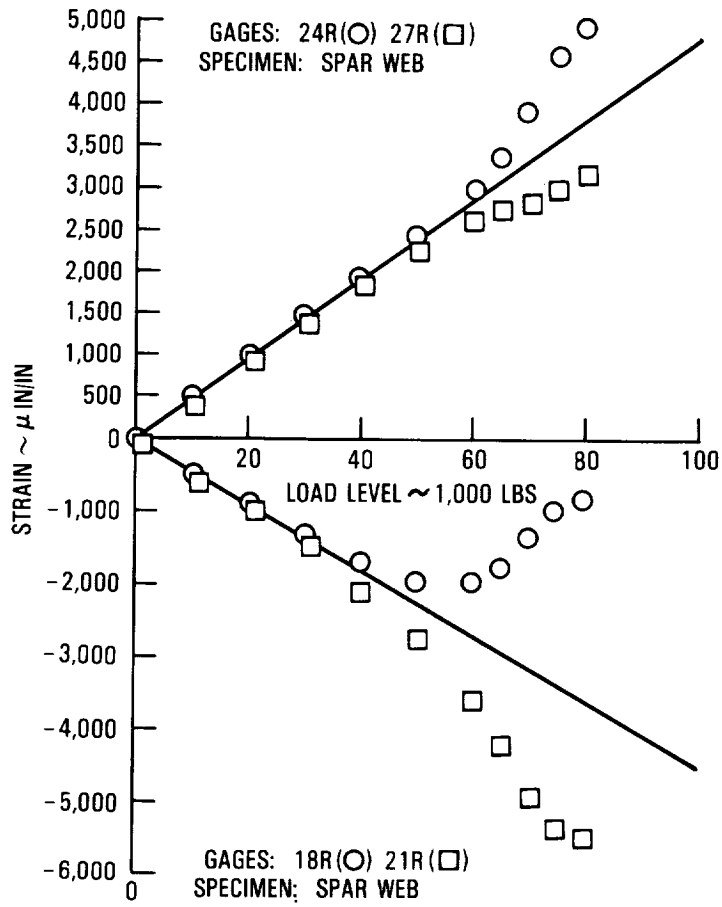
Figure 44. - Strain vs. load level - baseline "damaged" spar shear specimen.

for the back-to-back strain gage readings diverging sooner than actual initial buckling, and they may have contributed to the early initial buckling.

Both stiffeners separated from the panel at applied loads of 80,000 pounds tension and 78,464 pounds compression, or a calculated shear flow of 4980 lb/in. After stiffener separation, the load was increased to 85,000 lbs tension and 85,351 compression, at which point the unstiffened shear web failed along the tension diagonal.

Thermoplastic Spar

Design

The external configuration for the thermoplastic spar is identical to that of the baseline design. This facilitated the fabrication of test specimens by allowing existing designs for local reinforcing hardware and load introduction fittings to be utilized. One of the advantages of the thermoplastic matrix is in the capability for successive consolidations (or reconsolidations) of the material in a manner similar to that used in some heat-forming metal fabrication techniques. The spar design incorporated a roll-forming process as part of the transition from graphite/thermoplastic tape to a finished part.

Details of the selected design approach, which features the use of roll-formed angles for subsequent autoclave consolidation, are shown in Figure 45. Stiffeners for this design are also configured to be fabricated using this process and are attached to the spar web using a rivet/bonding technique, as illustrated in figure 46.

Fabrication

The high temperatures (700-750°F) needed to soften the thermoplastic resin (Polyetheretherketone -- PEEK) and the rapid cooldown rates desired during re-crystallization, restrict the choice of suitable tool materials to those which can maintain strength and thermal expansion/stability without warping or degradation. Lockheed selected steel tools with some aluminum details, and high-temperature autoclave bagging materials.

The thermoplastic spar bending specimen was fabricated using AS4/APC-2 (PEEK) tape, in the following manner:

Flat Panel Fabrication - Flat panels were made in ten-ply laminates to the required fiber orientations. The laminates were laid up by hand, tack-welded, cut in halves, bagged, and autoclave consolidated. A steel flat platen was used to produce these laminates. After ultrasonic inspection, the flat panels were shipped to Roll Forming Corporation, Shelbyville, Kentucky.

62

58 PLIES
(38%0/48%/±45°/14%90°)

0.12 R

PREFORMED ANGLES

UNIDIRECTIONAL TAPE

40 PLIES
(15%0/70%±45/15%90)

VIEW A

0.313

3.37

A

0.216

B

14.0
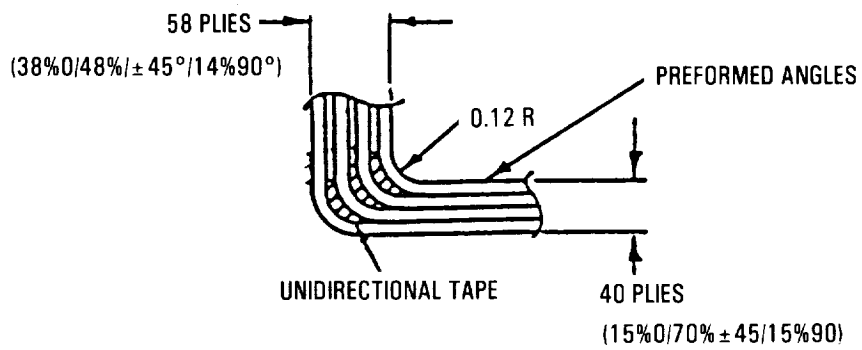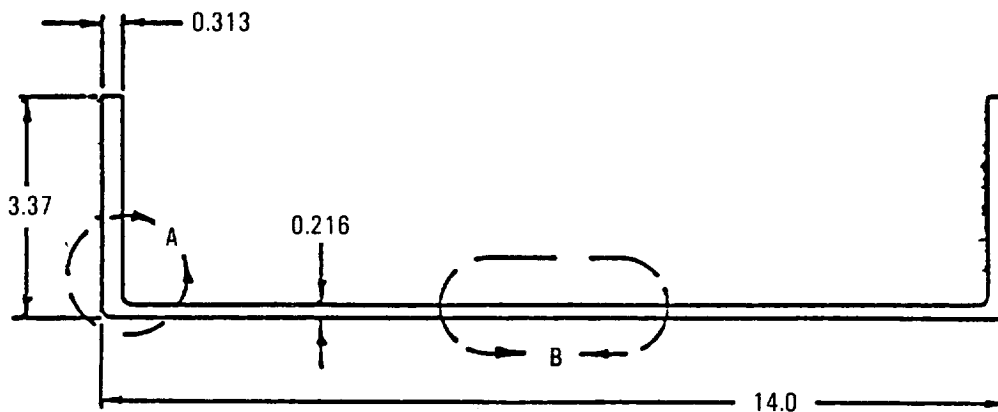
MATERIAL: AS4/APC 2
PREPREG TAPE (0.0054/PLY)

STAGGERED SPLICE
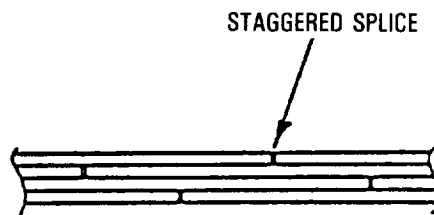
VIEW B

Figure 45. - Thermoplastic spar concept.
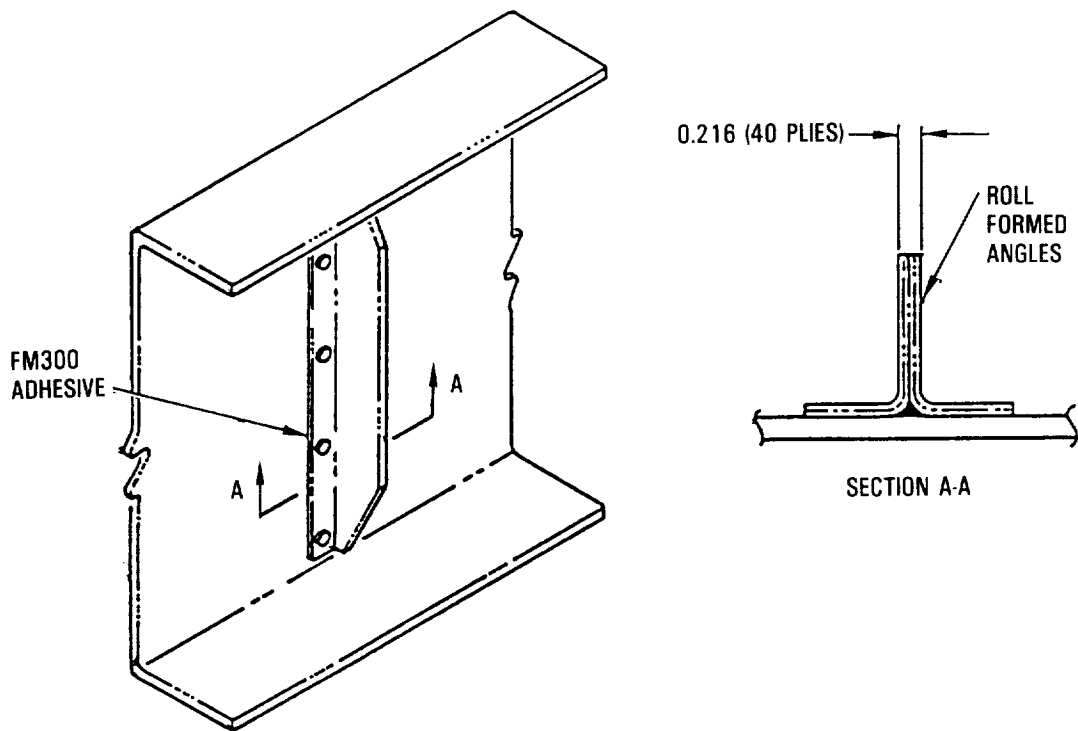
Figure 46. - Stiffener configuration - thermoplastic spar.

Roll Formed Angle Fabrication - Under a subcontract with Lockheed-
Georgia, Roll Forming Corporation used a metal-forming pilot line to convert
the flat panels into 90° "L"-shaped angles. They designed and made a steel
mandrel, caul plate, and forming rolls, selected rolling speeds and pressures,
and demonstrated the process capability. Figure 47 shows the pilot line,
while Figure 48 shows the mandrel, angle, and caul package emerging from the
last forming roll.

The fabrication process at Roll Forming Corporation was:

o The flat panel was placed on a steel mandrel instrumented with
   thermocouples.

o The panel, mandrel, and caul plate were placed in the oven and heated
   until the panel draped over the mandrel.

o The mandrel was quickly backed out of the oven and the caul plate was
   positioned on top.

o The mandrel was returned to the oven until it reached a temperature of
   730°F.
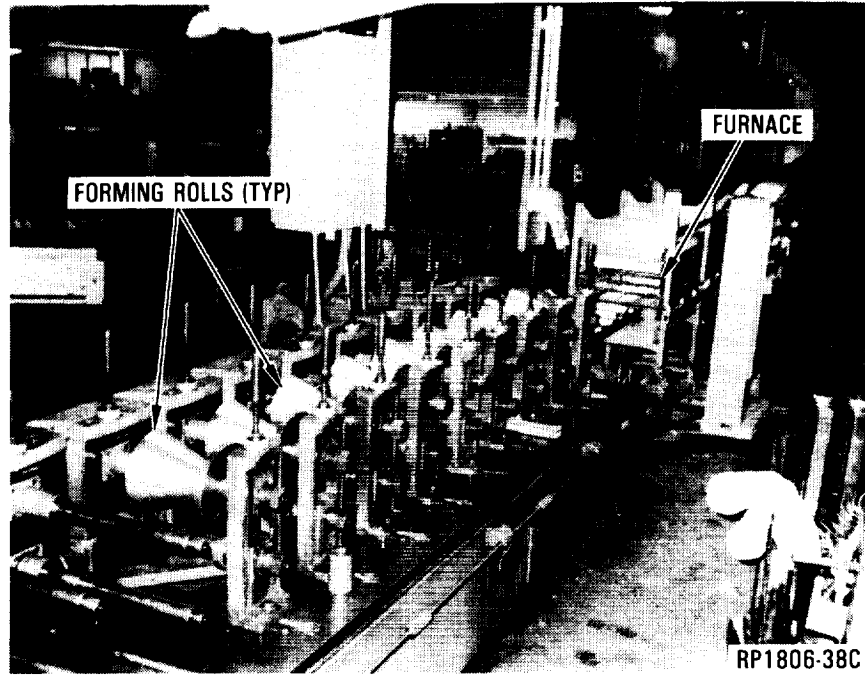
Figure 47. - Pilot line for roll forming angles.
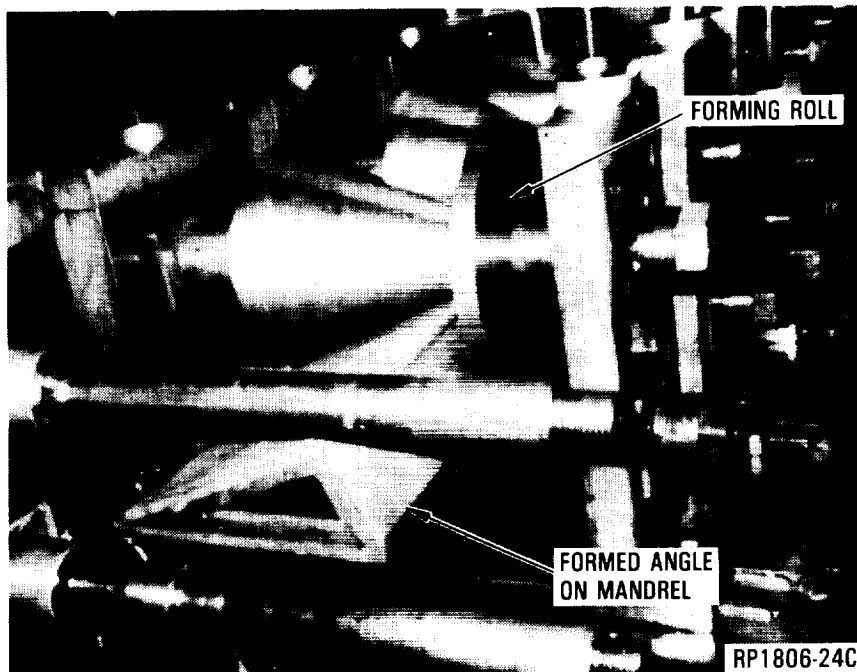
Figure 48. - Formed angle emerging from end of rolling line.

o The mandrel was pulled forward through the series of rollers to obtain the required shape and pressure for finish forming and consolidation.

o At the end of the rollers, a liquid nitrogen spray quickly cooled the panel/mandrel.

This process was repeated until all of the flat panels for the spar bending specimen and the stiffeners were roll formed. Three of the roll-formed angles are shown in figure 49.

Stiffener Fabrication - Stiffeners for both the spar bending and the spar shear specimens were fabricated from the roll-formed angles. The four stiffener angles were stacked back-to-back to form the blade stiffeners (fig. 50) by a final autoclave consolidation. The ultrasonic inspection revealed no voids, but dimensionally the angles closed 1-2 degrees.

Spar Final Consolidation - A final consolidation tool, illustrated in figure 51, was designed to hold a constant spar web height from room temperature to 730°F. This was achieved by using the different thermal expansion rates between the steel and the aluminum tool details.

Prior to final consolidation, a study was conducted to determine needed surface preparation of PEEK panels for final consolidation and the need for addition of PEEK film between panels. A surface preparation of glass bead blasting and solvent cleaning was used to remove any traces of mold release agent before final consolidation. A PEEK film interlayer (0.002-inch-thick) was placed upon the abraded surfaces prior to consolidation.

The spar bending article was final consolidated in the steel/aluminum tool. Figure 52 shows the tool loading arrangement to assemble the preconsolidated roll-formed angles, cap inserts, and fillets into the final consolidation tool. The parts were tack welded into position using heated air and neat PEEK resin film (fig. 53). This method worked well to hold the separate preconsolidated details in position and to prevent movement during installation of the aluminum cauls and bagging materials. After autoclave consolidation, the tool try spar was visually and dimensionally inspected. The spar cap angles were closed approximately 2.5 degrees, which was expected due to the large temperature change from consolidation to room temperature. Ultrasonic inspection showed moderate voids in the radius and flange areas. A second spar was final consolidated and reconsolidated to achieve better compaction in the radius and flange areas.

The fabrication of the thermoplastic spar shear panels was simpler than that of the spar bending specimens. Four unique, ten-ply laminates were processed in the same manufacturing method as those for the spar laminates. After autoclave consolidation and inspection, the laminates were machined, surface prepped, and tool loaded in a sequence representative of the spar web. The shear panels successfully passed ultrasonic inspection.
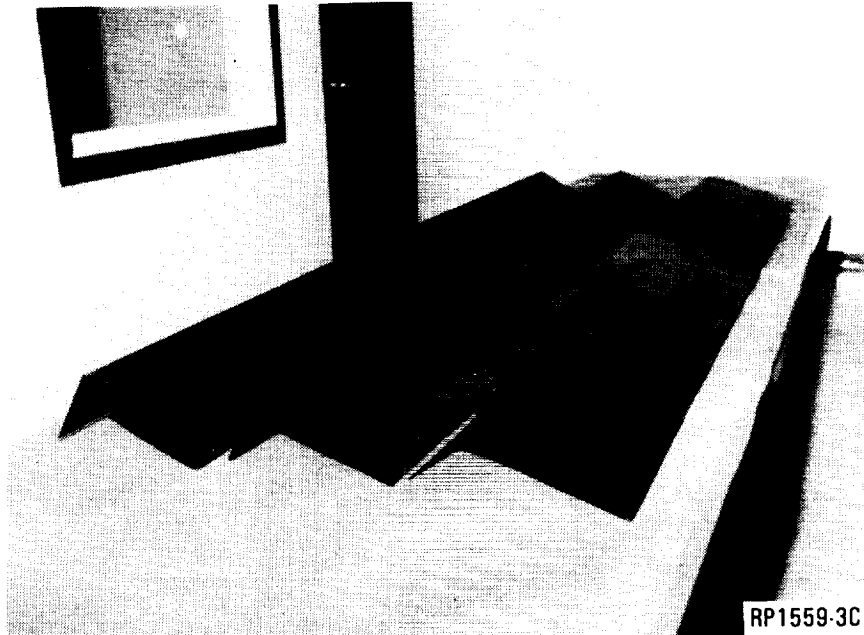
Figure 49. - Typical roll formed thermoplastic angles.
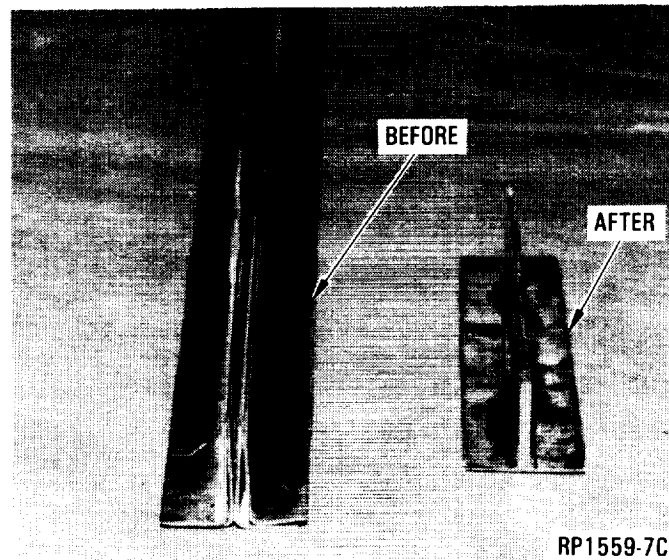
Figure 50. - Thermoplastic stiffener before and after consolidation.

67

0.06 GAP AT R.T.
(BOTH SIDES)
NO GAP AT 730°F

KAPTON BAG

── 30″ ──

── 14″ ──
*

SIDE PLATE
ALUMINUM

SPLIT MANDREL
ALUMINUM

BASE PLATE — STEEL

THERMOPLASTIC SPAR

*THIS DIMENSION REMAINS CONSTANT
FROM R.T TO 730°F
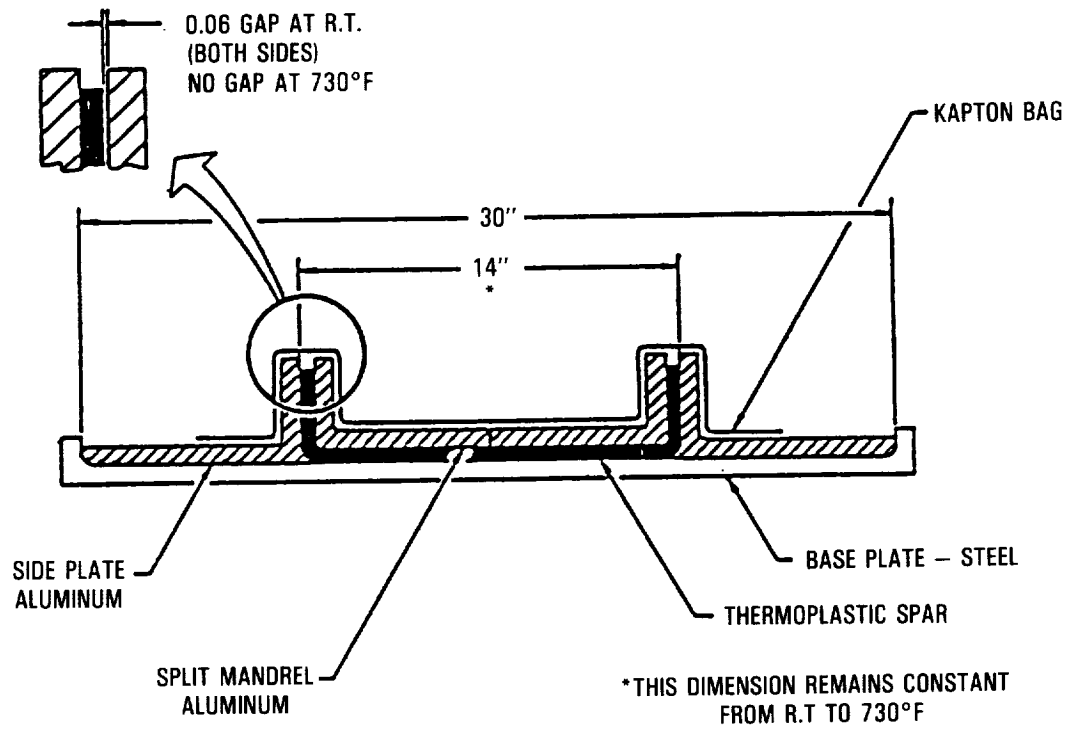
Figure 51. - T/P spar -- concept for final consolidation tool.

SPLIT MANDREL
ALUMINUM

ROLL FORMED ANGLES (4)
.002″ PEEK FILM (ALL FAYING SURFACES)
INSERTS (3)
FILLETS (3)

NOTE: SPAR LAYUP IS SYMMETRICAL
ONE SIDE SHOWN FOR CLARITY

SIDE PLATES
ALUMINUM

STAGGERED
PLY ENDINGS

14″

THERMOPLASTIC SPAR
BASE PLATE
STEEL

72″

30″
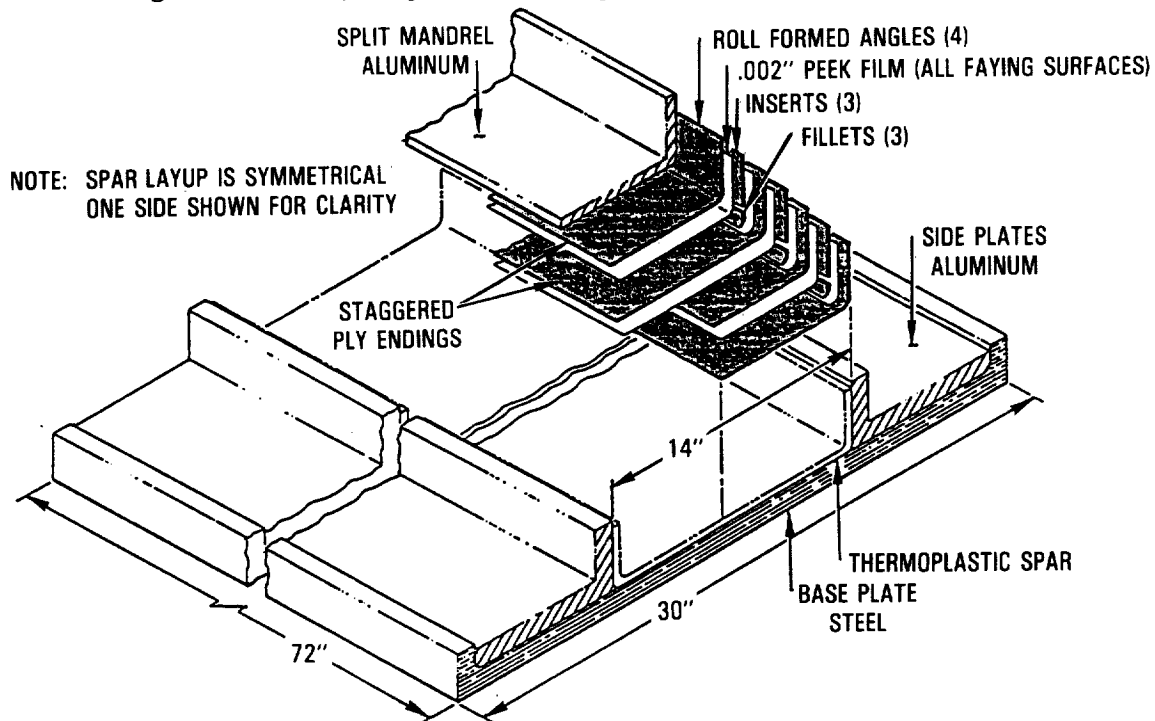
Figure 52. - Thermoplastic spar tool and loading plan for final
consolidation.

Figure 53. - Tack-welding thermoplastic angles and details in final
consolidation tool.

Stiffener-to-Panel Assembly - The thermoplastic stiffeners were bonded to
the spar web/shear panels with a 350°F curing adhesive, and mechanical
fasteners were installed. Metal test panel details were then bonded with a
room-temperature curing adhesive.

The completed spar bending assembly is shown in figure 54.

Test

Bending Specimen - The procedure for this specimen was identical to that
used for the baseline articles. The test fixture incorporated the
modification on the longitudinal constraint to prevent unwanted induced
bending loads and make the external loading statically determinant.

Test loads were applied in cycles up to limit load with no indication of
permanent set in the metallic structure. Test loads were re-applied to design
limit load, then on to specimen failure. During the loading, loud noises were
heard coming from the specimen at approximately 15% above limit load, but no
visual damage was found; the noises were attributed to possible local
disbonding between steel reinforcement parts in the non-test region and the
composite specimen. Load application was continued to 1.32 limit load, where
a small load drop was noticed. A close visual inspection of the specimen did

69
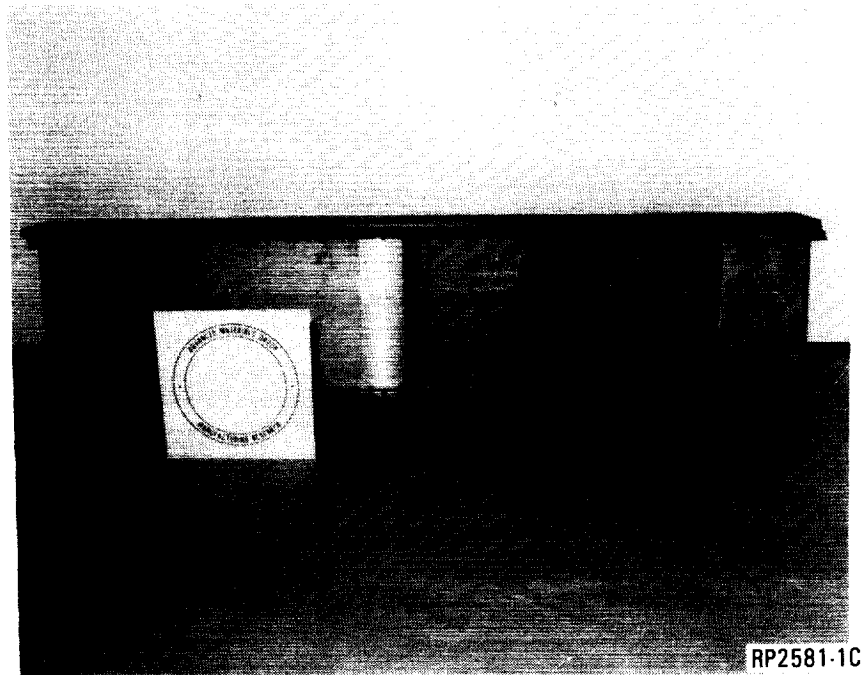
Figure 54. - Completed thermoplastic spar test specimen.

not reveal any damage. After restarting the test, loading proceeded uneventfully until final failure occurred at approximately 2.0 times limit load, or a calculated shear flow of 6071 lb/in.

Figure 55 shows a schematic of the failed article along with the critical gage locations. Photographs of the failed specimen are shown in figures 56 and 57 as viewed from the stiffener side and web side, respectively.

Buckling was indicated at a load level of 73,188 pounds, or a calculated average shear flow of 5228 lb/in. This shear flow is slightly higher than the value predicted (4942 lb/in.). Failure resulted at a calculated shear flow of 6071 lb/in. A post-test inspection revealed that multiple failures occurred, including compression failures of the stiffeners. Since the strain readings in the stiffener were relatively low just prior to failure, these failures are assumed to be secondary to the buckling overstress failure in the webs. The failure investigation also revealed that separation of the web had occurred along the four staggered web butt joints located near the spar's neutral axis. These joints are unique to the thermoplastic design because of the manufacturing process.

Generally, good structural performance was achieved by the thermoplastic design.

70
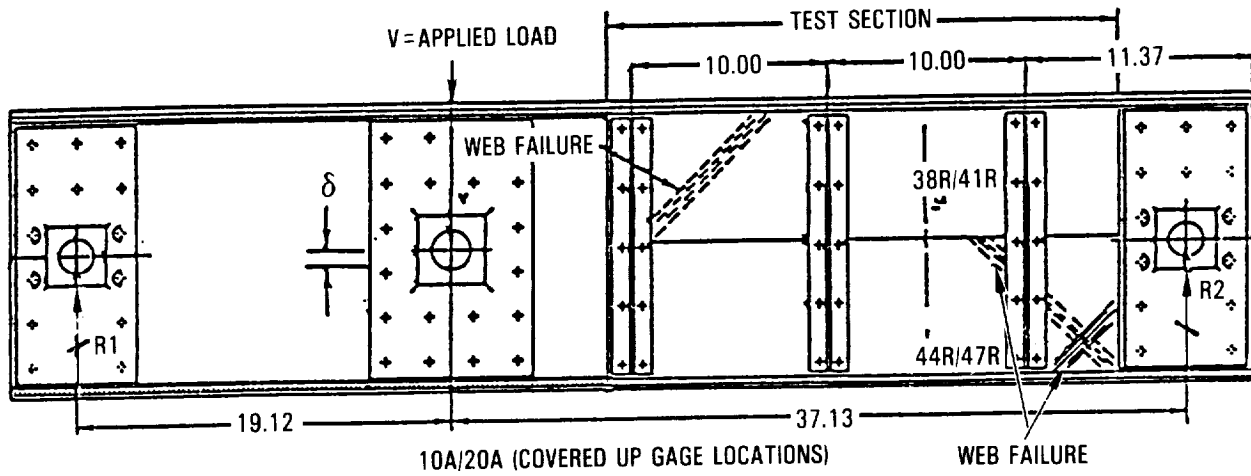
Figure 55. - Strain gage locations and failure description - thermoplastic spar bending specimen.

Figure 56. - Thermoplastic spar after test - stiffener side.
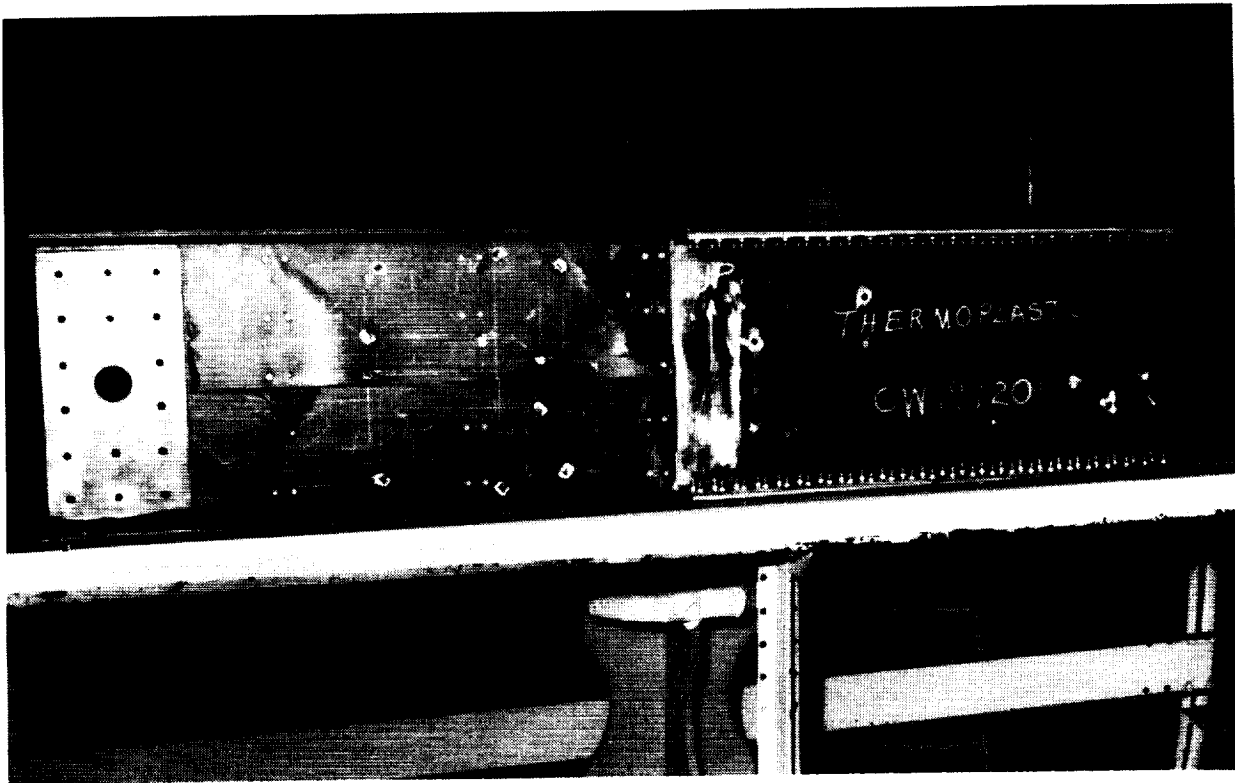
Figure 57. - Thermoplastic spar after test - web side.

Spar Shear Specimens - The two thermoplastic shear panels were tested in the same manner as the baseline specimens. A summary of the test and predicted shear flows is provided below.

SPECIMEN TYPE	PREDICTED BUCKLING LB/IN.	ACTUAL BUCKLING LB/IN.	COMPLETE FAILURE LB/IN.
"As-Manufactured"	4117	4038	5636
"Damaged"	4117	4054	5651

A summary of the impact data on these panels is provided below.

IMPACT SITE /1\	IMPACT ENERGY (FT-LBS)	IMPACT SIDE DAMAGE DEPTH (IN.)	DAMAGE AREA (SQ. IN.) /2\
1	60	.011	.413
2	100	.008	.710
A	100	.050	2.91
B	100	.028	3.06

/1\ Impact sites 1 and 2 are shown in figure 58 for the trial impact
specimens, and sites A and B are shown in figure 59.

/2\ Impact sites 1 and 2 - Ultrasonic C-Scan area
Impact sites A and B - Radiographic area

Failure modes for both specimens were similar with web failures at the
four staggered butt joints along the specimen center line (perpendicular to
the stiffener). The stiffeners remained attached to the web by their
mechanical fasteners.

Filament-Wound Spar

Design

Trade studies showed that filament winding had a high potential for low-
cost spar fabrication. The stiffened channel spar configuration is completely
adaptable to accommodate this fabrication technique. This concept uses
AS4/1806 12K prepreg tow material for all filament winding operations, and
hand laid AS4/1806 tape for axial reinforcing of the spar caps. Stiffeners
for this design are identical to those used on the baseline spar and are co-
bonded to the web during the spar cure cycle. One significant change from the
baseline ply layup for this design is that $\pm 20^\circ$ plies have been substituted
for 0° plies to accommodate the filament winding equipment utilized. The C-
channel ply layup used is depicted in figure 60.

Fabrication

The mandrel for winding spars was an open metal box, rectangular in
cross-section, with perforated sides, as illustrated in figure 61. The
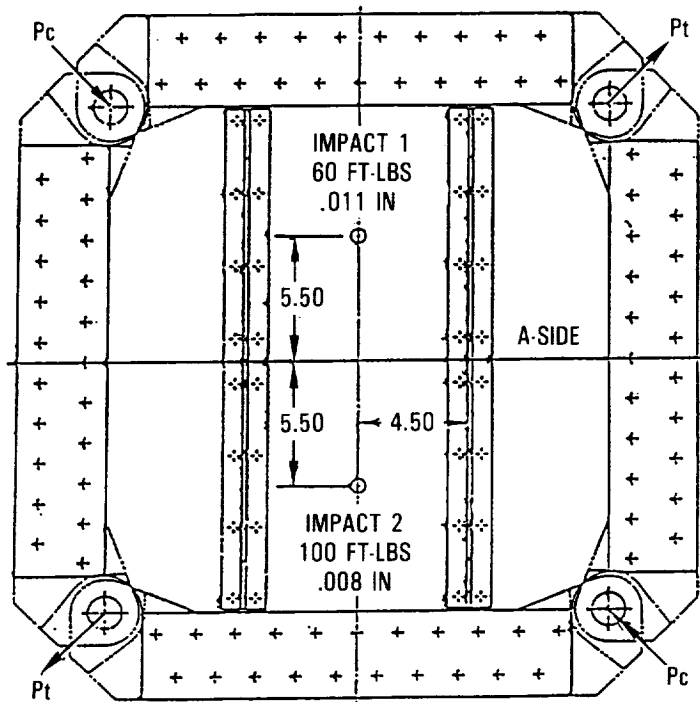
Figure 58. Trial impact locations - thermoplastic spar shear specimen.
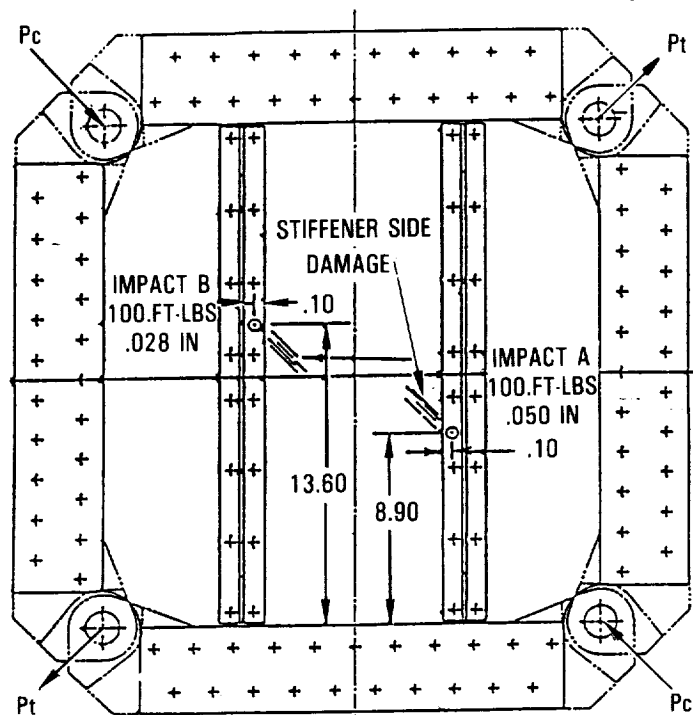
IMPACTS ON WEB SIDE OF PANEL.
STIFFENER SIDE SHOWN.

Figure 59. - Impact locations in thermoplastic "damaged" spar shear
specimen

CAP REINFORCING
TAPE (HAND LAY-UP)

.317 (20 PLIES TOWPREG. 18 PLIES TAPE)
(27%0°/14% ± 20°/42% ± 45°/17%90°

MATERIAL AS4/1806
PREPREG TOW .011/PLY
PREPREG TAPE .0054/PLY

.220 (20 PLIES)
(20% ± 20°/60% ± 45/20%90°)
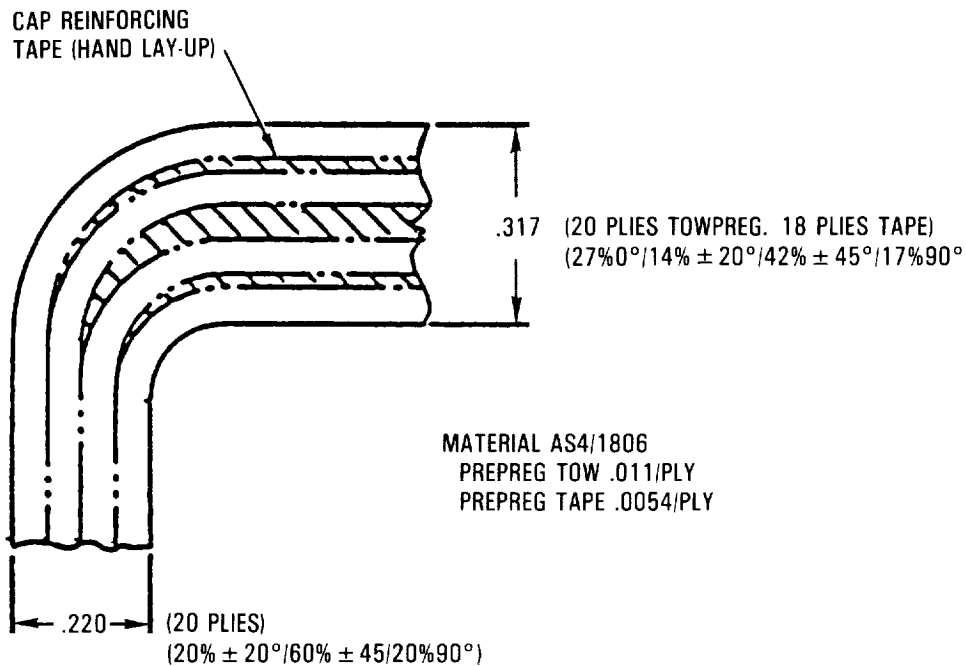
Figure 60. - Filament wound spar ply layup.

outer surface was covered with an expandable rubber bladder. Towpreg was
directly wound onto the rubber-covered mandrel and clamshell C-shaped
graphite/epoxy cauls were installed over the winding. The rectangular winding
was slit lengthwise (top and bottom) to let the expanded bladder force the
wound material into the cauls for curing. After bagging, the parts were
autoclave-cured. Attractive features of this tool concept include:

● Dimensional thermal compatibility of the graphite/epoxy cauls gives
  close control of finished part dimensions.

● Precise pressure is achieved on the curing laminate since both caul
  position and bladder expansion are controlled by autoclave pressure.

● Two spars of the same thickness and orientation can be fabricated in
  one winding and autoclave run, reducing fabrication cost.

● Required web stiffeners may be co-bonded, secondarily-bonded, or
  mechanically fastened to spars. During fabrication of filament-wound
  spars at Lockheed-Georgia, pre-cured blade stiffeners were placed in
  tool recesses on one half of the mandrel (the other half was smooth)
  before winding, bagging, and curing.

Completed filament wound spars are shown in figure 62. The spar on the
left has three co-bonded stiffeners; the other has a smooth web. Stiffeners
were made in the shop-aid stiffener tool for both filament-wound specimens.

FILAMENT WINDING MANDREL (ALUMINUM)

CLAM SHELL MOLDING FIXTURE (TOOLRITE GRAPHITE)

BAG (SEALED TO RUBBER BLADDER)

14"

8"

SECTION THROUGH ASSEMBLED TOOL

GR/EP WINDING (NOT SHOWN IN ISOMETRIC VIEW)

80"

SECTION A-A

RECESS FOR STIFFENER (3 PLACES)

EXPANDABLE BLADDER (RUBBER SHEET)

VENT HOLES
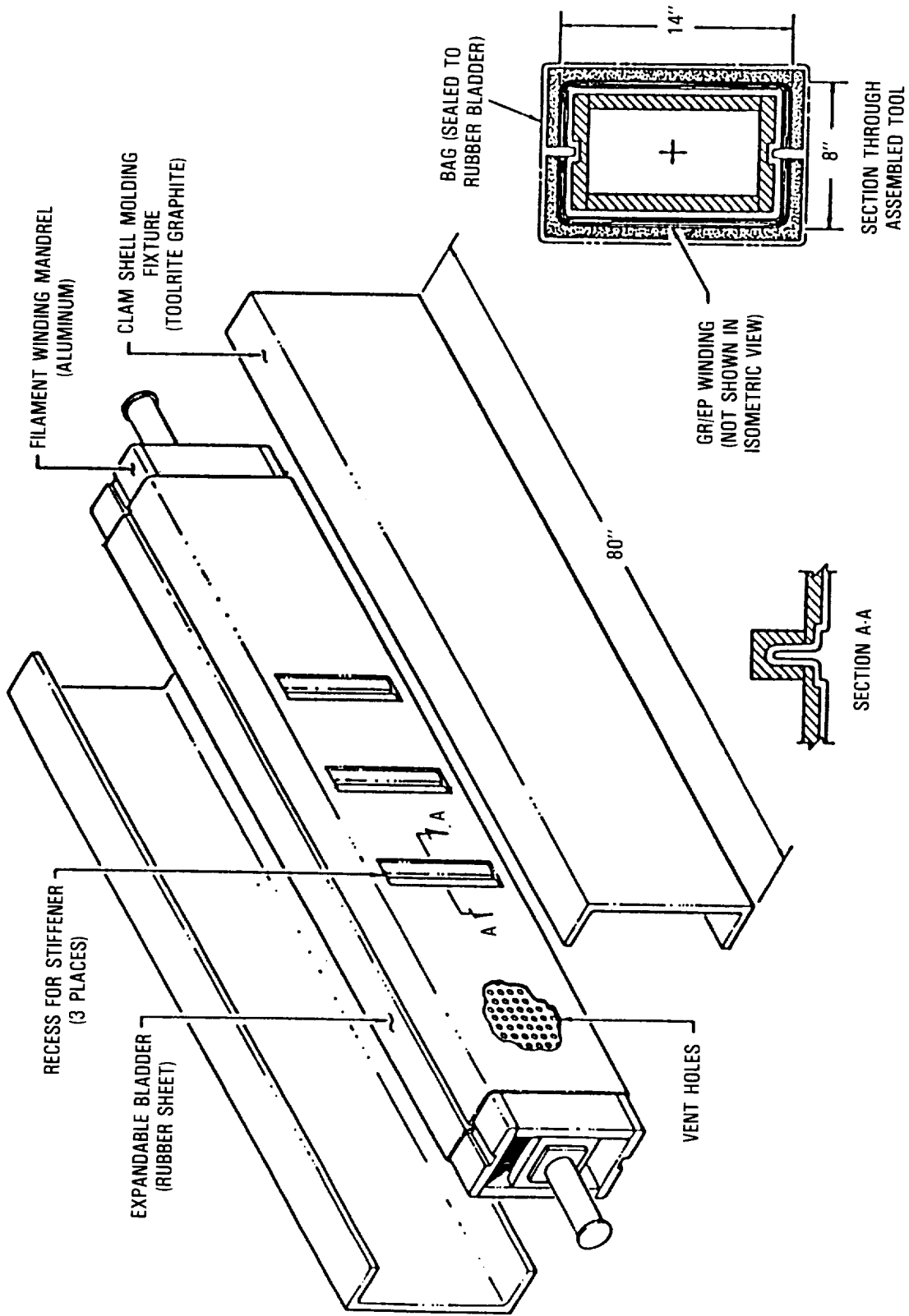
Figure 61. – Filament winding tool illustration.
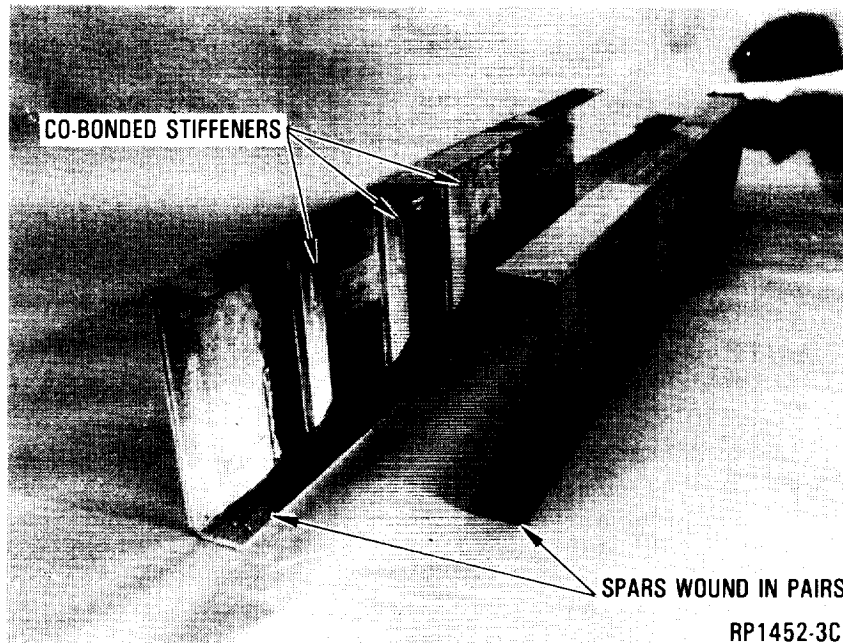
Figure 62. - Filament wound spars demonstrate low cost manufacturing.

Shear panels were drum wound to provide plies, which were cut, debulked, laid on a flat platen, bagged, and autoclave cured. Stiffeners were then bonded to the cured panel. No special tooling was used.

The internal rubber bladder on the spar bending tool worked well, pushing the graphite/epoxy winding out into the caul plates, and the pre-cured stiffeners and spar winding resulted in a good co-bond.

Tests

Spar Bending Specimen - For this test specimen, the steel covers were heat treated to avoid the nonlinearity effects experienced on the baseline test article in the cap region. Also, the test fixture was modified to allow the two end reaction points freedom of movement relative to each other along the specimen longitudinal axis.

The filament wound specimen's critical web buckled at a calculated shear flow of 6468 lb/in, significantly higher than that observed for the baseline specimen (4710 lb/in). The difference observed was attributed to four basic causes: .

77

(1) The available filament winding machine could not wind longitudinal plies (0 degrees) but could achieve a 20 degree angle. Thus, ±20 degree plies were substituted for the 0 degree plies. This enhances the shear buckling strength over that of the hand layup article.

(2) The baseline test article was longitudinally constrained; thus, when the center loading was applied, horizontal forces were induced. These forces were applied in a tensile direction below the neutral axis, thereby introducing additional bending (N_x) forces in the web to be combined with the N_{xy} shear.

(3) Per-ply thicknesses were higher than expected for crossplied laminates (10.5 mil. became 11.5 mil.).

(4) Yielding of the steel covers on the baseline test article created a higher bending strain in the composite web.

The resulting buckling level of 6182 lb/in., compares with a predicted shear flow of 6126 lb/in., from the analysis. No attempt was made to predict the final spar failure, which occurred when the three co-bonded stiffeners separated simultaneously at a calculated shear flow of 7587 lb/in.

Figure 63 shows the failed specimen and the shear buckling failure in the web along the tension diagonal. Strain versus load level plots are presented in figure 64 for critical web gages and show the onset of buckling. The linear behavior of the cap strains below ultimate design load are depicted in the strain versus load level plot shown in figure 65.

Spar Shear Specimen - The two filament wound shear panels were tested in the same manner used for the baseline: as-manufactured testing to failure; trial impacting of the as-manufactured failed specimen; and testing the second article to failure after impacting. The results of the impacting are tabulated below. They show a significant reduction from the baseline in dent depth and visible damage at the 100 ft-lb energy level. The radiographic damage area does not show as large a reduction.

SPECIMEN TYPE	IMPACT SITE I.D.	IMPACT ENERGY FT-LBS	IMPACT SIDE DAMAGE DEPTH (IN)	RADIOGRAPHIC DAMAGE AREA (IN^2)
Trial Impact Specimen	1B	100	.007	1.13
"Damaged" Specimen	2A	100	.008	1.23
	2B	100	.011	0.60

78

Figure 63. – Failed filament wound spar after test.

79

GAGES: 35R(O) 38R(□)
SPECIMEN: BEND NO. 2

GAGES: 55R(O) 62R(□)
SPECIMEN: BEND NO. 2
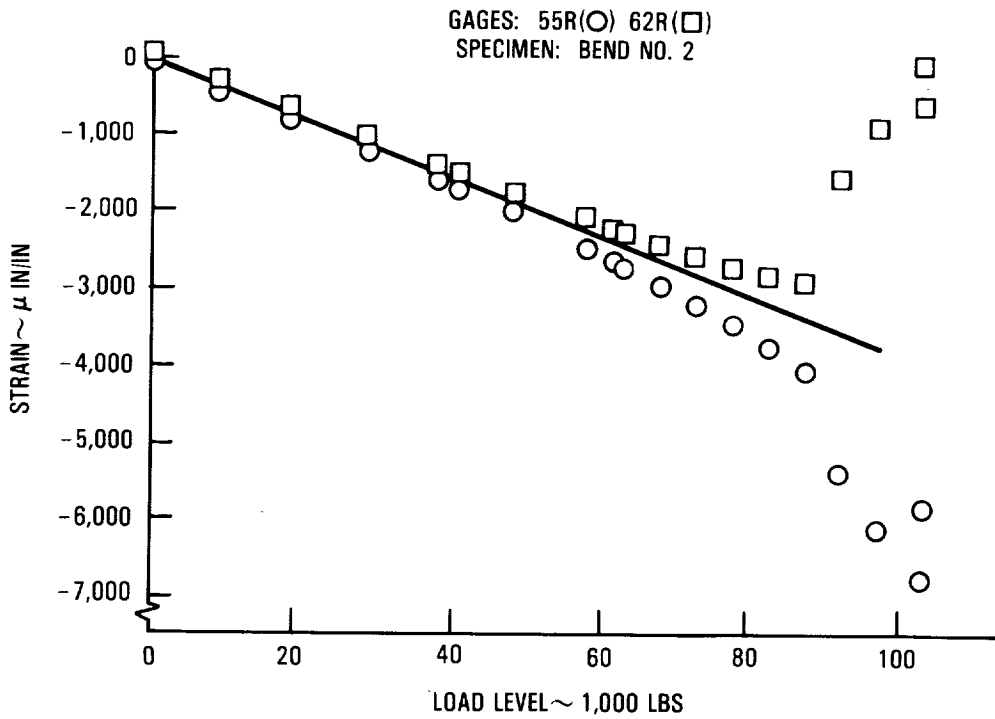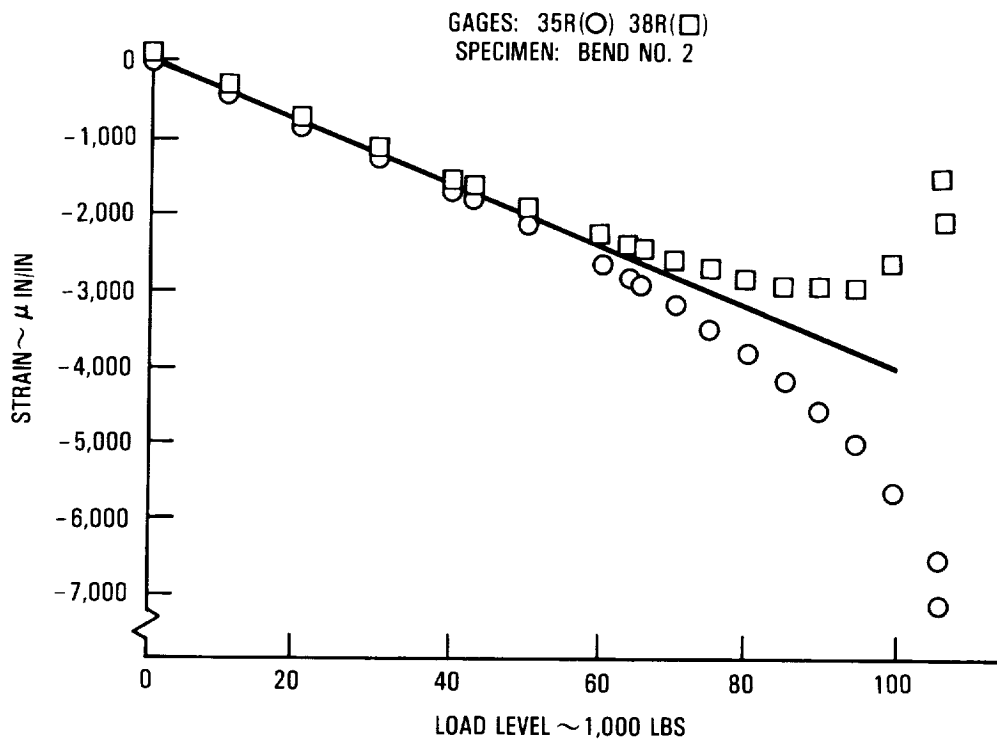
Figure 64. - Strain versus load level - filament wound spar bending
specimen - web gages.

80
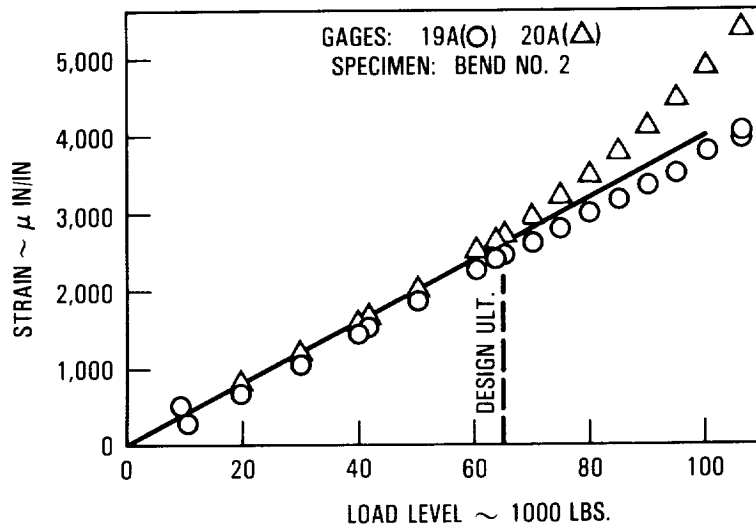
Figure 65. - Strain versus load level - filament wound spar bending
specimen - lower cap gages.

Since the fiber and resin type were the same for the baseline and
filament wound specimens, this difference in dent depth and damage area is
assumed to be a result of the winding process.

A summary of the calculated shear flow from measured test results at
initial buckling and final failure is tabulated below for both specimens.

SPECIMEN TYPE	PREDICTED BUCKLING LB/IN.	ACTUAL BUCKLING LB/IN.	*COMPLETE FAILURE LB/IN.
"As-Manufactured:"	4,949	5,539	7,159
"Damaged"	4,949	5,322	6,279

*Failure for both specimens occurred simultaneously with stiffener
separation and shear buckling.

81

Postbuckled Spar

Design

Weight saving in metal aircraft structure is often increased by allowing some elements to deform "out-of-plane" or buckle at a pre-determined load level. To evaluate this buckled effect, a wing spar was designed, fabricated, and tested.

The spar configuration selected to evaluate postbuckled capability was similar to that of the baseline, except that web thickness was reduced to allow the spar web to buckle at limit load. Details of the spar bending test specimen are shown in figure 66. The spar web thickness for this configuration was reduced to 0.156 in., as compared to the baseline thickness of 0.216 in. This change results in an additional weight reduction of approximately 10 percent.

Postbuckled Spar Tooling and Fabrication

The postbuckled spar was fabricated with the baseline tooling, bagging, and curing techniques described in the Fabrication section. The graphite/airpad caul was modified to accommodate the ply terminations in the web region, and expansion joints were added at the spar web-to-cap radius for better compaction. Later, the airpad was replaced by an elastomeric rubber caul. A new shop-aid stiffener tool was made to accommodate an increase in the blade height.

The postbuckled spar bending and spar shear specimens were fabricated by hand layup of AS4/1806 knit and woven fabric. Mylar ply templates were used to cut and locate the plies. Figure 67 shows the shear panel ready for bonding the "picture-frame" test fixture, and the completed spar bending article is shown in Figure 68.

Postbuckled Spar Test and Evaluation

Spar Bending Specimen - Tests conducted on this specimen were the same as those run on the baseline, filament-wound, and thermoplastic specimens. In addition, Moire' fringe data were obtained during the test, to correlate with analytical mode shapes and deformations.

Test loading proceeded normally up to 1.35 limit load (57,400 pounds R_2). At this load the middle stiffener in the test section cleanly disbonded from the web, remaining attached by the stiffener end fasteners. No other damage was noted, and the specimen continued to hold load. Load was removed, and the middle stiffener was rebonded with a room temperature adhesive without removing it from the test machine. Additional 3/16-in. diameter fasteners were installed on 2.25 in. centers in the three vertical stiffeners to reduce the possibility of early stiffener separation precipitating an early complete failure.
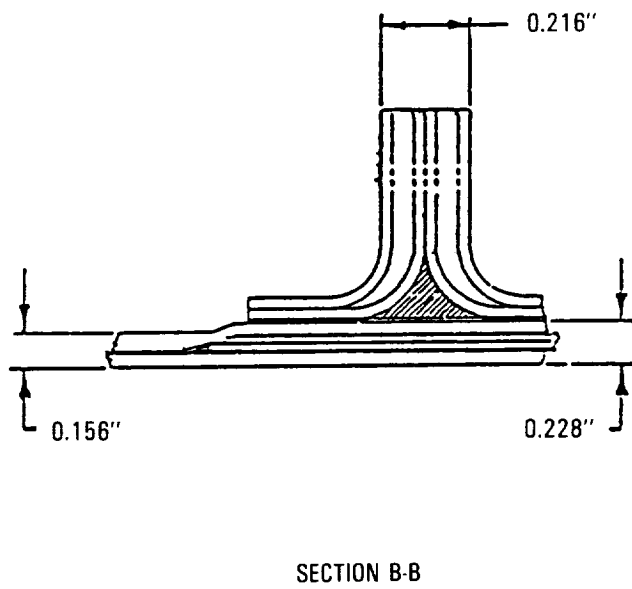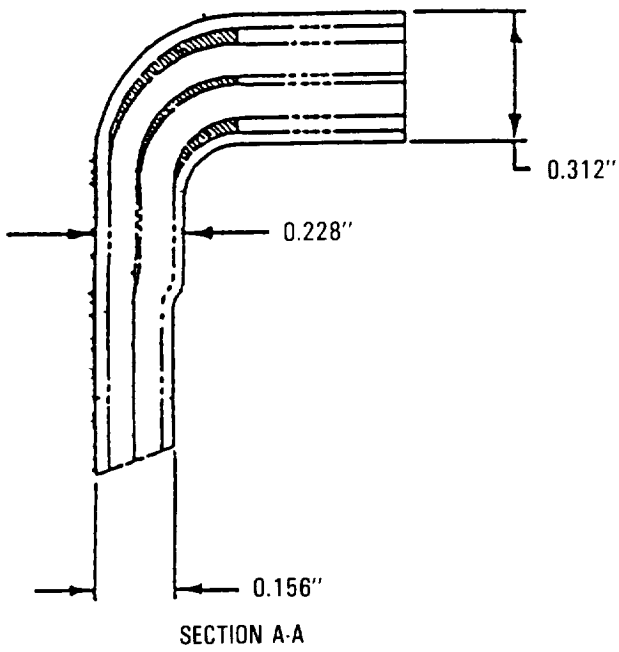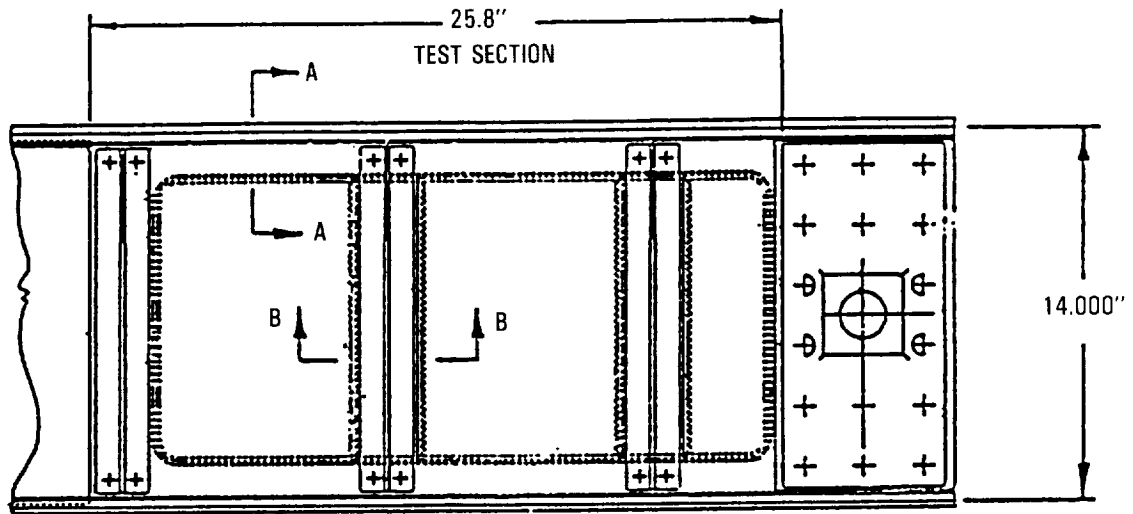
Figure 66. - Postbuckled spar design.
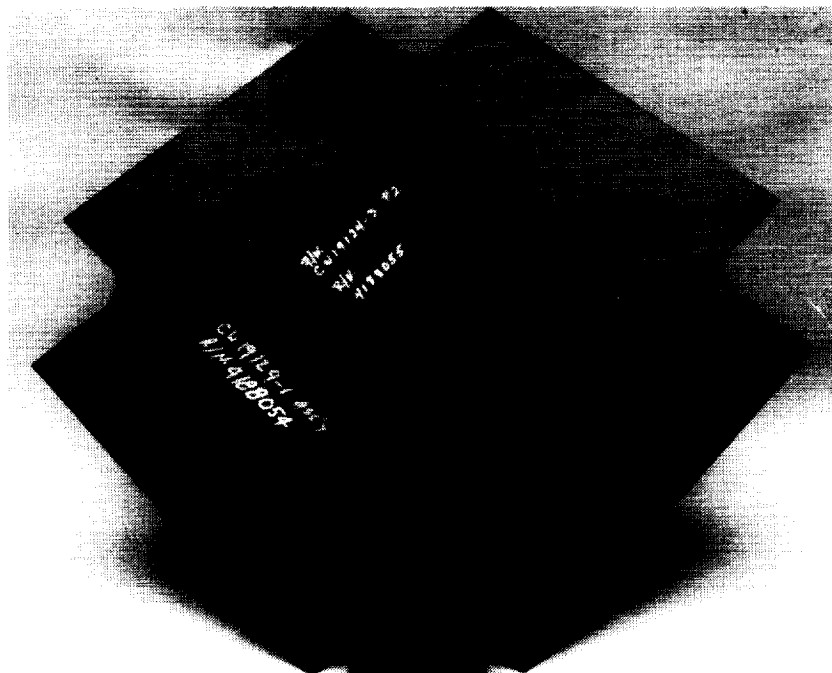
Figure 67. - Postbuckled spar shear test specimen.
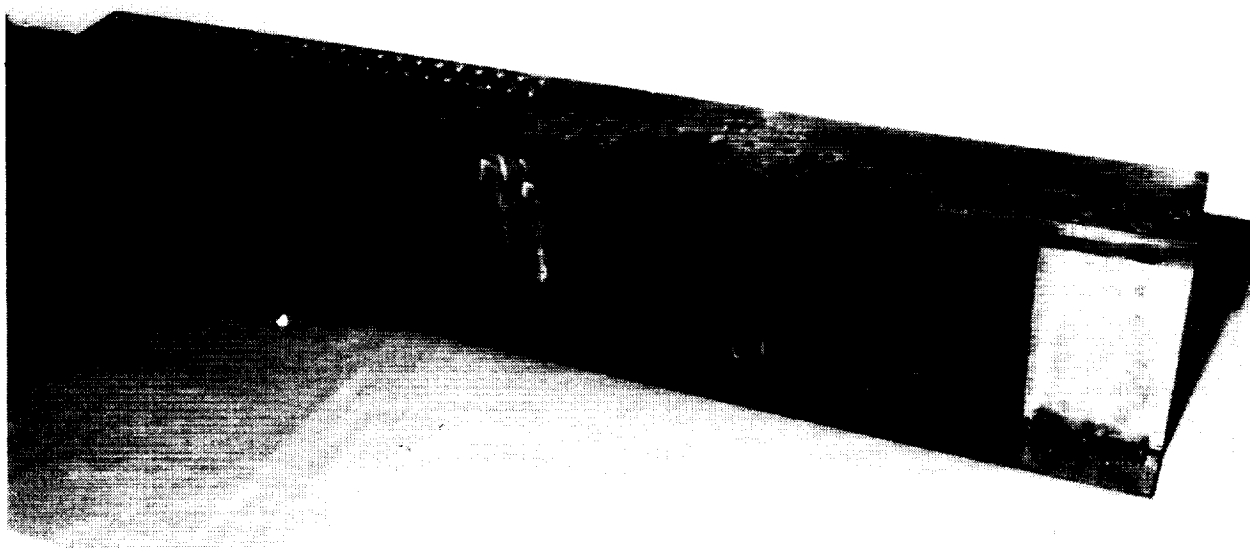
Figure 68. - Postbuckled spar bending specimen ready for test.

84

After completing the repair, tests proceeded to final failure at a load
level of 81,000 pounds R_2, or a calculated shear flow of 5786 lb/in.
Figure 69 shows a schematic of the failed specimen. The majority of the
failures were along the web tension diagonal, with one web failure extending
into the lower tension cap as indicated in Section A-A of that figure.
Several fastener pull-throughs were observed.

Outputs from several strategically-located strain gages are shown in
figures 70 and 71 with analytical results. Good correlation with test results
is evident, especially in the design range. Slight divergence at the higher
strains may be due to nonlinear material behavior, which is not accounted for
in the analysis.

The indicated onset of buckling is shown in figure 70 at 44,125 pounds R_2
(q = 3152 lb/in.), which is slightly sooner than the prediction of 49,600
pounds R_2 (q = 3543 lb/in.).

Buckling mode shapes and deflection were computed with the finite element
model. A typical contour plot slightly below ultimate load is presented in
figure 72. The analytic mode shape/web deflections compare favorably with
Moire' fringes observed during test. A Moire' fringe pattern from the
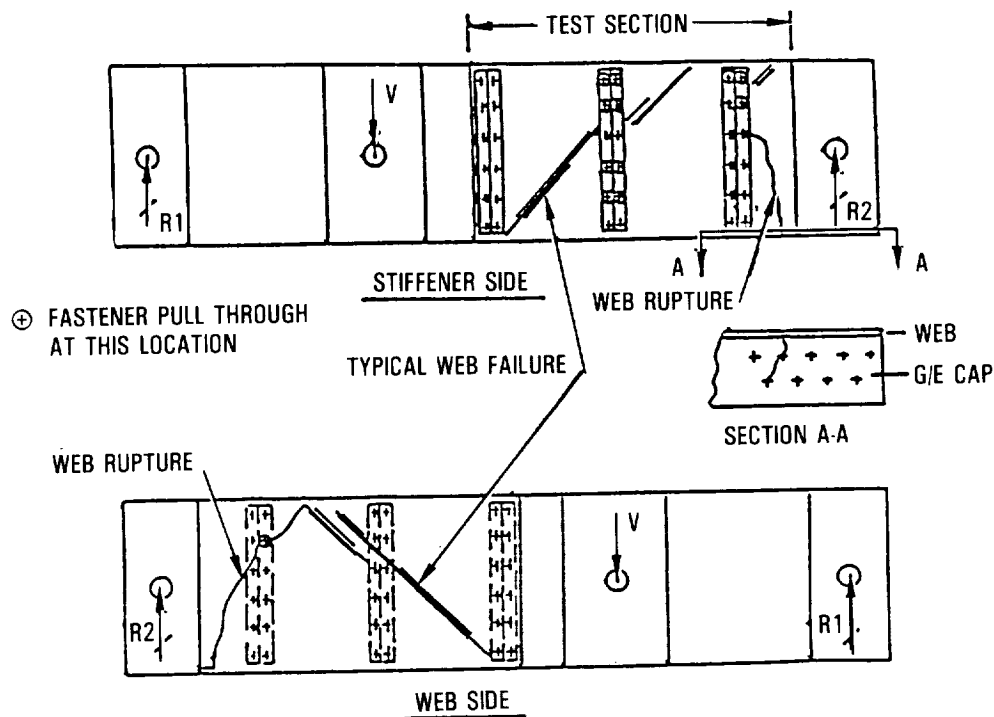
Figure 69. - Failure description - "post-buckled" spar bending specimen.
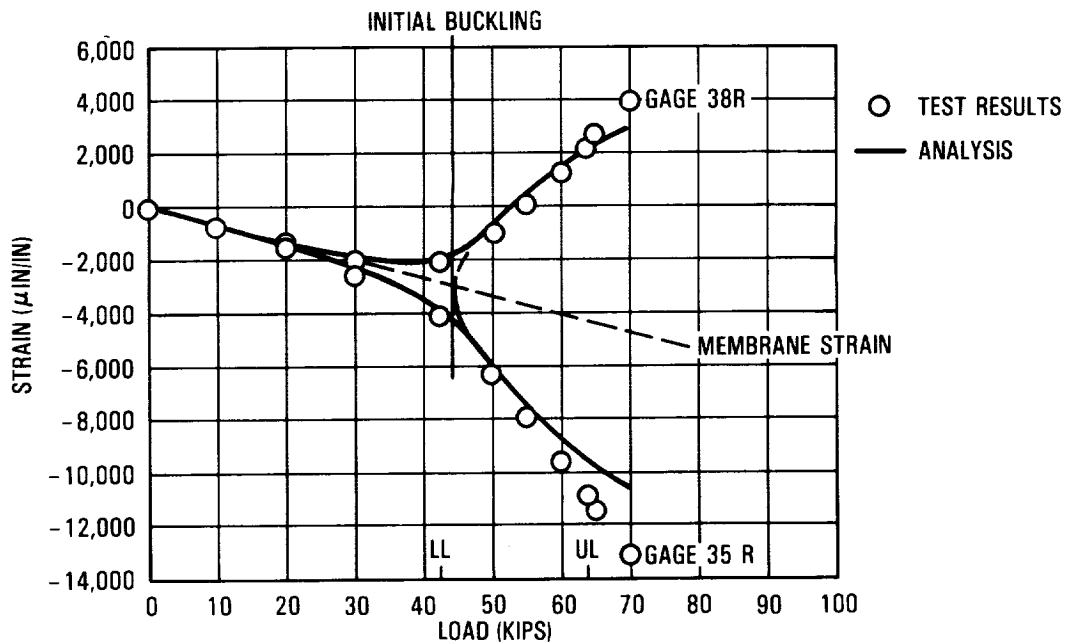
Figure 70. - Strain vs. load level "post-buckled" spar bending specimen.

specimen's critical panel at ultimate load is shown in figure 73. To show analysis correlation with test results, out-of-plane deflections along the web diagonal for the critical panel were plotted. The test deflections were obtained from the fringes shown in figure 73 (line A-B-C), with calibration correlated to wedges in each corner of the panel. Figure 74 shows the favorable comparison.

Spar Shear Specimen - Tests for the "post-buckled" shear panel test were identical to those described for prior panels. The following summary of test and predicted shear flows shows good correlation.

SPECIMEN TYPE	PREDICTED BUCKLING (LB/IN.)	ACTUAL BUCKLING (LB/IN.)	ACTUAL FAILURE (LB/IN.)
"As-Manufactured:"	2573	2430	4658
"Damaged:"	2573	2363	4338
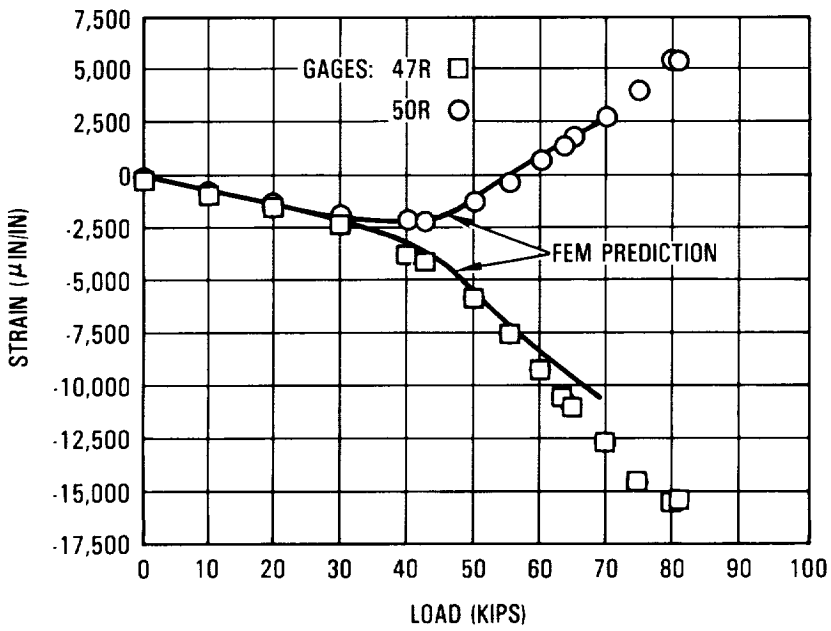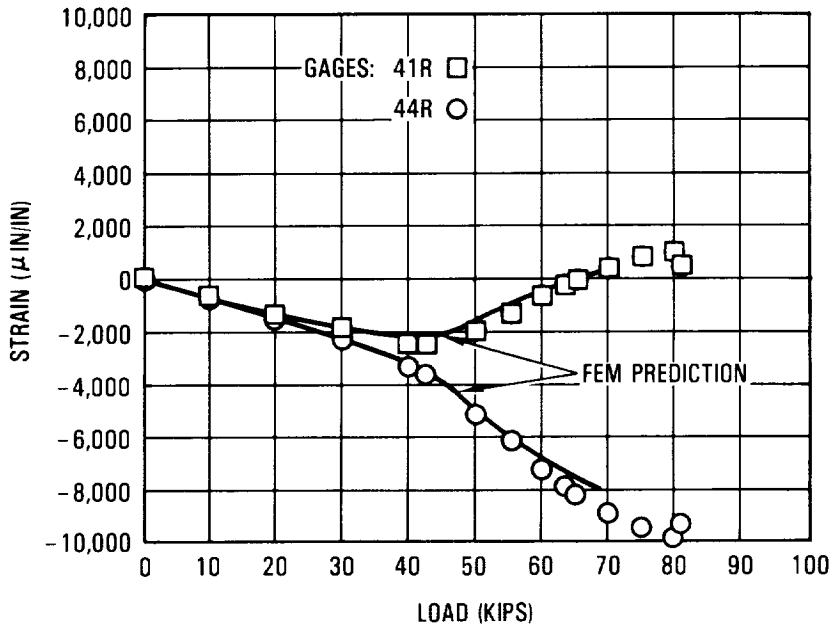
Figure 71. - Strain vs. load level "post-buckled" spar bending specimen.

C-2

POST BUCKLED BENDING SPAR — NONLINEAR ANALYSIS
P = 63.0 KIPS

DIAL

CONTOUR PLOT U2

CONTOUR	
1	−0.180E+00
2	−0.160E+00
3	−0.140E+00
4	−0.120E+00
5	−0.100E+00
6	−0.800E−01
7	−0.600E−01
8	−0.400E−01
9	−0.200E−01
0	−0.000E+00
A	0.200E−01
B	0.400E−01
C	0.600E−01
D	0.800E−01

MIN = −0.187E+00
MAX = 0.857E−01

MESH PLOT
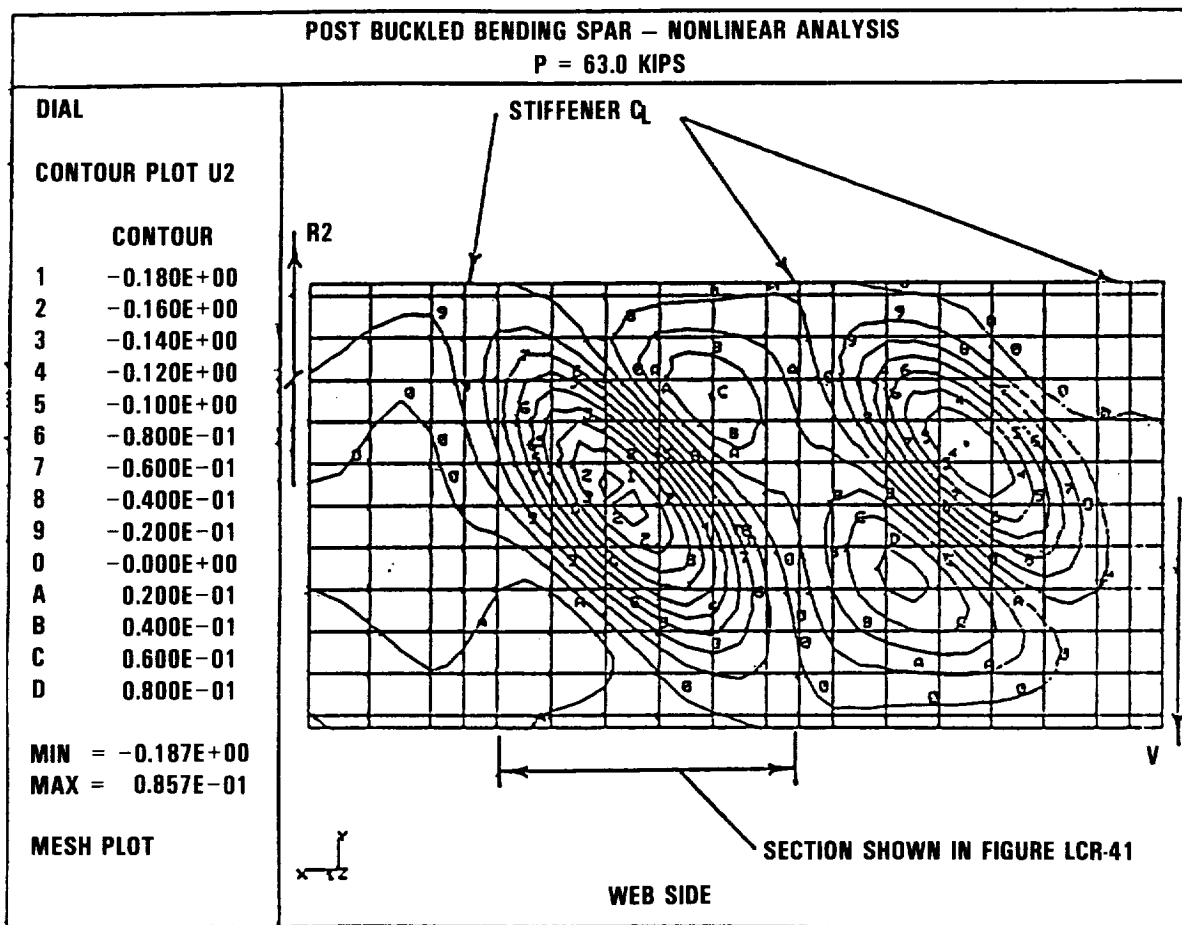
Figure 72. – Analytical deformation plot for the post-buckled web.

The impact data on the post-buckled panels is summarized below.

IMPACT SITE [1]	IMPACT ENERGY FT-LBS	WEB THICKNESS (IN)	IMPACT SIDE DAMAGE DEPTH (IN) [2]	RADIOGRAPHIC DAMAGE AREA (IN^2)
1	100	.228	.051	2.27
2	100	.228	.019	1.43
3	50	.156	.084	2.84
4	80	.156	Through Hole	2.55
5	100	.228	.134	2.46
6	100	.228	.137	2.11

[1] Impact sites shown in Figure 75.

[2] Sites 1, 2, 5, and 6 were impacted on smooth side of the web; sites 3 and 4 on stiffener side of web.

Figure 73. - Moire'fringe at ultimate load - post-buckled spar web.

Initial failure of the "as-manufactured" post-buckled spar shear specimen was detected audibly at applied loads of 74,000 pounds tension and 74,332 pounds compression, or 4658 lb/in., shear. After the load was reduced to zero, the test specimen was checked for visible damage, but none was found. Load was reintroduced, and full specimen failure occurred at 72,000 pounds tension and 72,487 pounds compression. Web failure prior to, or coincident with, stiffener separation was the primary mode of failure. A buckling ratio, τ/τ^{cr}, of 1.91 was obtained.

Initial failure of the impacted post-buckled spar shear specimen was detected by cracking noises at 55,000 pounds tension and 55,379 pounds compression, or 3469 lb/in. shear. the specimen failed at 69,000 pounds tension and 69,021 pounds compression. The web failed generally parallel to the two load axes, with severe rupture along the compression axis through impact site 7A (same location as site 5 in figure 75). The stiffeners did not separate from the web, although some disbonding did occur. One stiffener sustained damage in the fastener areas at the top and bottom of the web. figure 76 shows the failed specimen viewed from the impacted side.

ALL MOIRE' FRINGE OUT-OF-PLANE
DIMENSIONS ARE ±0.023 IN.

WEB BUCKLE SHAPE AT
63.6 KIPS (ULTIMATE LOAD)

0.140 MAX AT B

0.140   0.128

A   B   C

4.40   3.95

MOIRE FRINGE

WEB BUCKLE SHAPE AT
63.0 KIPS

0.180 MAX AT B

0.020   0.060

A   B   C

4.40   3.95

FINITE ELEMENT MODEL
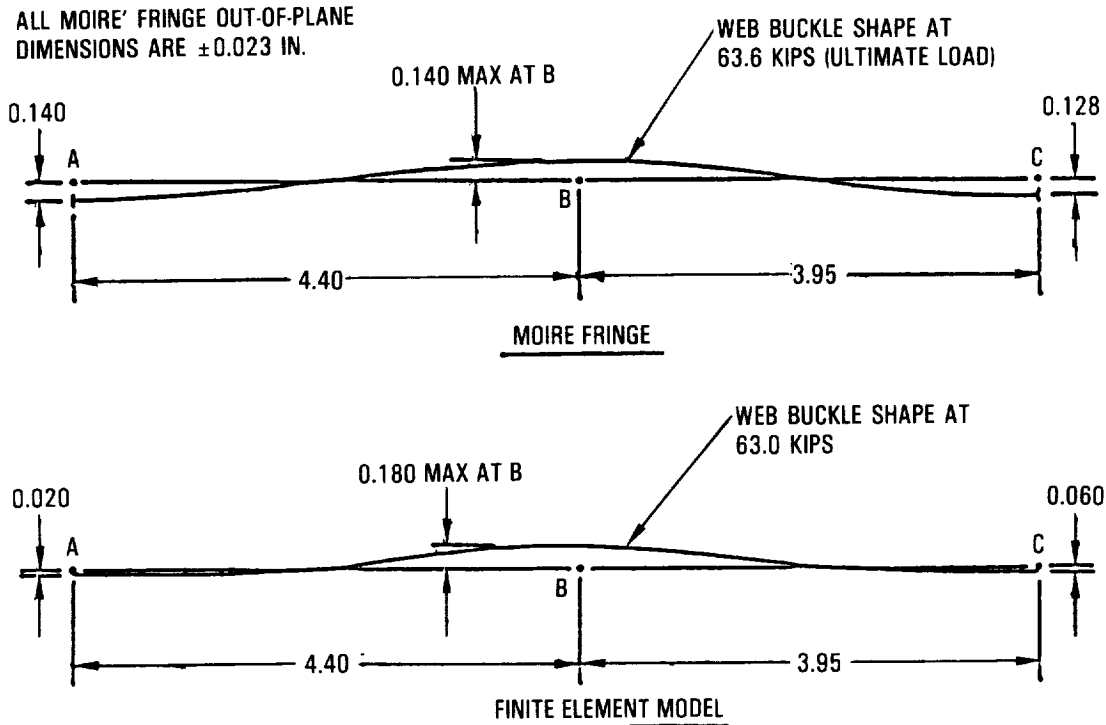
Figure 74. - Moire' vs. Analytical out-of-plane deflection at ultimate
load - post-buckled spar web.

CONCLUSIONS

Numerous design concepts, materials and manufacturing methods were
investigated for the covers and spars of a transport wing box. Cover panels
and spar segments were fabricated and tested to verify the structural
integrity of the design concepts and fabrication techniques.

Table 11 summarizes compression test results obtained for various wing
upper cover designs. These data show that the impact damaged condition
establishes the design allowable strains for panels loaded in compression.
Damage tolerance can be improved by modifying the design to arrest
delamination growth as was demonstrated with the addition of pad-ups in the
'T' stiffened panel designs. Tougher materials can also improve damage
tolerance as is shown by comparing the performance of the AS4/2220 blade
stiffened panel versus the IM7/8551-7 panels. Figure 77 compares the
structural efficiency of the stiffened cover panels which were tested. The
structural efficiency index used is the end load at failure for impacted
panels divided by the panel areal weight. To obtain a panel weight savings of
35 percent compared to the aluminum baseline a structural efficiency index of
79×10^4 in., must be achieved. Of the six designs tested, all except the 'T'
stiffened panel without the pad-up and the AS4/2220 blade stiffened panel met
or exceeded the design goal. Note also that although the IM7/8551-7 blade

90
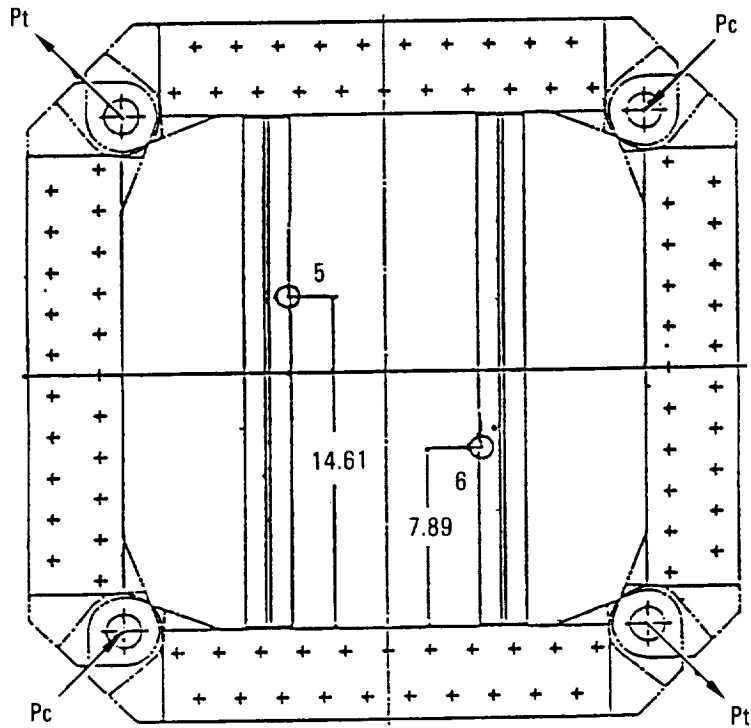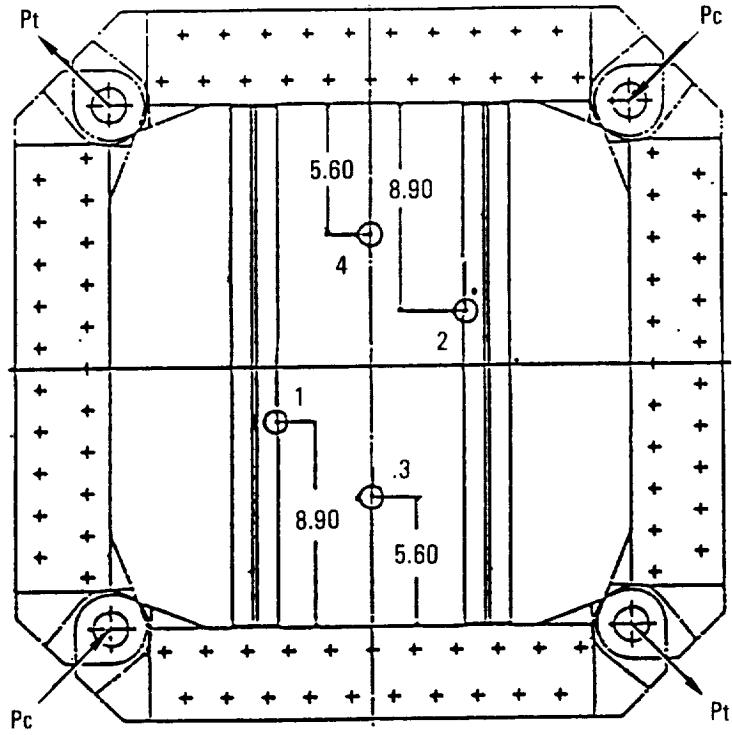
Figure 75. - Impact location - "post-buckled" spar shear specimen.
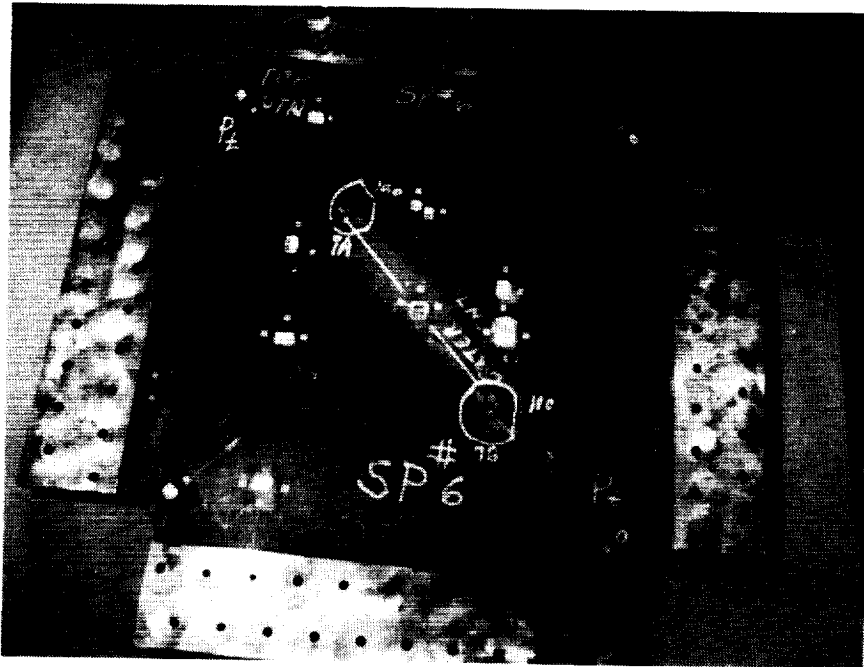
Figure 76. - Failed spar shear specimen - "post-buckled/damaged."

stiffened panel failed at the same strain level as the 'T' stiffened panel without pad-ups, use of the higher modulus fiber results in a significant improvement in structural efficiency.

Figures 78 and 79 compare the performance of the various spar designs which were fabricated and tested. A summary of the weights for each design is given in Table 12. Of the six designs tested, all except the foam sandwich and geodesic concepts met or exceeded the design load level. With the exception of the foam sandwich design, impact damage caused only a slight degradation of performance in the shear web specimens. Very good correlations between predicted buckling loads and measured buckling loads were obtained on all designs. The best performance to weight ratio was obtained from the filament wound spar design, demonstrating the ability of this low cost manufacturing approach to produce parts having excellent structural quality.

Fabrication costs for the cover panel and spar test specimens were tracked to accumulate composite manufacturing information from which data can be extracted to develop cost estimating relationships. Comparative cost data for the various cover and spar concepts fabricated is shown in figures 80 and 81 respectively. The relative costs presented are based on actuals and reflect current market prices. Material costs are a small percentage of the total fabrication cost, since labor costs are always higher for single parts than for production quantities. High volume production would reduce labor costs so that they would represent a smaller contribution to overall costs, making material costs more significant.

TABLE 11. COVER COMPRESSION TESTS — STRAIN RESULTS

CONCEPT / MATERIAL	NOTCHED [1] FAILURE (μIN./IN.)	IMPACTED FAILURE (μIN./IN.)
'T' Stiffened [4] — AS4/1806 Tape		
No Pad-up	6400	4700 [2]
Discrete Pad-up	N/A	4900 [2]
Integral Pad-up	N/A	5600 [2]
'J' Stiffened — AS4/1806 Fabric		
Discrete Pad-up	6400	4800 [3]
Blade Stiffened		
AS4/2200	N/A	3500 [3]
IM7/8551-7	5200	4600 [3]
Sandwich [4] IM7/8551-7		
Between Spar Panel	N/A	4200 [3]
Spar Cap Insert Panel	5000	5100 [3]

[1] 0.25 in. diameter holes

[2] 80 ft-lb at skin (results lower than 100 ft-lb impact)

[3] 100 ft-lb at skin

[4] Separately funded results

93
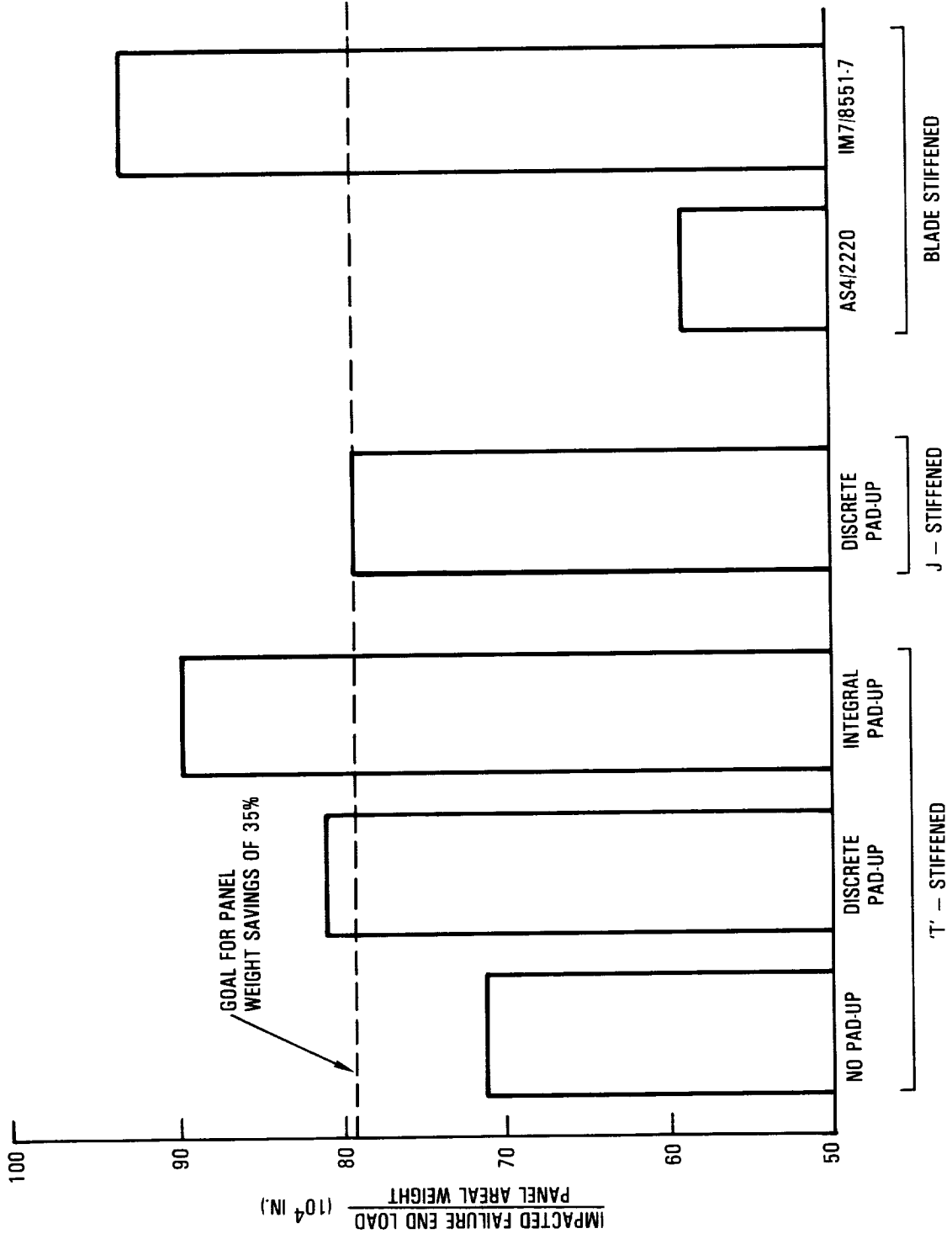
Figure 77. – Stiffened cover designs – structural efficiency comparisons.
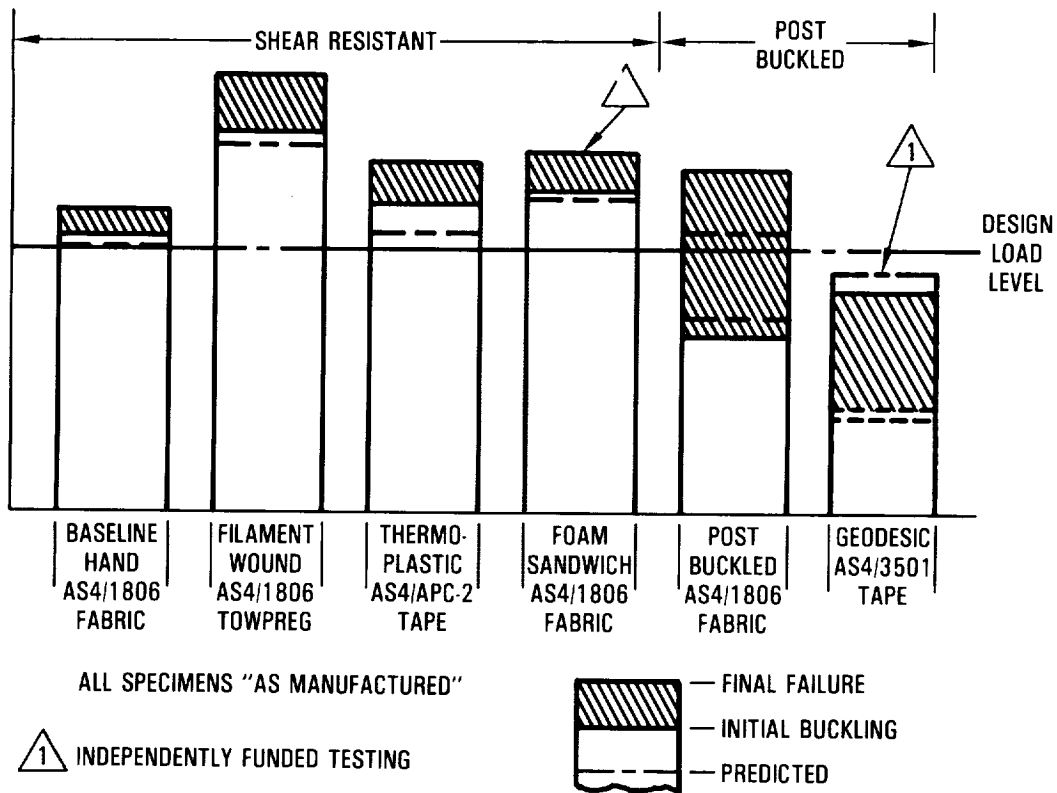
Figure 78. - Spar bending test summary.
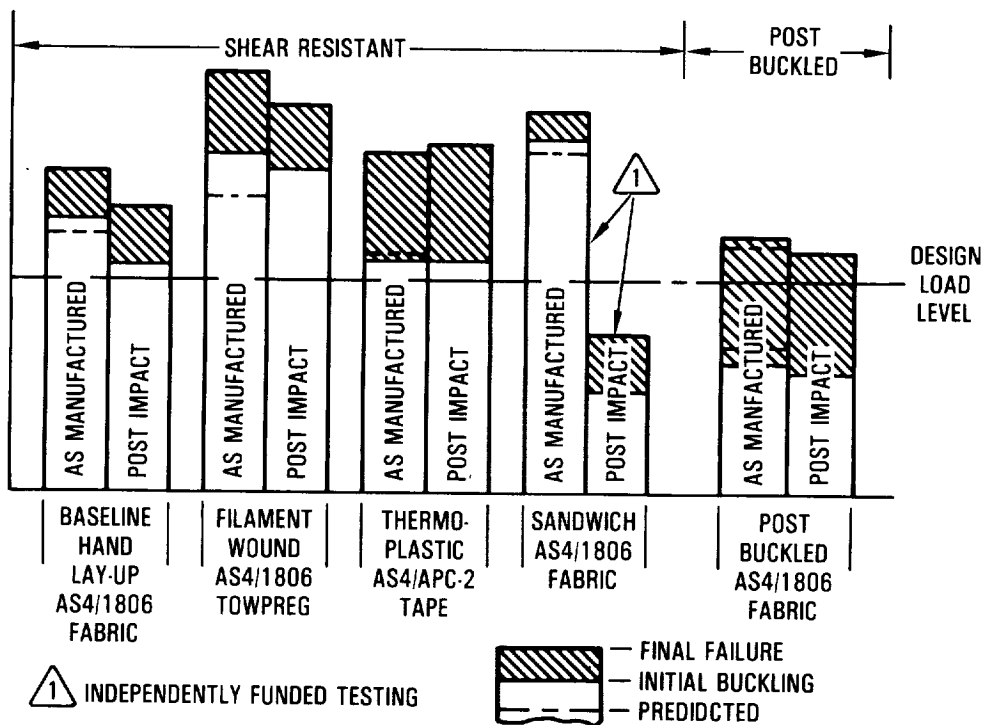
Figure 79. - Spar-shear test summary.

TABLE 12. - SPAR WEIGHT SUMMARY

SPAR CONCEPT	TYPICAL WEB AREAL WEIGHT (LB/IN^2)	AVERAGE WEIGHT/UNIT LENGTH (LB/IN)	SPAR WEIGHT (LB)
Baseline	.0130	.671	295
Filament Wound	.0130	.671	295
Thermoplastic	.0137	.706	311
Postbuckled	.0122	.647	285
Sandwich ① ②	.0111	.626	275
Geodesic ① (Postbuckled)	.0136	.744	327

① Separately funded designs.

② Does not meet damage tolerance criteria.

The towpreg used for the filament wound spar is the most expensive material, but this cost could be reduced significantly with high volume production. The thermoplastic tape is the second most expensive material. Material costs for the baseline spar and postbuckled spar are roughly equivalent.

Labor hours were tracked by operation for each test article. Shop orders were generated for all specimens. From these shop orders, each major operation was defined, and separate work order numbers were established for each operation category. Where possible, like items were combined to eliminate unnecessary effort in recording fabrication time. The time spent for each operation category was recorded to the attendance and labor recording system computer and reported on a weekly basis. Figures 82 and 83 show the typical labor breakdown for the J-stiffened cover panels and baseline spar bending specimens.

Based on the results reported herein, the designs, materials and manufacturing methods have been selected for a technology integration box beam which will be a full scale section of a wing box. The covers will be a blade stiffened design fabricated with AS4/1806 fabrics. A low percentage of 0° plies will be used in the skins to maximize damage tolerance. This design concept and material was selected because they offer the best cost and weight performance of all the candidates evaluated. Pultrusion will be used to lay up and form the channel sections which constitute the blade stiffeners. For the spars, a shear resistant filament wound design was selected. As with the covers, this decision was made based on the attainment of the greatest weight savings for the lowest fabrication cost. The additional weight saved by
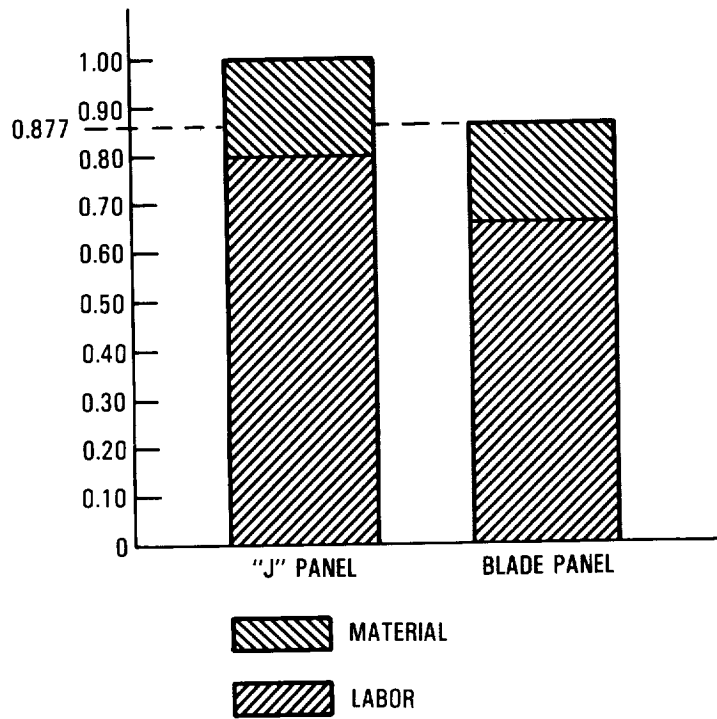
Figure 80. - Relative costs of composite covers.
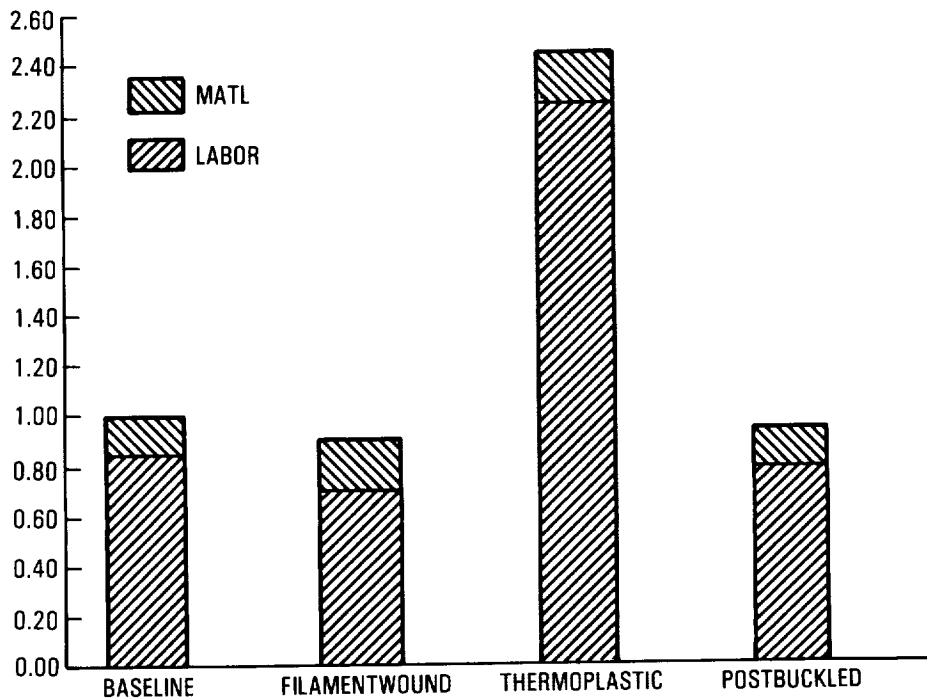
Figure 81. - Relative costs of composite spars.
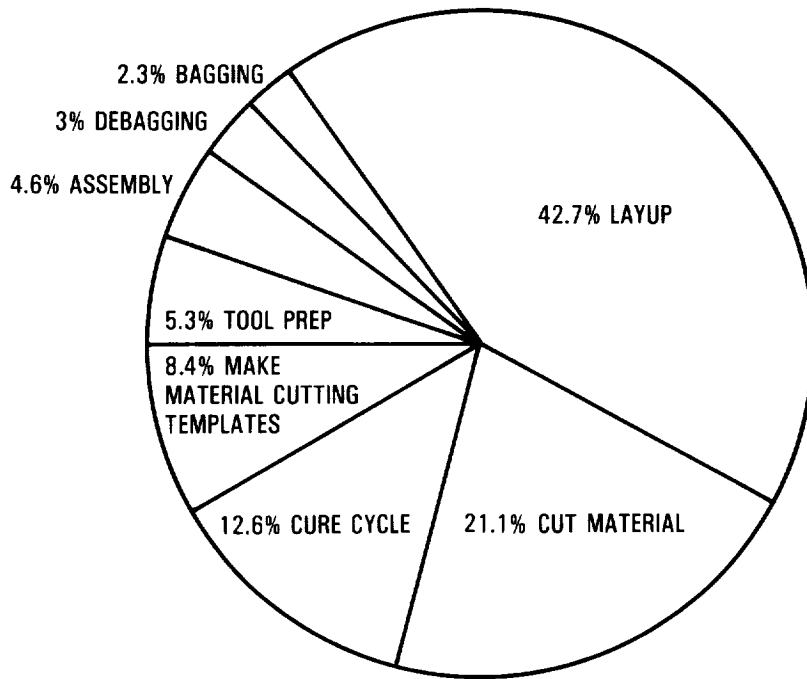
Figure 82. - J-stiffened cover labor costs.
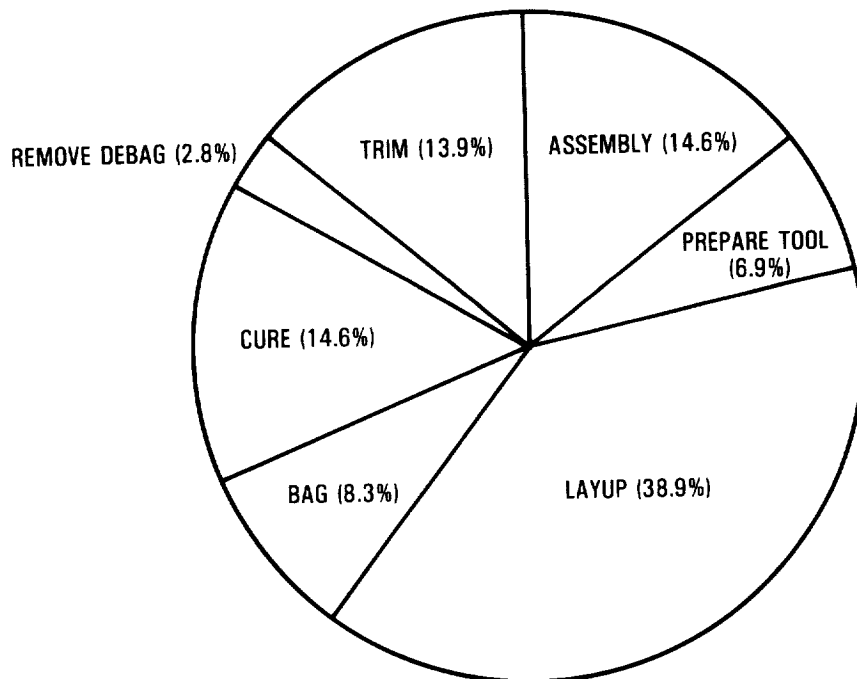
Figure 83. - Baseline spar labor costs.

selecting a post-buckled design did not justify the greater manufacturing complexity required for the stiffener pad-ups in the webs and therefore the additional cost. A combination of AS4/1806 towpreg and fabric will be used to fabric the spars. When completed, the data obtained by fabricating and testing the box beam will demonstrate the structural integrity of an advanced composite wing design which is 25 percent lighter than the baseline wing box.

NASA

National Aeronautics and Space Administration
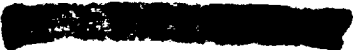
Report Documentation Page

1. Report No. NASA CR-4177	2. Government Accession No.	3. Recipient's Catalog No.
4. Title and Subtitle Composite Transport Wing Technology Development - Design Development Tests and Advanced Structural Concepts		5. Report Date September 1988
		6. Performing Organization Code 76-20
7. Author(s) Charles F. Griffin and William E. Harvill		8. Performing Organization Report No.
		10. Work Unit No. 505-63-01-06
9. Performing Organization Name and Address Lockheed Aeronautical Systems Company P.O. Box 551 Burbank, California 91520		11. Contract or Grant No. NAS1-17699
		13. Type of Report and Period Covered Contractor Report
12. Sponsoring Agency Name and Address National Aeronautics and Space Administration Langley Research Center Hampton, VA 23665-5225		14. Sponsoring Agency Code

16. Abstract

Numerous design concepts, materials and manufacturing methods were investigated for the covers and spars of a transport wing box. Cover panels and spar segments were fabricated and tested to verify the structural integrity of design concepts and fabrication techniques.

Compression tests on stiffened panels demonstrated the ability for graphite/epoxy wing upper cover designs to achieve a 35 percent weight savings compared to the aluminum baseline. The impact damage tolerance of the designs and materials used for these panels limits the allowable compression strain and therefore the maximum achievable weight savings.

Bending and shear tests on various spar designs verified an average weight savings of 37 percent compared to the aluminum baseline. Impact damage to spar webs did not significantly degrade structural performance. Predictions of spar web shear instability correlated very well with measure performance. The structural integrity of spars manufactured by filament winding equaled or exceeded those fabricated by hand lay-up.

The information obtained will be applied to the design, fabrication, and test of a full-scale section of a wing box. When completed, the tests on the technology integration box beam will demonstrate the structural integrity of an advanced composite wing design which is 25 percent lighter than the metal baseline.

17. Key Words (Suggested by Author(s)) Composites, Materials, Primary, Aircraft Structure, Wings, Graphite/Epoxy, Damage Tolerance	18. Distribution Statement ███████████ Subject Category 24
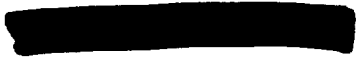
19. Security Classif. (of this report) Unclassified	20. Security Classif. (of this page) Unclassified	21. No. of pages 112	22. Price